KWAME NKRUMAH UNIVERSITY OF SCIENCE AND TECHNOLOGY, KUMASI

COLLEGE OF SCIENCE

FACULTY OF PHYSICAL AND COMPUTATIONAL SCIENCES

Synthesis and characterization of nanocrystalline Zeolite Socony Mobil-5 using some Ghanaian clays as the starting raw materials

By

Benjamin Kwadzo Kokloku

(B.Sc. Chemistry)

A thesis submitted to the Department of Chemistry, Kwame Nkrumah University of Science and Technology, Kumasi-Ghana, in partial fulfillment of the requirements for the award of the degree of

MASTER OF PHILOSOPHY IN CHEMISTRY

November, 2023

Declaration

I hereby declare that this thesis is my work toward a Master of Philosophy degree in Chemistry and that to the best of my knowledge, it contains no material previously published or written by another person nor one which has been accepted for the award of any other degree or diploma at the Kwame Nkrumah University of Science and Technology, Kumasi or any other educational institution, except where due acknowledgment is made in the thesis.

Benjamin Kwadzo Kokloku	……..	…….
(PG 4265420)	Signature	Date

Certified by:

Prof. Johannes A. M. Awudza	……..	…….
(Supervisor)	Signature	Date

Certified by:

Prof. Godfred Darko	……..	…….
(Head of Department)	Signature	Date

Acknowledgments

I thank God Almighty whose immeasurable grace has brought me this far in life. I express my sincere gratitude to my supervisor, Professor Johannes A. M. Awudza, for his constant guidance, support, and encouragement throughout this research work. His expertise and insightful feedback were invaluable in shaping the research and writing the thesis. My appreciation also goes to Prof. Francis Kemausuor and Dr. (Mrs.) Mizpah A. D. Rockson for shaping my thoughts into reality.

Furthermore, I want to thank the faculty members of the Department of Chemistry, KNUST for their invaluable feedback, and suggestions on my research work. I was able to upgrade the standard of my work thanks to their suggestions. A special thanks to Dr. Michael B. Mensah and Dr. Gershon Amenuvor for giving me access to their laboratory to do the major part of the experiments. I want to extend my appreciation to the laboratory technicians of the Department of Chemistry, KNUST for their assistance and valuable resources in accomplishing this work.

An acknowledgment to the following Departments and their laboratory technicians for allowing me to use their facilities: The Department of Materials Engineering, Department of Industrial Art (Ceramic section), Department of Civil Engineering, and Department of Soil Sciences, KNUST. An acknowledgment to KNUST Central Laboratory, the Department of Physics, the Department of Earth Sciences, and the Department of Materials Science & Engineering, University of Ghana for helping me with the sample characterizations.

My heartfelt gratitude to my parents and family for their prayers, unwavering support, love, and encouragement throughout my academic journey. Finally, I am appreciative of the financial assistance received from the Ministry of Education and Research (BMBF) in Germany under the Hybrid Waste to Energy as a Sustainable Solution for Ghana Project, and the Brew-Hammond Energy Centre (TBHEC), KNUST.

Abstract

Zeolites are aluminosilicate crystals having a porous structure and are useful as catalysts, adsorbents, and ion exchange materials. The synthesis of zeolites using clay minerals is a promising approach because it utilizes inexpensive and widely available starting materials. However, clays originate from different sources and the parameters of synthesis vary depending on the environment and nature of the clay. Therefore, the process requires suitable pre-treatment of the raw clay and the optimization of the synthesis parameters to ensure that the synthesized zeolite has the desired properties. In this work, a protocol to be used in the synthesis of ZSM-5 zeolite using Anfoega, Mfensi, Teleku-Bokazo, and Tetebu clays was developed. These clays serve as silica and alumina sources. The raw clays were first calcined, followed by acid leaching to dealuminate the calcined samples to increase the SiO_2/Al_2O_3 molar ratio while removing impurities, and finally hydrothermal zeolitization. From the results obtained, acquiring the ZSM-5 phase in the final product depended greatly on the pre-treatment technique applied to the raw clay. ZSM-5 zeolite was effectively synthesized from all four clay sources at a crystallization temperature and crystallization period of 190 °C and 24 h, respectively. The relative crystallinity and crystallite sizes of the ZSM-5 phase were calculated to be 41.23% and 36.08 nm, 32.02% and 35.53 nm, 35.37% and 34.75 nm, and 54.43% and 29.74 nm for Anfoega, Mfensi, Teleku-Bokazo, and Tetegu clays respectively. The synthesis conditions of the ZSM-5 zeolite using Tetegu clay were further investigated in more detail and the parameters were optimized. Hence, for the Tetegu clay, the effects of key synthesis parameters, i.e., temperature, time, aging conditions, and reactant molar ratios were investigated. The optimal production conditions of nano-crystallite ZSM-5 zeolite using the Tetegu clay were found to be a molar ratio of SiO_2/Al_2O_3 = 51.97, $NaOH/SiO_2$ = 0.032, $TPABr/SiO_2$ = 0.072, H_2O/SiO_2 = 25; crystallization temperature = 190 °C; crystallization time = 24 h, with aging at room temperature (without stirring) for 24 h. This study has established

the viability of clay samples obtained from Anfoega, Mfensi, Teleku-Bokazo, and Tetegu as starting materials for the production of ZSM-5 zeolite, and the appropriate optimal production conditions were established for Tetegu clay.

Keywords: Clay, pre-treatment, hydrothermal synthesis, ZSM-5 zeolite, optimal conditions.

Table of content

List of Tables

List of Figures

List of Abbreviations

AFC	Anfoega Clay
CAFC	Calcined Anfoega Clay
CMFC	Calcined Mfensi Clay
COD	Crystallography Open Database
CTBC	Calcined Teleku-Bokazo Clay
CTTC	Calcined Tetegu Clay
DSC	Differential Scanning Calorimetry
DTA	Differential Thermal Analysis
FTIR	Fourier Transform Infrared
FWHM	Full Width at Half Maximum
IL	Ionic Liquid
MFC	Mfensi Clay
MSW	Municipal Solid Waste
OSDA	Organic Structure Directing Agent
PDF	Powder Diffraction File
PDS	Particle Distribution Size
SEM	Scanning Electron Microscope
TBC	Teleku-Bokazo Clay
TGA	Thermogravimetric Analysis
TPABr	Tetrapropylammonium Bromide
TTC	Tetegu Clay
XRD	X-ray Diffraction
XRF	X-ray Fluorescence
ZSM-5	Zeolite Socony Mobil–5

CHAPTER ONE

INTRODUCTION

1.1 Background

The effects of Municipal solid waste (MSW) mismanagement are among some of the pressing issues confronting humanity. MSW is affecting the environment, human health, and economy negatively in most developing countries. About 1.3 billion tons of MSW is generated every year in most developing countries due to fast urbanization and population growth, as well as the rising standard of living (Miandad *et al.*, 2016). These waste materials come from homes, healthcare facilities, industries, and other establishments. Most frequently, an open dumping system is used to manage it. This results in air pollution, contamination of water, and land degradation (Sipra *et al.*, 2018). Among solid wastes, waste plastics have become a serious global concern in recent years. The global plastic waste generation was at 370 million tons in 2019. Just 9% of it is recycled, 12% of it is burned, and the rest ends up in landfills or the environment. Waste plastics that end up in the environment can cause serious issues like blocking waterways and creating stagnant water that can serve as a breeding ground for mosquitoes, pests, and other vectors of diseases (Kumar *et al.*, 2021). Burning plastics in open places releases toxic gases like dioxins, and polycyclic aromatic hydrocarbons into the atmosphere, and poses dangers to vegetables, and human and animal health (Zhang *et al.*, 2020).

In Ghana, 26,000 metric tons of various plastic products are manufactured each year. Additionally, the nation imports more than 10,000 metric tons of finished plastic goods every year (Tulashie *et al*., 2019). According to Zhou *et al*. (2021), more than 80% of plastic manufactured is discarded indiscriminately in the environment or ends up in landfills (Zhou *et al.*, 2021). Therefore, about 30, 600 metric tons of these plastics will end up in the environment

as waste. Rapid growth in Ghana's population will require an increase in the production of plastics, as well as their uses and applications, which will increase the amount of plastic waste generated in the country. Waste management is a major challenge facing many metropolitan, municipal, and district assemblies in Ghana (Miezah *et al.*, 2015). Further, Petroleum is the main energy source that the country significantly depends on with little variation in its energy mix (Tulashie *et al*., 2019).

Being derived from petroleum sources, plastics have a high energy content (Zhang *et al.*, 2020). Energy in these materials is stored in chemical bonds within chemical species and is released when broken down (Sipra *et al.*, 2018). With the current high-energy demand and the depletion of indigenous fossil fuels, these waste plastics present an opportunity. The conversion of plastic waste into fuel *via* pyrolysis could reduce its negative environmental impact and also add to the available energy sources (Zhang *et al.*, 2020). By using catalytic pyrolysis, 70-80% of plastic wastes may be transformed into liquid oil with properties matching those of typical diesel fuel. For example, both of them have a high heating value of 38-46 MJ/kg. Thus, the liquid oil produced by catalytic pyrolysis is of high quality and may be utilized in a range of energy-related applications, including the production of electrical power, fuel for vehicles, and heating sources (Miandad *et al.*, 2016).

During the catalytic pyrolysis process, several reactions may occur including cracking, dehydrogenation, oligomerization, cyclization, and aromatization (Lok *et al*, 2019). Zeolites, especially zeolite-Y, and ZSM-5 are utilized mostly as a catalyst in the pyrolysis process. They have a great impact on the composition of the resulting product. Additionally, these catalysts speed up the process by lowering the activation energy for the conversion process. Zeolite-Y and ZSM-5 zeolites are desired because of their thermal stability, acidity, and porous nature which enhances their activity and product selectivity (Hu *et al.*, 2020). They are known to be selective toward the production of aromatics and branched hydrocarbon during plastic

pyrolysis (Seo *et al*., 2003). ZSM-5 zeolite in particular is considered an effective catalyst for industrial-scale catalytic cracking of plastics into gasoline-range hydrocarbons (Zhou *et al.*, 2021).

The active sites that are crucial to the diverse catalytic activities are the Brønsted and Lewis acid sites in the framework of the zeolite catalysts (Verdoliva *et al.*, 2019). The removal of hydride ions from the polymer structure by Lewis acid sites or the insertion of a proton to the C-C bond by Brønsted acid sites of the zeolite initiates the catalytic breaking process in plastic pyrolysis (Fadillah *et al.*, 2021). Carbonium ions may be generated as an intermediate which promotes cracking, or chain scission leading to bond cleavage thereby producing shorter chain molecules (Daligaux *et al.*, 2021). Additionally, the successful application of zeolites is based on their main inherent shape-selective structure, which is a function of their porous nature (Koohsaryan and Anbia, 2016).

Despite these advantages of zeolites, synthetic zeolites are expensive due to the high cost of production, thus making the employment of catalytic pyrolysis using zeolites relatively expensive (Cocchi *et al.*, 2020). To lower the cost of zeolite production, scientists now focus on the use of low-cost raw materials for low-cost zeolite synthesis. Several inexpensive materials have been used for the synthesis of various zeolite types, which are predominantly composed of silica and alumina. These materials include kaolin, bauxite, clay, rice husk ash, fly ash from coal furnaces, paper sludge, blast furnace slag, municipal solid waste, and lithium slag (Khaleque *et al.*, 2020; Tran-Nguyen *et al.*, 2021). Amongst these materials, clay is the most frequently used since it has both silica and alumina in its crystalline structure, which can be transformed into a zeolite framework. Furthermore, clay has several advantages for ZSM-5 production including its abundance, easy accessibility, affordability, and ecological friendliness. Therefore, it could be employed as raw material for large-scale production of ZSM-5 zeolite (Nguyen *et al.*, 2023).

1.2 Problem statement

ZSM-5 zeolite has proven to be an efficient solid acid catalyst for the conversion of plastic wastes into transportation fuel *via* pyrolysis (Zhou *et al.,* 2021). However, the cost of this zeolite makes the overall cost of the process expensive. Fortunately, the use of clay as a low-cost starting raw material for the production of ZSM-5 zeolite has been known to reduce its cost. Thus, reducing the overall cost of fuel production from plastic waste. Clay reserves in commercial quantity are found in Ghana; however, an extensive literature search gave no information on the use of Ghanaian clays for the synthesis of ZSM-5 zeolites.

Furthermore, there is no standard procedure for zeolite synthesis when using clay. This is because the mineralogical compositions and crystalline phases present in clay vary from one geographical location to another. Consequently, the clay pre-treatment process and synthesis parameters vary per the environment in which the clay is obtained (Gandhi *et al*., 2021). Upon an extensive literature search, Ghanaian clays have not been explored for the synthesis of ZSM-5 zeolite. Hence, a need to determine the viability of these clays as potential raw material and to develop a protocol for the synthesis of ZSM-5 zeolite type using some Ghanaian clays for different applications.

1.3 Justification

The primary chemical components of clay are silica (SiO_2) and alumina (Al_2O_3), which are the chemical composition of zeolites. Clay minerals are well known to be suitable raw starting materials for the production of different zeolite types. Paquin *et al*. (2015) reported the successful production of ZSM-5 zeolite using clay as the only source of silica and alumina. Clay deposits are distributed over the entire land of Ghana and every region is endowed with

clay deposits (Asamoah *et al.*, 2018). Some Ghanaian clays, Anfoega and Awaso clay have been used successfully to synthesize zeolite types, A, X, and Y (Kwakye-Awuah *et al.*, 2014, 2018, 2019, 2021; Osei *et al.*, 2021). Zeolite P has been synthesized using Teleku-Bokazo clay as the silica and alumina source (Tabi *et al.*, 2021). These clays could be potential clays for ZSM-5 synthesis since they are suitable for other zeolite-type production. However, an extensive literature search gave no information about the use of Ghanaian clays as a precursor for the synthesis of ZSM-5.

1.4 Main objective

This research aimed at exploring the use of some Ghanaian clays as potential sources of silica and alumina for the syntheses of nanocrystalline Zeolite Socony Mobil-5 (ZSM-5).

1.4.1 Specific objectives

1. To collect and characterize Anfoega clay (Volta Region), Tetebu-Bokazo clay (Western Region), Mfensi clay (Ashanti Region), and Tetebu clay (Greater Accra), from clay deposits located in Ghana.
2. To develop suitable dealumination conditions for each of the selected clays.
3. To determine the viability of the four Ghanaian clays for the synthesis of ZSM-5 zeolite.
4. To study the effects of synthesis parameters such as reactant's molar ratios, aging conditions, crystallization temperature, and crystallization time on the zeolite structure formed.

1.5 Scope of study

The scope of this study was to collect and characterize clay samples from some clay deposits in different geographical areas located in Ghana. Subsequently, evaluate the viability of these clay samples for the synthesis of ZSM-5 zeolite, and optimize the synthesis parameters. Finally, use the as-synthesized zeolites for the catalytic pyrolysis of Municipal solid wastes into liquid fuel focusing on plastic waste conversion. However, time and resource constraints could not permit the applications of the zeolites produced.

CHAPTER TWO

LITERATURE REVIEW

2.1 The genesis of zeolites

The earliest naturally occurring zeolites were discovered in the voids and vugs of volcanic rocks. Alex Fredrik Crönstedt, a mineralogist was the first to recognize naturally occurring zeolite as a mineral in 1756 after he examined crystallites collected from a copper mine in Sweden. He noticed the mineral discovered released a lot of water vapor when heated fast after absorbing water. Based on this behavior, he named the new mineral "boiling stone" which was taken from the Greek words ζ΄εω, "boil" and λ΄ιθος, "stone" (Cataldo *et al.*, 2021). Later, Barrer and Milton paved the way for the synthesis of zeolites in the 1940s. Ever since, much work has gone into the synthesis of novel zeolite structures (Liu and Yu, 2016). To date, 234 varieties of zeolite structures have been documented (Narayanan *et al.*, 2021).

2.2 The chemistry of zeolites

Zeolites are microporous aluminosilicate crystals made up of $[SiO_4]^{4-}$ and $[AlO_4]^{5-}$ tetrahedra and they are joined by four oxygen atoms forming a well-defined three-dimensional framework (Sumari *et al.*, 2019). Figure 2.1 and Figure 2.3 show the primary structure of zeolite and its framework. The framework is composed of channels, tunnels, and cavities inside where cations, which are typically group I and II metals, water molecules, or other small mobile molecules may be found (Smail *et al.*, 2019). Zeolites are one of the most used inorganic solids in industry and they have a wide spectrum of applications. They have found extensive use in areas like catalysis, ion exchange, adsorption, optoelectronics, and medicine (Mei *et al.*, 2021). In catalysis, they are used to carry out a wide range of reactions including cracking, alkylation,

isomerization, dehydration, dewaxing, and hydrodeoxygenation due to their tunable porosity and molecular shape selectivity (Zhang *et al.*, 2018).

The tetrahedral unit of zeolite is made of tetravalent silicon (Si^{4+}) and trivalent aluminum (Al^{3+}) linked together by sharing four oxygen atoms giving rise to the unique architectural structure of zeolites (Afridi *et al.*, 2021). A pure SiO_4 unit is neutral, however, the addition of trivalent aluminum into the framework leaves a net negative charge and is countered by counterions that are most often Na^+, K^+, Ca^{2+}, or Mg^{2+} (Schroeder *et al.*, 2020). Moreover, these cations are exchangeable ions, and their presence makes zeolites good ion exchangers and widely applicable in industries like water purification and softening (Hammond *et al.*, 2018).

Zeolites have a general chemical formula of:

$$M_{x/n}[(AlO_2)_x(SiO_2)_y].zH_2O \quad \ldots\ldots\ldots\ldots\ldots\ldots\ldots\ldots\ldots\ldots\ldots\ldots\ldots\ldots\ldots \quad (1)$$

where M is a compensated cation with a valence n. x, y, and z are empirical variables of molar ratios of aluminum, silicon, and water of hydration respectively (Bacakova *et al.*, 2018).

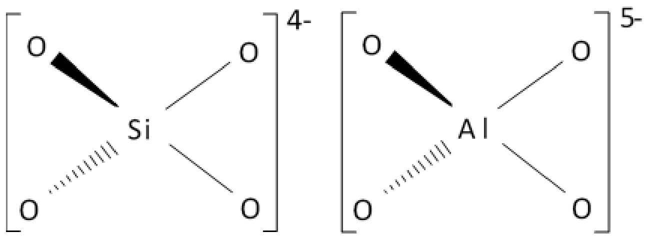

Figure 2.1: Primary unit block of zeolites (Moshoeshoe *et al.*, 2017)

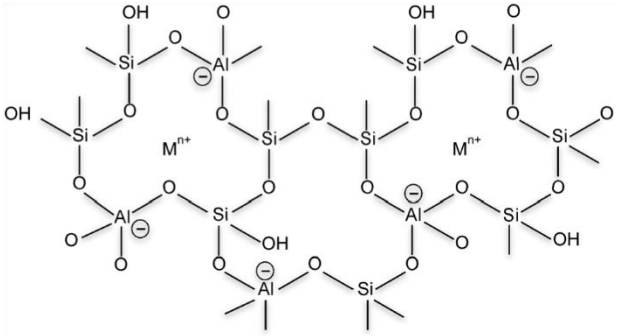

Figure 2.2: A typical view of a zeolite framework (Baile *et al.*, 2019)

Apart from cations from group one and group two, positively charged organic structure directing agents such as tetrapropylammonium cation (TPA^+) could serve as compensated cations during zeolite synthesis. Moreover, the cation can be post-synthetically exchanged with NH_4^+ and thermally decomposed into H^+ giving rise to Brønsted acid sites (see Figure 2.3). The H^+ covalently bonds to one of the oxygen atoms in the AlO_4^- unit Brønsted acid sites. Due to the polarizing action of the Al atom, the bond length between the Al atom and the oxygen atom bearing the proton is changed from ~1.7 to ~1.9 Å resulting in a relative decrease in the bond strength of O-H when compared with the isolated silanol groups in the structure (Schroeder *et al.*, 2020). The protonated form of zeolites (Si-O(H)-Al) exhibits a high level of Brønsted acidity with high acidity comparable to 100% H_2SO_4 (Hammond *et al.*, 2018).

The catalytic potential of zeolites can largely be ascribed to the existence of Lewis and Brønsted-Lowry acid sites in its framework. The Brønsted acid site arises when trivalent Al^{3+} metal is added to the zeolite structure. Moreover, an increase in Al content (Si/Al ratio) enhances the hydrothermal stability and hydrophobicity of the zeolite. Lewis acid site arises through the dealumination of the zeolite, dislodging Al^{3+} out of the framework. This forms an 'extra-framework' site found within the zeolite cavities (see Figure 2.4d). These sites are known as Lewis acid sites (Djoko *et al.*, 2016).

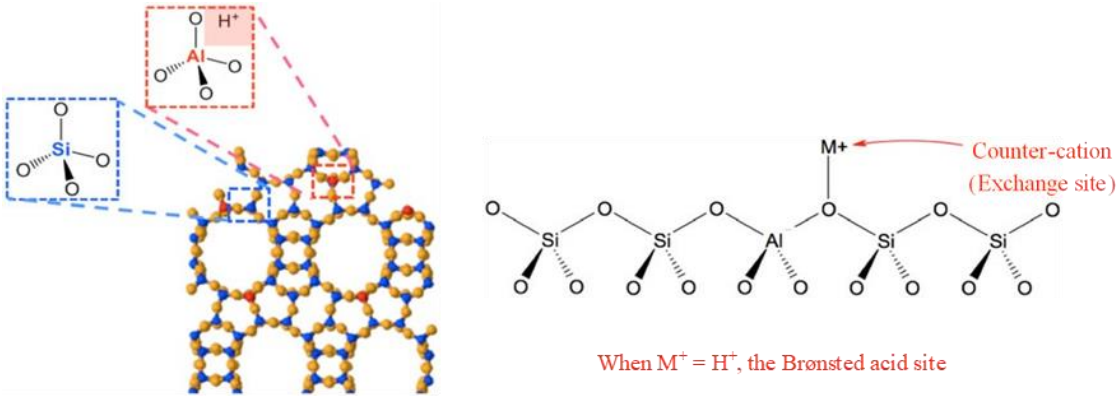

Figure 2.3: A typical view of Brønsted acid site and its formation (Hammond *et al.*, 2018).

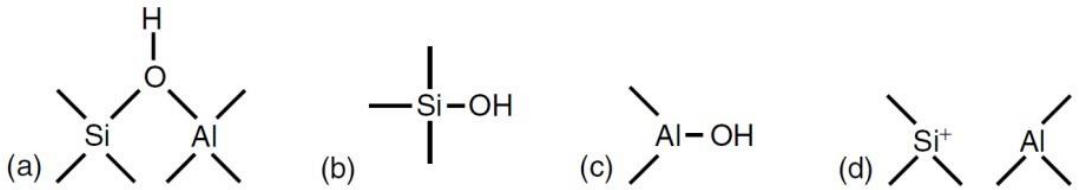

Figure 2.4: Types of hydroxyl groups and acid sites (Kianfar, 2020).

Shape-selective catalytic reactions are a function of the porosity nature of the zeolite structure, thus enabling selectivity on a molecular scale (Feliczak-Guzik, 2018). The mechanism of their shape-selective process is divided into three stages; i) the reactants stage, ii) the transition/intermediate state, and iii) the product selectivity stage (see Figure 2.5) (Kerstens *et al.*, 2020). Shape selectivity in catalysis was first described by Weisz and Frilette in 1960 (Weisz and Frilette, 1960). Most heterogeneous catalysis occurs in the inner surfaces of catalyst cavities, giving rise to the idea of intra-crystalline catalytic activity. In catalysis, the reactant molecule must first diffuse into the zeolite pores to the catalytic active sites where it undergoes a transformation and then diffuse out of the cavities. This enter/exit concept is controlled by the dimensions and configuration of the pores in the zeolite (Zhou *et al.*, 2018).

Three types of shape selectivity concepts have been identified based on whether pore size and shape allow or restrict the entry of the reacting molecule, the departure of the product molecule,

or the development of certain transition states. Reactant selectivity arises when only a portion of the reactant molecules are tiny in size enough to permeate through the catalyst pore mouths while blocking the bulky ones. Product selectivity arises when some of the molecules that are produced inside the catalyst cavities are too big to exist through the catalyst pores. They ultimately either become less substantial molecules to exit the pores or plug the pores, which deactivates the catalyst. When specific reactions cannot occur because the relevant transition state would take up more space than is present in the pore cavity, restricted transition-state selectivity is evident. Additional selectivity may be molecular traffic control. The catalysts with many types of intersecting pore systems exhibit this particular form of selectivity. Reactant molecules to enter the catalyst cavity may preferentially use one of the pore systems. While the other pore system, which typically has a larger pore allows the product molecules to exit (Csicsery, 1984; Jia *et al.*, 2019). Apart from selective catalysis, zeolites are applied as molecular in filtration and separation processes due to their unique porous channels. The channel dimensions are crucial to its application because a slight change in the dimension can make a difference between success and failure in its application (Xie, 2021).

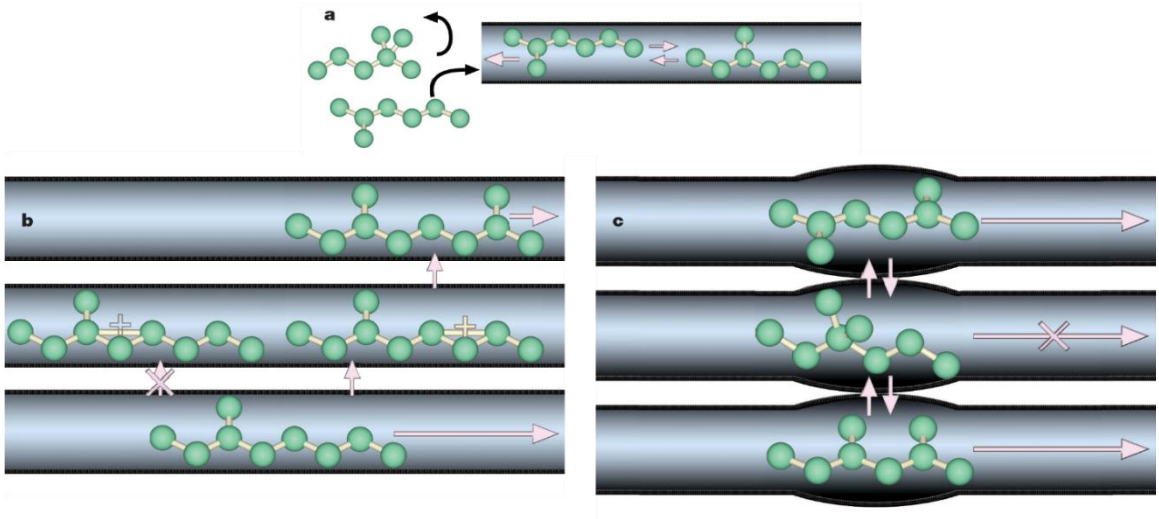

Figure 2.5: The figure shows the three mechanisms giving rise to shape selectivity in zeolites. (a) Reactant (b) Transition state (c) Product-shape, selectivity (Smit and Maesen, 2008).

Shape-selective catalysis helps increase the targeted product while reducing the by-products, thereby increasing the reaction efficiency. One advantage zeolites have over other solid acid catalysts is the possession of channels in addition to their acid-active sites. Different zeolite framework poses different ring membered and ring dimensions.

2.3 Classification and types of zeolites

More than 250 different topologies of zeolites have been identified by the International Zeolite Association (IZA) and are assigned a three-letter code (Kerstens *et al.*, 2020). They can be classified into three categories based on their different characteristics: classification based on pore sizes, classification based on silica/alumina ratio, and classification based on the source. Based on the source, they can be natural or synthetic zeolite.

The pore cavities of zeolites are built of tetrahedral atoms (T-atom, such as Si and Al) forming ring members typically 8-, 10-, and 12-membered rings (see Figure 2.6). They may be divided into small, medium, and large pore zeolites due to the dimensions of their pores, which are determined by the membered ring and pore diameter (Kerstens *et al.*, 2020). According to Petrov and Michalev (2012), zeolites can be classified based on their pore size (pore diameter) as follows:

a.) The first class is 8-membered rings or small-pore zeolites: They possess 0.30-0.45 nm pores in diameter.

b.) The second classification is 10-membered rings or intermediate-pore zeolites: They possess 0.45-0.60 nm pores in diameter.

c.) The third classification is 12-membered rings or large-pore zeolites: They possess 0.60 to 0.80 nm pores in diameter.

d.) A special class known as extra-large-pore or 14-membered rings zeolites: This class has extra-large free pore diameter ranges from 0.80 to 1.00 nm (Petrov and Michalev, 2012).

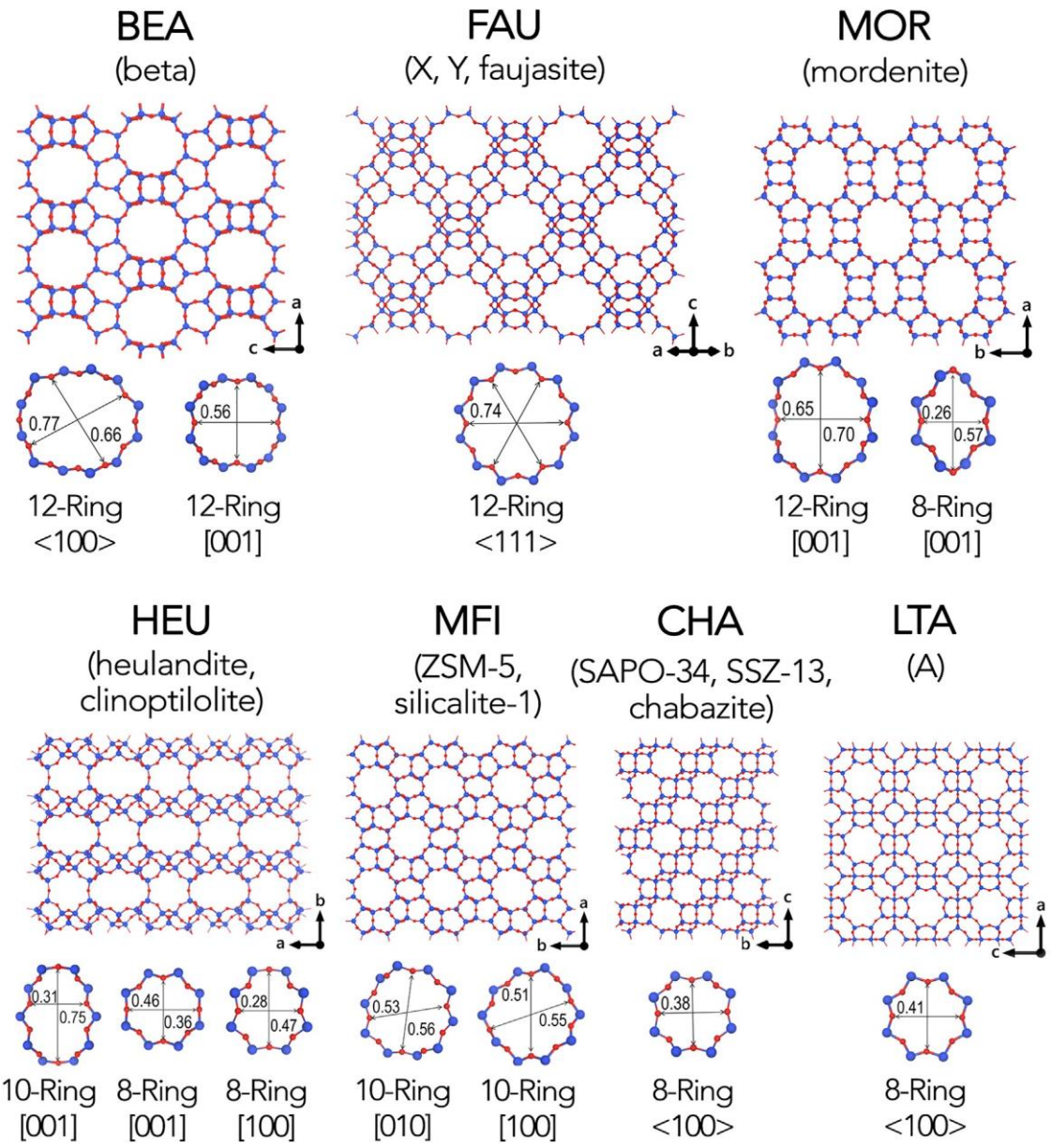

Figure 2.6: Some zeolite frameworks, ring members, and ring diameters (Li *et al*., 2017).

Zeolites are further classified based on their chemical makeup, specifically their Si/Al molar ratio and they are as follows (Ramesh *et al.*, 2010):

a.) Low Si/Al molar ratio (1.0 to 1.5) zeolites

b.) Intermediates Si/Al ratio (2 to 5) zeolites

c.) High Si/Al ratio (above 5 to ω) zeolites

Table 2.1: Some examples of zeolite-based Si/Al ratio classification (Jha and Singh, 2011; Yoldi *et al*., 2019).

Zeolite class	Si/Al	Some examples
Low silica	< 2	Zeolite A, Sodalite, Cancrinite, Phillipsite, Natrolite, etc.
Intermediate silica	2 to 5	Faujasite, Mordenite, Chabazite, etc.
High silica	5 to ω	ZSM-5, β-Zeolite, etc.

The Si/Al molar ratio influences some zeolite properties. Acid resistivity, hydrophobicity, and thermal stability increase with a rise in Si/Al ratio whereas acid site density, hydrophilicity, and structural cation decrease (Yoldi *et al.*, 2019).

2.3.1 Zeolite Linde Type A

Zeolite Linde Type A (Zeolite A or Zeolite LTA) is a low silica zeolite having a Si/Al ratio of 1, which is the minimum possible molar ratio a zeolite could possess according to Löwenstein's rule (Collins *et al.*, 2020). Löwenstein's rule of "aluminum avoidance", an established axiom of zeolite science, states that, "on forming the aluminosilicate zeolite framework, there is a disinclination for tetrahedral units of alumina to bond adjacent to one another, forbidding formation of Al-O-Al bonds, and thereby limiting the minimum Si/Al ratio of any zeolite to be

one" (Fletcher, Ling and Slater, 2017). Zeolite LTA was the first synthesized zeolite to be made commercially available. It has a general formula in sodium exchangeable form; $Na_{12}[(AlO_2)_{12}(SiO_2)_{12}] \cdot 27H_2O$. When the exchangeable cation is potassium, sodium, or calcium, it is commonly referred to as zeolite 3A, 4A, or 5A, respectively. Its unique cation exchangeable property makes it beneficial for ion exchange techniques like water softening. Zeolite LTA has a framework structure made up of two kinds of cages: α-cage and β-cage (sodalite cage). Eight sodalite cages are linked *via* double four-membered rings to form a huge α-supercage in the mid-way of eight-membered rings (see Figure 2.7) (Collins *et al.*, 2020).

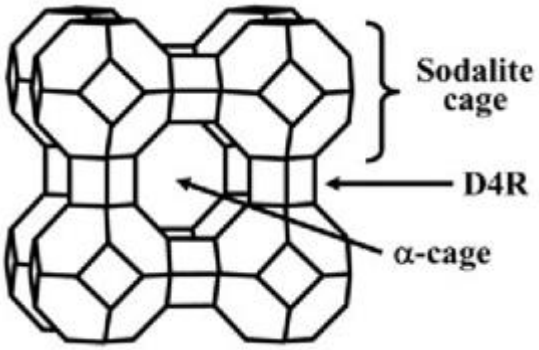

Figure 2.7: Structure framework of zeolite LTA (Wakihara *et al.*, 2005).

2.3.2 Faujasite zeolites

Faujasite zeolites are intermediate silica zeolites. Zeolite X and zeolite Y are the two types of this class of zeolite, and they can be differentiated based on their Si/Al ratio content. Zeolite X has Si/Al ratio between 1 and 1.5, whereas zeolite Y including ultra-stable zeolite Y (USY) has Si/Al ratio above 1.5 (Belaabed *et al*., 2017). They are molecular sieves with a three-dimensional pore opening of a diameter equal to 7.4 Å (Taufiqurrahmi *et al*., 2011). The basic structure framework unit for the faujasite family is sodalite cages, which combine to form super-cages large enough to contain spheres up to 1.2 nm in diameter (Garcia *et al.*, 2016).

2.3.3 Analcime zeolite

Analcime (ANA) zeolite has the smallest pore openings among all zeolites and has a compact structure (Novembre and Gimeno, 2021). The pores are arranged in four, six, and eight-fold rings (Azizi *et al*., 2013). It has a basic general formula of $NaAlSi_2O_6.H_2O$, and the sharing of the tetrahedral unit (TO_4) creates irregular channels, while certain voids in the crystal lattice are filled by exchangeable Na ions (Chen *et al.*, 2017). Analcime is normally synthesized using the hydrothermal method, combining silica and alumina sources in alkaline conditions and at a temperature ranging from 100 to 310 ^oC. Some studies show that it can be crystallized at lower temperatures if more Na_2O is used in the starting material (Novembre and Gimeno, 2021).

2.3.4 Zeolite Socony Mobil-Five (ZSM-5)

Zeolite Socony Mobil-Five (ZSM-5) is another aluminosilicate class of zeolites, and it belongs to the pentasil family. The first to synthesize this type of zeolite was Argauer and Landolt from Mobil Oil Corporation in the 1960s and it was patented by the corporation in 1972 (Knott *et al.*, 2018). ZSM-5 is a ten-membered ring zeolite with a pore diameter of range 5 Å (angstroms). It has two kinds of channels, which are the straight channels along [010] and zigzag channels along [100] (see Figure 2.8). The zigzag or sinusoidal channels have an elliptical aperture of 0.51 nm to 0.55 nm, whereas the straight channels have a circle-like opening of 0.53 nm to 0.56 nm (Pan *et al.*, 2010; Widayat and Annisa, 2017). The hydrated ZSM-5 has a chemical formula of $Na_xAl_xSi_{96-x}O_{192}\cdot 16H_2O$ ($0<x<27$). The Si/Al ratio ranges from 12 to ∞ and it has an orthorhombic unit cell (Zoubida and Hichem, 2018; Afridi *et al.*, 2021).

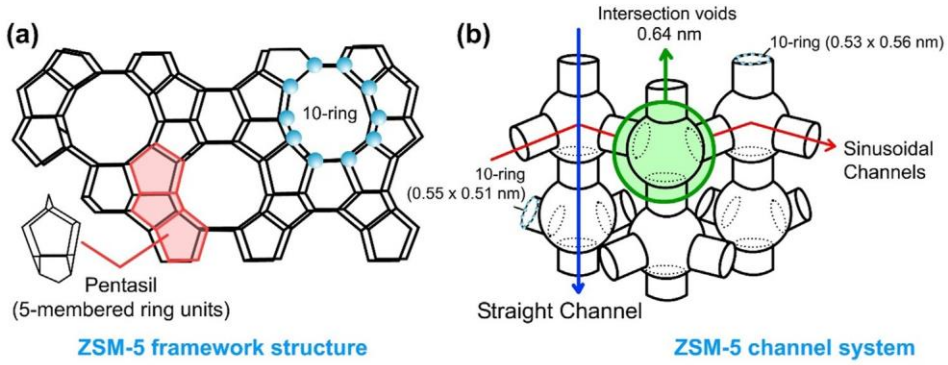

Figure 2.8: The structure framework (a) and channel system (b) of ZSM-5 (Sharbini *et al.*, 2022).

The composite building units (CBUs) its framework (MFI framework) are mor, cas, mfi, and mel (Santos *et al.*, 2020). Traditionally, it is synthesized at high temperature and high pressure in a Teflon-coated autoclave using tetrapropylammonium cation (TPA^{+}) as an organic structure directing agent (OSDA). Equation (2) below describes the chemical reaction;

$$SiO_2 + NaAlO_2 + NaOH + N(CH_2CH_2CH_3)_4Br + H_2O \longrightarrow ZSM-5 + [Analcime + \alpha - quartz] \ldots\ldots\ldots\ldots\ldots\ldots\ldots\ldots\ldots (2)$$

As equation (2) demonstrates, analcime zeolite and quartz are potential crystal phases that can compete with the formation of the ZSM-5 phase during its synthesis.

The ZSM-5 is classified among molecular sieves with an MFI-type structure that encourages widespread use. It is highly employed in industrial activities such as petrochemical cracking, separation of gases or fluids, production of fine chemicals, space research, as a solid acid catalyst, and among others (Mei *et al.*, 2021).

2.4 Methods of zeolite synthesis

In nature, zeolites are formed when Alkaline aqueous fluids interact with rocks at low pressure and low temperature, which may take tens to thousands of years (Szerement *et al.*, 2021). The

natural conditions and the chemical composition of the rock influence the type of zeolite formed. Zeolite synthesis started in the laboratory by mimicking the natural process and conditions.

Zeolite synthesis proceeds through gradual transformation processes. It is often synthesized by converting the amorphous phase of the starting precursors through a semi-stable form and finally into a stable zeolite (Inagaki *et al.*, 2013). Since the primary chemical constituents of zeolites are silica and alumina, zeolites are usually synthesized from chemical sources of silica and alumina. The process is usually carried out in an aqueous alkaline medium at a temperature from 30 to 200 ^{o}C and may take minutes or days to form (Yoldi *et al.*, 2019; Szerement *et al.*, 2021).

2.4.1 Approaches to zeolite production

In general, zeolite synthesis can be approached in two main ways namely, bottom-up and top-down. The top-down method aims to produce hierarchical zeolites by incorporating mesopores (pores with a diameter of 2-50 nm) and macropores (pores with a diameter greater than 50 nm) into the microporous pore network system of the zeolite (Kerstens *et al.*, 2020). This method is known as post-synthesis treatment and it is performed on zeolites that have already been synthesized in advanced or commercially available. These post-treatments may involve dealumination, desilication, direct metallation, and recrystallization processes (Dapsens *et al*., 2015). The modification is to tune acidity, increase intra-crystalline diffusion, decrease steric limitations, change product selectivity, and decrease coke formation of the zeolite during catalysis (Jia *et al.*, 2021). In another way, the bottom-up approach involves the use of hard-templating, soft-templating, and non-templating processes. Hydrothermal conditions are usually applied here under high autogenous pressures to crystallize alumino-silicate gel (Zhang

et al., 2018). The bottom-up technique of zeolite synthesis can further be divided into two broad methods: i) Solvothermal method of synthesis and ii) Solid-like synthesis or solvent-free or green synthesis method. Over the years, many methods have been employed in the production of zeolites (Li *et al.*, 2019). The hydrothermal method is the earliest and most well-developed among them, and it is widely and most used (He *et al.*, 2021).

2.4.2 Hydrothermal method of zeolite synthesis

The hydrothermal method of synthesis makes use of water as a solvent and high temperature during zeolite synthesis. This method involves mixing solutions of a silica source, alumina source, and mineralization agent like alkali hydroxide with or without an organic template, and then proceeding with crystallization (Derbe *et al*., 2021). A solvent must be present because it serves as a medium for the reactants to be transported (Maghfirah *et al.*, 2020). The hydrothermal method consists of two stages: i) the aging period where hydrated aluminosilicate gel is formed and ii) the crystallization period at elevated temperature and autogenous pressure. The crystallization period can further be subdivided into; i) condensation of poly-silicate and poly-aluminate anions, ii) nucleation of zeolite, iii) growth of nuclei, and iv) crystal growth of zeolites (see Figure 2.9) (Derbe *et al*., 2021). The stages of hydrothermal processes of zeolites are as follows (Cundy and Cox, 2005; Kornas *et al.*, 2021):

1. Aqueous solutions of Si and Al sources are homogeneously mixed with the mineralizing agent, often sodium hydroxide.

2. The optional addition of a templating agent.

3. The resultant mixture may be allowed to age for a period that may take a few minutes to several days to allow the formation of a gel.

4. The gel obtained is transferred into an autoclave vessel.

5. The autoclave vessel is then sealed, and the hydrothermal conditions are created by heating it., normally by placing it in a preheated oven.

6. Agitation may optionally be applied. However, it must be noted that a variation in these conditions may cause competition in the formation of crystalline phases.

7. The heat energy generated at the hydrothermal condition is used up in the formation of Si-O-Si and Si-O-Al chemical bonds. No significant enthalpy change would be expected since the bond type present in the product and that of the precursor oxide are quite similar. The total free energy change is typically small, making the process most often kinetically controlled.

8. Zeolite crystalline gradually grows during the synthesis timeframes that range from a few h to several days, influenced by the process parameters and the targeted zeolite phase.

9. The autoclave is cooled and opened after the crystallization period.

10. The resulting product is collected by filtration, followed by washing to a pH less than 8 and drying.

11. In Synthesis where OSDA is used (step 2), they are removed by calcination at elevated temperature for the organic molecule to decompose.

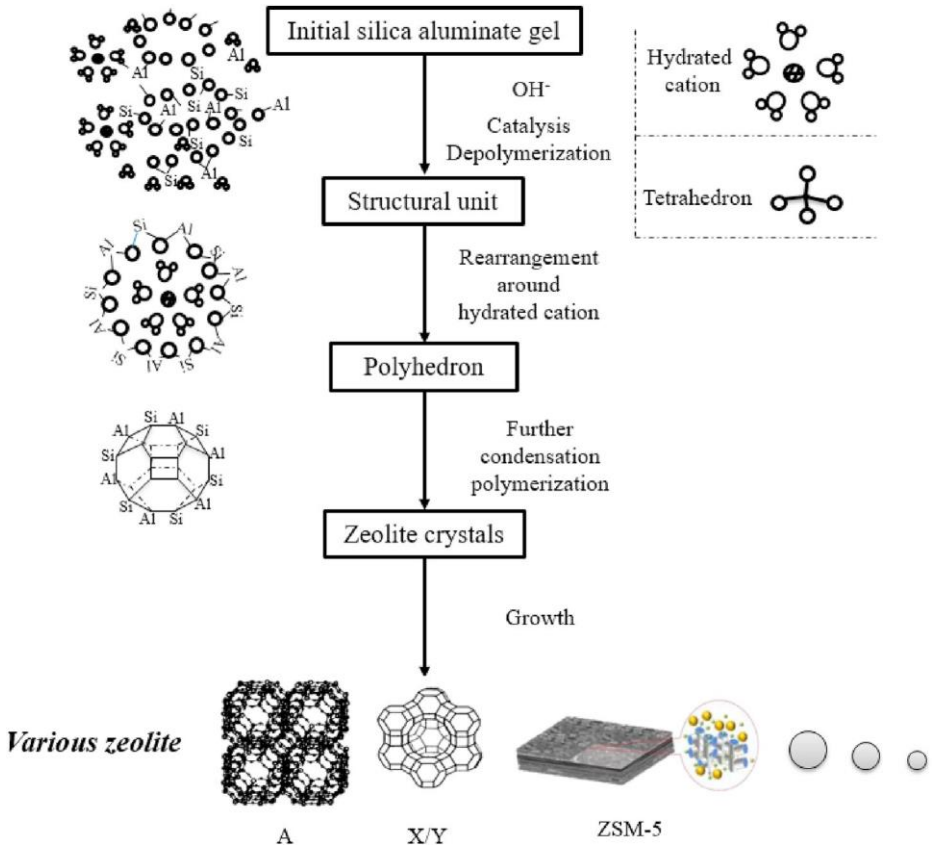

Figure 2.9: Stages in zeolite synthesis and crystal formation (He *et al.*, 2021).

2.4.3 Solid state or solvent-free method of zeolite synthesis

Solvents are commonly used in zeolite production to enable the effective transport of the reactants. However, they take up a lot of space in the autoclave reactors, thus having significant effects on the quantity of product obtained. This approach often results in a low product yield due to the use of a significant volume of solvent, which occupies a large space in the reaction vessel. Concerns about safety and the environment are also brought on by excessive autogenous pressure and waste solvent generated. Therefore, notable attempts have been made to reduce or eliminate solvents in zeolite synthesis by using solvent-free approaches (Wu *et al.*, 2014). Unlike the hydrothermal process where solvent wastes are discharged after the production process, the solvent-free method does not involve the use of solvent, and no solvent waste is

generated. Solvent-free method of synthesis is a technique used to produce zeolite in the absence of added solvent (Nada *et al*., 2019). Is solvent necessary for zeolite production?

Wu *et al.,* (2018) proposed the following mechanisms for the role of water acting as a catalyst in zeolite production.

$$Si(OSi)_4 + nH_2O \longrightarrow Si(OSi)_{4-4}(OH)_m \qquad (1 \leq m \leq 4) \ldots\ldots\ldots\ldots\ldots\ldots (3a)$$

$$Si(OSi)_{4-m}(OH)_m \longrightarrow Si(OSi)_4 + nH_2O \qquad (1 \leq m \leq 4) \ldots\ldots\ldots\ldots\ldots\ldots (3b)$$

Equation (3a) depicts the period of depolymerization reaction as a result of the hydration of silica species and equation (3b) depicts the condensation of hydrated species.

When silica species are being hydrated (3a), water is used up, and it is then regenerated when the silica species are being condensed (3b). It stands to reason that a huge volume of water is not required in zeolite production if water acts only as a catalyst during the crystallization process (Wu *et al.*, 2018).

Xu *et al*. discovered a unique method for zeolite creation in 1990 known as vapor-phase transport. It was used successfully to synthesize ZSM-5 zeolite by using water vapor without the reaction mixture coming into contact with the mixed solution of the solvent directly. This proved that a large amount of water is not necessary for the crystallization process (Xu *et al.*, 1990). Is at least a trace of water a requirement for the synthesis of zeolites?

In 1994, Althoff and co-workers demonstrated that water is not necessary to be present at the crystallization stage by substituting ammonium fluoride (NH_4F) for water vapor. Pure ZSM-5 zeolite was obtained without amorphous impurities (Althoff *et al.,* 1994). Wu *et al.* (2015) also reported the synthesis of MFI, BEA, EUO, and TON zeolites *via* the solvent-free method using NH_4F and OSDA including grinding of the anhydrous reactants and crystallizing at 140 - 240

^{o}C. They point out that, the crystallization of the zeolites was driven by the presence of F^- from the NH_4F (Wu *et al.*, 2015). The following reaction was suggested.

$$SiO_2 + 6NH_4F \longrightarrow SiF_6^{2-} + 2NH_4^+ + 2H_2O + 4NH_3 \ldots\ldots\ldots\ldots\ldots\ldots\ldots\ldots (4a)$$

$$SiF_6^{2-} + 2H_2O + 4NH_3 \longrightarrow SiO_2 + 4NH_4^+ + 6F^- \ldots\ldots\ldots\ldots\ldots\ldots\ldots\ldots (4b)$$

where reaction (4a) illustrates the depolymerization of silica species by ammonium fluoride, and reaction (4b) illustrates the condensation of the depolymerized species.

Combining reactions (4a) and (4b) suggests that F^- species could act as a catalyst in the reaction process. From reaction equation (4a), it could be seen that water has been generated as a byproduct in the depolymerization process with the consumption of F^- species. This water is enough for the formation of zeolite, and the addition of a trace of water is not required for the reaction to proceed (Wu *et al.*, 2018). Ren *et al*. (2012) described a process of mechanically grinding and heating precursors to produce ZSM-5 zeolite without the need for any extra solvent. The solvent-free approach is a simple, effective, high-yield, and inexpensive way to synthesize zeolites. It will have a significant impact on the industrial production of zeolites in the future. Moreover, further research into the mechanism of zeolite synthesis by the solvent-free method is still required (Mei *et al.*, 2021).

2.4.4 Important factors that influence zeolite synthesis

The synthesis of zeolites is an intricate process comprising several reactions and equilibria that are controlled by a combination of thermodynamics and kinetic factors. Many kinds of research are geared toward the preparation of tailor-made zeolites and the discovery of new zeolite structures. Many synthetic factors influence the outcome of synthesized products which include the nature of the raw materials, solvent content, molar ratios of precursors, synthesis

temperature and time, nature of structure directing agent, and others. These important parameters have been investigated and are known to significantly govern the zeolite type obtained and its morphology. Although pressure is a significant thermodynamic factor, it is not taken into account as an independent variable. This is because, the zeolite crystallization process is normally done under autogenous pressure, which depends on the synthesis temperature, chemical constituents, and reactor fill level (Tan *et al.*, 2020).

2.4.4.1 Sources of silica and alumina

Silica and alumina are the primary and most important reactants in zeolite synthesis. A variety of silica sources are employed in the synthesis of zeolite, which includes silicic acid, colloidal silica forms, fused silica, tetraethoxysilane, silicate solutions such as sodium metasilicate, etc. The choice of silica source influences how quickly silica is dissolved into the solution, which controls how homogeneous the initial growth of the solution is (Oleksiak and Rimer, 2014). The aluminum source includes aluminum hydroxide, sodium aluminate, and aluminum salts (Nazir *et al.*, 2020).

Synthetic inorganic sources of silica and alumina are expensive and with a negative environmental impact. This has called for the search for cost-effective, environmentally benign, and sustainable starting materials leading to the utilization of clay minerals such as kaolinite for the production of zeolites (Abdullahi *et al.*, 2017). Other affordable raw materials are rice husk ash, coal fly ash, high silicon flay ash, waste sandstone cake, waste porcelain, oil shale ash, etc. Kaolin is the most used clay in the synthesis of zeolite types among other materials mentioned (Hartati *et al.*, 2020). Clays are available cheap natural resources that contain silica and alumina in large quantities, which can serve as silica and alumina sources for zeolite production. There are two stages in transforming kaolinite mineral into zeolite phase:

(i) metakaolinization and (ii) zeolitization (Abdullahi *et al.*, 2017). Metakaolinization is the activation of kaolin clay into metakaolin typically by calcination at elevated temperatures leading to the decomposition of the clay structure. Al and Si species in the form of $2Al(OH)_4^-$ and $[SiO(OH)_3]^-$ respectively, are released into the solution when the metakaolin is treated with an alkaline solution. These species further recombine in the polycondensation and polymerization process to form the zeolite framework (Hartati *et al.*, 2020).

2.4.4.2 Solvent

Although solvent is not a requirement, a large volume of solvent is normally used for manufacturing zeolite (Wu *et al.*, 2015). Notably, zeolites are often synthesized with the involvement of solvents like water, alcohol, and ionic liquids under hydrothermal, solvothermal, or isothermal conditions (Jin *et al.*, 2013).

The ionothermal synthesis approach as the name suggests, involves the utilization of ionic liquids as solvents and elevated temperature. Most often the solvent serves as a structure-directing agent as well. This contradicts conventional hydrothermal/solvothermal synthesis where solvents are mostly molecular. Ionic liquid (IL) is a type of molten salt made up of organic cations and complementary anions. The ionothermal method was first developed by Morris and colleagues in 2004 to synthesize zeolite materials and has subsequently attracted a lot of interest. Ionic liquids have great solvating qualities as solvents due to their moderate polarity. Because of their low melting points, a homogenous mixture of chemical reagents can be prepared using them at ambient temperatures. They offer a robust medium for synthesis at high temperatures (<250 °C) because they are thermally stable (<300 °C). Because ILs in particular have low vapor pressure, the synthesis may be carried out at room conditions, which removes the dangers of the high-pressure reactions. Therefore, rather than using a more typical

Teflon-lined stainless-steel autoclave, the ionothermal reactions can take place in open reaction vessels. In the ionothermal approach of zeolite materials production, 1-methyl-3-ethylimidazolium bromide ([EMim][Br]) is the most often utilized ionic liquid (Cooper *et al.*, 2004; Liu and Yu, 2016). There are very few publications on the production of high silica zeolites due to the low dissolution ability of silica in ILs and deep eutectic solvents (DES). Therefore, a small quantity of water is often added in most cases (Lin and Huang, 2016a). Ionothermal method has been successfully used in the synthesis of ZSM-5, zeolite Y, ZSM-22, SAPO-34, sodalite, ZSM-39, TON, MTT, and ITW zeolite types (Cai *et al.*, 2010; Wheatley *et al.*, 2010; Wen *et al.*, 2014; Yuan *et al.*, 2015; Lin and Huang, 2016b; Wu *et al.*, 2019; Han *et al.*, 2021). The ionothermal method of zeolite synthesis looks promising to conventional hydrothermal synthesis, however, the high-cost ionic liquids and long reaction time hinder their applications in industrial-scale productions (Luo *et al.*, 2017).

Water is the most widely used solvent in the production of many different types of zeolites (Lin and Huang, 2016a). Cheng et al. studied the effects of the amount of water utilized for ZSM-5 zeolite production without the use of a template. The results show that the product obtained does not contain the ZSM-5 phase. It was rather amorphous when the amount of water was below 200 mol. However, the %crystallinity of ZSM-5 zeolite was 20%, 100%, 83%, 71%, 67%, and 66% when the water quantity was 2000, 2500, 3000, 4000, 5000, and 6000 moles respectively (Cheng *et al.*, 2008). The amount of water present determines the concentrations of the reactants in the reaction mixture. Generally, low water content results in higher concentration leading to faster supersaturation, and high crystallization. It suggests that the proximity of the nutrients in the reaction mixture has facilitated nucleation and, consequently, crystallization (Cheng *et al.*, 2008). Water has also been documented to play the role of a co-templating agent during the hydrothermal synthesis of zeolites (Asgar and Sebakhy, 2022).

2.4.4.3 Mineralization agents

The physicochemical properties of a zeolite after synthesis depend on the chemical constituents of the reaction mixture during synthesis and the crystallization conditions. Over the years, our understanding of the intricate zeolite formation has advanced significantly. For instance, the synthesis can be carried out in both basic medium (OH^-) and fluoride medium (F^-) and they serve as mineralizing agents (Qin *et al.*, 2014). Mineralizing agents are chemical species that regulate the dissolution and mobility of the sources of the structure atoms in the synthesis gel through processes of depolymerization and poly-condensation. The hydroxyl anion (OH^-), which enables zeolite crystallization in alkaline conditions (pH > 10), is the most often utilized mineralizing agent (Moliner *et al.*, 2013). Aluminosilicate gel dissolves more easily when there is OH- present. It also facilitates the condensation of Si-OH species together or with a combination of Al-OH species (Li *et al.*, 2019). However, there are some circumstances in which carrying out the synthesis at a neutral pH value might be more suitable. This is especially true when the organic structure directing agents cannot be synthesized at high pH levels at the appropriate temperature (Moliner *et al.*, 2013). However, there are significant variations between the zeolite formation mechanisms of the two mineralization catalysts resulting in different zeolite morphology. Zeolites can crystallize in a little acidic to slightly basic media (pH<10), as opposed to typical zeolite production, which is carried out at high pH. Zeolite crystallized near a neutral pH minimizes the number of non-bridging ≡SiO defects, consequently, fluoride medium-produced crystals have fewer structural defects (Qin *et al.*, 2014). In addition, F^- involvement can go beyond the silica mineralizing action and could function in directing the zeolite framework during the synthesis (Li *et al.*, 2019). However, a fluoride medium for zeolite synthesis generally leads to a larger crystalline formation (Qin *et al.*, 2014).

Louis and Kiwi-Minsker (2004) investigated the synthesis of ZSM-5 in a fluoride medium at a neutral pH and with varied Si/F ratios ranging from 0.3 to 1.6. They obtained the ZSM-5 phase with crystalline sizes spanning from 10 to 75 μm, with specific surface areas of 60 to 350 m^2/g. They reported that the level of crystallinity, the surface area, and the crystal size are greater than those of the zeolites produced using an alkaline medium. It appears that the development of both large and well-crystallized crystals can be achieved by the substitution of F^- ions for OH^- ions as the mineralizer (Louis *et al.*, 2001; Louis and Kiwi-Minsker, 2004).

2.4.4.4 Structure directing agents or Templates

The presence of structure-directing agents (SDAs) (or templates) is typically necessary for the majority of zeolite syntheses. SDAs can be classified as inorganic cations like sodium, and the second category is organic structure-directing agents (OSDAs) which are organic cations. They direct nutrients in the reaction solution and control the crystallization process of zeolites. Zeolite seeds are used in seed-assisted synthesis pathways and they can be logically regarded as a third form of SDA (Ji *et al.*, 2016). OSDAs have dimensions and geometries that mimic the channels of zeolite type. As a result, they promote the creation of specific pore dimensions within the zeolite framework. They change the kinetics of crystallization and occasionally control the incorporation of aluminum at certain tetrahedral locations within the crystal lattice. With sodium ions acting as inorganic structure-directing agents, ZSM-5 may be produced without the need for an OSDA, but the resulting product will contain high Al content (Si/Al <20). High Si-content zeolite, which is frequently preferred for catalytic applications, must be attained by using an OSDA in the crystal growth. Tetrapropylammonium cations are the most typically used OSDA for ZSM-5 zeolite production (Chawla *et al.*, 2018).

Several OSDAs have been reported for the synthesis of the ZSM-5 phase. They include tetrapropylammonium hydroxide (TPAOH), tetrapropylammonium bromide (TPABr), and tetrabutylammonium hydroxide (TBAOH) (Karimi *et al.*, 2012). Sang *et al*. (2014) studied the influence of n-butylamine (BTA), ethylamine (ETA), isopropylamine (IPA), ethylenediamine (EDA), ethanol (ETL), ethanol-ammonium (ETL-AM), and no template (NT) as templates on ZSM-5 synthesis. They reported that ZSM-5 could be made comparatively more easily using organic templates than it could without them or with inorganic templates. The SEM results revealed different shapes and particle sizes of the produced ZSM-5 when they varied the templates. In the sample using ethanol as a template, the Si/Al ratio and BET-specific surface area were the lowest. The sample produced without any templating agent contained fewer strong acid sites than other samples (Sang *et al.*, 2004). Normally, the template-free synthesis approach requires a long synthesis time to obtain ZSM-5 with good crystallinity, phase purity, and yield.

Moreover, the kind of OSDA employed in the synthesis strongly impacts the size and morphology of the zeolite crystal produced. For example, MFI-type zeolite synthesized using TPA^+ as OSDA possesses coffin-shaped crystals and is 5 μm in size. This differs from the MFI-type produced using quaternary ammonium cations, which produce crystals with a variety of morphologies including octagonal, leaf-shaped, and plate-like crystals. Furthermore, the impact of the amount of OSDA on zeolite crystal morphology and size has also been investigated. The result of the study for TPA-MFI has shown that lower amounts of OSDA resulted in rod-like shape crystals with large sizes. However, in contrast, nano-range zeolite crystals were produced when a large amount of OSDA was applied (Asgar-Pour and Sebakhy, 2022). Notably, OSDA plays a role in the crystallite and particle size of the product obtained. During the aging process, the ions of OSDA approach silica particles intimately, interact with

them, and prevent tiny silica species from aggregating consequently causing the growth of smaller crystallites (Alipour *et al.*, 2014).

Although OSDAs have presented us with many advantages, they also present some drawbacks. The most widely used OSDAs are quaternary ammonium-based or amines, and they are expensive. This in return raises the cost of zeolite production. To create open pores that are unique to zeolites, the OSDAs are often eliminated from the pores by calcination at high temperatures. The combustion process consistently goes together with the emission of dangerous gases that are mostly NOx and CO_2. Furthermore, substantial energy is consumed, and there is some degree of zeolite structural degradation during the calcination. This strategy is typically harmful and not eco-friendly. Therefore, innovative environmentally friendly processes such as employing less toxic OSDAs, recycling the OSDAs, and OSDA-free synthesis are crucial for the manufacture of zeolites in large quantities (Meng and Xiao, 2014). Cheng and co-workers successfully synthesized nano-sized ZSM-5 at 180 °C for 24 h without organic SDA. They reported that the Na^+ ion plays the role of both structure-directing and charge-balancing agent (Cheng *et al.*, 2008).

2.4.4.5 Molar ratio

The various reactants' molar ratios (amount to each other) present in a reaction mixture is a key factor that influences the final zeolite phase and its morphology after synthesis. These reactant components include Al_2O_3, SiO_2, OH^-, H_2O, SDA, and Na_2O, and their ratios influence the morphology and degree of crystallinity of the product obtained. In the synthesis of ZSM-5, SDA/Si and OH/Si ratios are the two key parameters that determine the crystallinity and the crystallite size of the final product obtained. The two ratios determine the alkalinity of the reaction medium since most OSDA is acidic and OH from metal hydroxide impacts alkalinity.

Higher alkalinity increases the crystallinity of the product and smaller crystal due to higher saturation of the solution, which enhances nucleation. The major function of Na_2O in the reaction is to adjust the pH of the medium, especially when SDA is involved in the synthesis. Although high alkalinity is essential when targeting nano-sized SZM-5, the rate of crystallization decreases subsequently when the optimum pH is exceeded. Moreover, an inappropriate Na_2O/Si ratio may result in the formation of an undesired zeolite phase or the formation of amorphous products. Surface characteristics like surface charge and acidity can vary depending on the SiO_2/Al_2O_3 ratio. Additionally, a decline in the SiO_2/Al_2O_3 ratio promotes the formation of MOR over the MFI phase (Alipour *et al.,* 2014). Another crucial variable that controls the resultant crystal size is the H_2O/SiO_2 ratio of the starting ZSM-5 synthesis solution mixture. Increasing this ratio leads to a decrease in the concentration of all other reactant species present in the solution. Subsequently resulting in the production of bigger crystal sizes due to low supersaturation. According to research done by Hu and colleagues (2009) on the effect of the H_2O/SiO_2 ratio on ZSM-5 synthesis, the results indicated that the particle size raised from 170 to 300 nm when the ratio was more than 13.87. This outcome was explained to be due to the decrease in alkalinity (lowers the pH), and dilution of SDA, SiO_2, and Al_2O_3 species concentrations. Even at constant pH levels, a high H_2O/SiO_2 ratio promotes the growth of bigger crystallites by lowering the supersaturation level of the original solution, and hence the effectiveness of crystal nucleation decreases. Notably, a certain level of water is required in the production of ZSM-5, because when the H_2O/SiO_2 ratio was too low, the MOR zeolite phase was formed instead of the MFI phase (Hu *et al.,* 2009; Alipour *et al.,* 2014).

2.4.4.6 Aging conditions

Aging in zeolite synthesis refers to the period where the solutions of reactants are mixed at a temperature lower than the crystallization temperature, to allow crystal nucleation (Oleksiak and Rimer, 2014). Nucleation is a phenomenon in which the "nucleus," usually a tiny seed crystal or dust particle, initiates crystallization in a solution's amorphous phase. The crystallization process begins with nucleation and it happens during the aging period. At greater supersaturation levels, a large energy barrier can be overcome. There will be more nuclei generated if supersaturation is very high. The rate of nucleation is inversely proportional to the degree of temperature and is directly linked to concentration. The zeolite formation mechanism consists of complex nucleation and crystal growth stages (Afridi *et al.*, 2021). It is well known that prolonged aging could enhance the number of nuclei formation and speed up the crystallization process. Extended aging, however, is not advantageous for industrial applications since it is time-consuming. Although reactions involved in aging are uncertain, it is thought that chemical rearrangements giving rise to crystal nuclei occurred throughout this period (Selvin *et al.*, 2011). Selvin *et al.*, (2011) studied the effects of aging temperature on nanocrystalline ZSM-5 formed. The findings demonstrated that the particle sizes remained nearly constant at 48 nm during the temperature range of 25 ^{o}C to 75 ^{o}C. However, an additional rise to 100 ^{o}C in the aging temperature increases the particle size to 85 nm.

2.4.4.7 Crystallization temperature and time

It has been proven that crystallization temperature and time have a substantial impact on the size of the resulting crystallites or particles, their degree of crystallinity, their phase composition, and their morphology. They control the rate and extent of nucleation and crystal growth (Javdani *et al.*, 2019). The temperature at which crystallization occurs (crystallization temperature) affects the time it takes the product to form (crystallization time). At higher

temperatures, the time has less of an impact, however at lower temperatures; time can play a substantial role in regulating the size of the particles in the finished product. When the temperature is high enough, the crystal growth rate speeds up and this causes the crystal growth equilibrium to be reached so quickly that the influence of time variation is ignored. As the synthesis temperature rises, the nutrients in the initial gel dissolve more quickly, causing crystal nuclei to develop more quickly. Conversely, a lower synthesis temperature promotes nuclei formation as opposed to growth (Alipour *et al.*, 2014).

An investigation into the impact of crystallization temperature and crystallization period on the size of the silicalite-1 seed revealed a linear relationship between temperature and particle size. Dai *et al.* mathematically studied the silicalite-1 seed's crystallization analytically and proposed an equation that connects the average seed size (d, nm) and crystallization temperature (T, ^{o}C) as (Dai *et al.*, 2017);

$$d = 1.7T - 59 \dots\dots\dots\dots\dots\dots\dots\dots\dots\dots\dots\dots\dots\dots\dots\dots\dots\dots\dots (5)$$

The rate of crystal formation is a function of crystallization temperature and activation energy as demonstrated by the Arrhenius equation (6) below.

$$\ln k_g = \ln A - \frac{E_a(g)}{RT} \dots\dots\dots\dots\dots\dots\dots\dots\dots\dots\dots\dots\dots\dots (6)$$

where k_g is the rate constant of linear crystal growth at the reaction temperature T. R is the gas constant with the value of 8.3143 J K^{-1} mol^{-1}, and T is the absolute temperature. A is the appropriate constant and Eα(g) is the activation energy of the crystal growth process. As a result, raising the crystallization temperature reduces activation energy, the rate of crystal formation to be accelerated, and bigger crystals to be produced (Javdani *et al.*, 2019). Song *et al.* (2004) investigated the impacts of time on the crystallite size of silicate-1 (or ZSM-5)

synthesized. They noticed that lengthening the crystallization period produces bigger crystals. Smaller crystals were obtained since crystals formed quickly and had little time to grow.

Although crystallization pressure is a significant thermodynamic factor, it is not taken into account as an independent parameter. This is because hydrothermal synthesis is typically carry-out under autogenous pressure. Synthesis pressure is a function of synthesis temperature and it is also dependent on the chemical makeup of the reaction mixture, and the fill level of the reactor. At a fixed volume of the autoclave reactor, an increase in synthesis temperature results in a corresponding increase in pressure. While, more fundamentally, higher temperatures and pressures increase the kinetic energy of the electrons or particles. Because of this, high pressure can occasionally cause phase transitions or modifications to reaction pathways that are not possible at ambient pressure. Additionally, high pressure could make certain species more soluble in water, raise the supersaturation level, and enhance the nucleation in response to stimuli. Zeolite crystallization could greatly be controlled by such distinctive characteristics of the water-mediated environment at high pressure (Tan *et al.*, 2020).

2.5 Applications of zeolites

Crystalline aluminosilicate zeolites are extensively employed in the separation and refinery sectors. They are useful there as catalysts, adsorbents, and ion exchangers because of their unique architecture. Zeolites have strong catalytic activity and selectivity due to their huge internal surface area, numerous exposed active sites, uniformly sized pores, thermally stable, and superior chemical inertness (Bayati *et al*., 2008; Taufiqurrahmi *et al*., 2011). They are employed in several petrochemical and chemical processes as industrial catalysts for catalytic cracking, hydrocracking, isomerization, disproportionation, aromatics alkylation, methanol to gasoline conversions, and dewaxing processes (Zhang *et al.*, 2018; Afridi *et al.*, 2021). Zeolites

are also utilized in the mineral and detergent industry, as well as for treating radioactive liquid wastes. In terms of environmental remediation, zeolites are crucial in the thorough co-treatment of waste gas and sewage (He *et al.*, 2021).

Zeolites are biocompatible, potentially non-toxic, and they are generally edible. These qualities explain their varied applicability in several medical fields. It must be indicated that using natural zeolites like Clinoptilolite as a food additive not only gives people access to vital minerals but also protects against being poisoned by noxious compounds in the environment - air, water, and food. Additionally, zeolites are widely used in biomedical areas due to their exceptional physical and chemical characteristics, such as their unique porosity, ion exchange-ability, anti-oxidative potential, biocompatibility, and lasting biological stability. These qualities increase their applicability in drug and gene delivery systems, wound healing, as scaffolds in tissue engineering, anti-microbial agents, implant coating, absorbers of harmful ions, harmful gas absorbers, hemodialysis, and teeth root filling materials (Serati-Nouri *et al.*, 2020; Servatan *et al.*, 2020).

2.6 Formation of clay and clay minerals

Clay is a form of fine-grained natural soil material, natural rock, or earthy substance that is free-bound, has a diameter smaller than 0.005 mm, and contains clay minerals. They may have a plastic character, have an amount of water in them, and can become hardened when dried or fired (Kausar *et al.*, 2018).

The genesis of clay largely depends on the original parent material and environmental factors. The weathering of rocks and other soil materials is the fundamental process through which clay minerals originate. The weathering procedure brings about a physical breakdown and a chemical transformation of pre-existing earthy minerals into clay minerals. This process is

enhanced when the rocks interact with water and are in contact with air or steam. The resultant clay minerals undergo transportation and metamorphosis through mechanisms known as diagenesis to more stable forms. During the diagenesis process, silicate materials including quartz, feldspar, volcanic glasses, primary clay minerals, and amorphous metal oxides are converted into more stable clay minerals. Dissolution and recrystallization processes are dominant during this transformation. In addition, the makeup of the original rock, variables influencing rock decomposition, and soil formation play crucial roles. Other environmental factors including the amount of water in contact with the rock, temperature, topography, the presence of organisms and organic material, and the length of time all have a significant impact on the type of clay mineral formed. The characteristics of weathered rock will therefore be greatly influenced by these elements under various climatic circumstances. Common silicate minerals including feldspar, mica, amphibole, pyrite, and olivine are earthy materials that frequently weathered into clay minerals like kaolin, smectite, illite, serpentine, and vermiculite depending on environmental factors. These clay minerals respond to environmental changes, erosion, transportation, and deposition. These processes lead to ion exchange, the rebuilding of material that has decomposed, and the formation of a particular type of clay mineral from another or simpler mineral (Zhou and Keeling, 2013; Aboudi-Mana *et al*., 2017). Equation 7 illustrates the formation of kaolinite from feldspar.

$$2KAlSi_3O_8 + 2CO_2 + 11H_2O \longrightarrow Al_2Si_2O_5(OH)_4 + 2K^+ + 4H_4SiO_4 + 2HCO_4^- \ldots(7)$$

$$K - feldspar + carbon\ dioxide + water \longrightarrow Kaolin + potassium, silica\ and\ carbonate\ ions$$

Table 2.2: Some earthy materials and their possible corresponding products after weathering (Wilson, 2004).

Primary Silicates	Weathering Product (clay mineral)
Potassium feldspar	Kaolin (and illite normally less)
Plagioclase feldspar	Kaolin (particularly kaolinite and halloysite)
Olivine	Smectite
Amphibole and Pyroxene	Smectite, chlorite, vermiculite, and talc
Biotite	Vermiculite, kaolin

Clays can be divided into two categories: (1) residual clay, which is found in the location of origin and is created by surface weathering of parent materials like rocks, and (2) transported clay, which is also referred to as sedimentary clay, are the ones removed from the location of origin by erosion means and got deposited in a new distant geographical location (Do-Nascimento, 2021).

2.6.1 Clay minerals

Clay minerals are seen as a gift for humans, they are always researching, and discovering new uses since clay minerals are inexpensive, environmentally benign, readily available, and non-toxic. Class minerals can be classified based on their chemical constituents and structural orientation as it is illustrated in Figure 2.10.

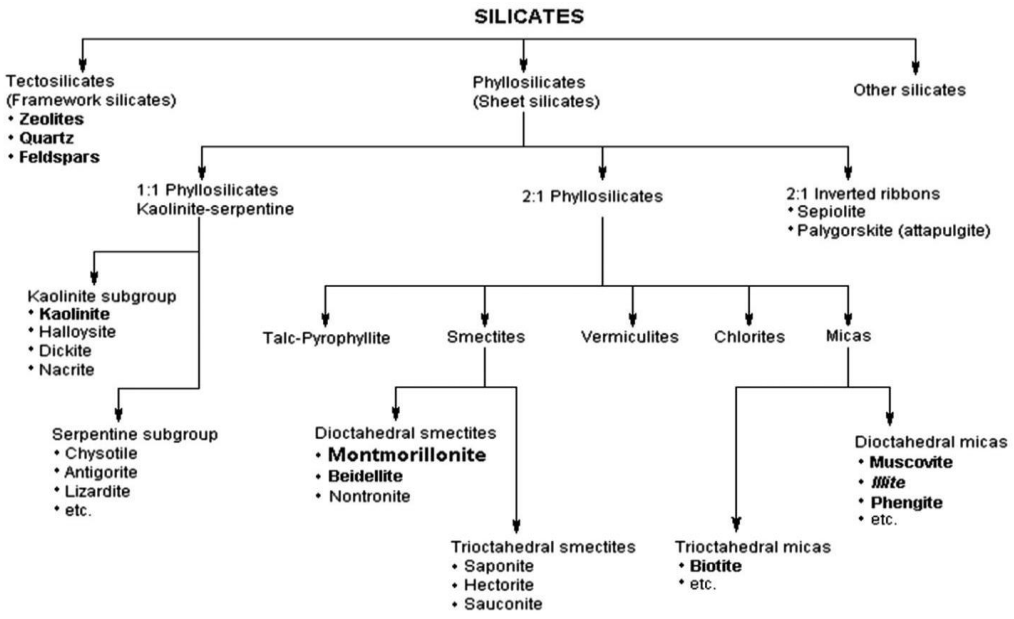

Figure 2.10: Classification of clay minerals according to Bailey in 1980 (Aboudi *et al.*, 2017).

The main chemical constituent of clay minerals is tetrahedral silicate sheet and octahedral aluminum sheet. A layer of a clay mineral may be made up of one $AlO_4(OH)_2$ octahedron sheet and one or two SiO_4 tetrahedron sheets depending on the type of clay mineral. Generally, clay minerals can be classified as type 1:1 and type 2:1 (see Figure 2.11). Type 1:1 as in kaolinite and halloysite, the crystal layer unit system contains one mono-sheet of SiO_4 and one mono-sheet of $AlO_4(OH)_2$ which are connected by sharing of oxygen atoms. On the other hand, type 2:1 clay minerals have a layering system made of two SiO_4 and one $AlO_4(OH)_2$, which are connected by the sharing of oxygen atoms forming tri-sheets of SiO_4-$AlO_4(OH)_2$-SiO_4 sandwiched structure. Unlike1:1 type class that which the layers are connected by hydrogen bonds, there is no hydrogen bond between each inter-layers of the 2:1 class making the layers relatively independent. Examples of 2:1 types of aluminosilicate clay minerals include smectite, illite, chlorite, and vermiculite (Zou *et al.*, 2022).

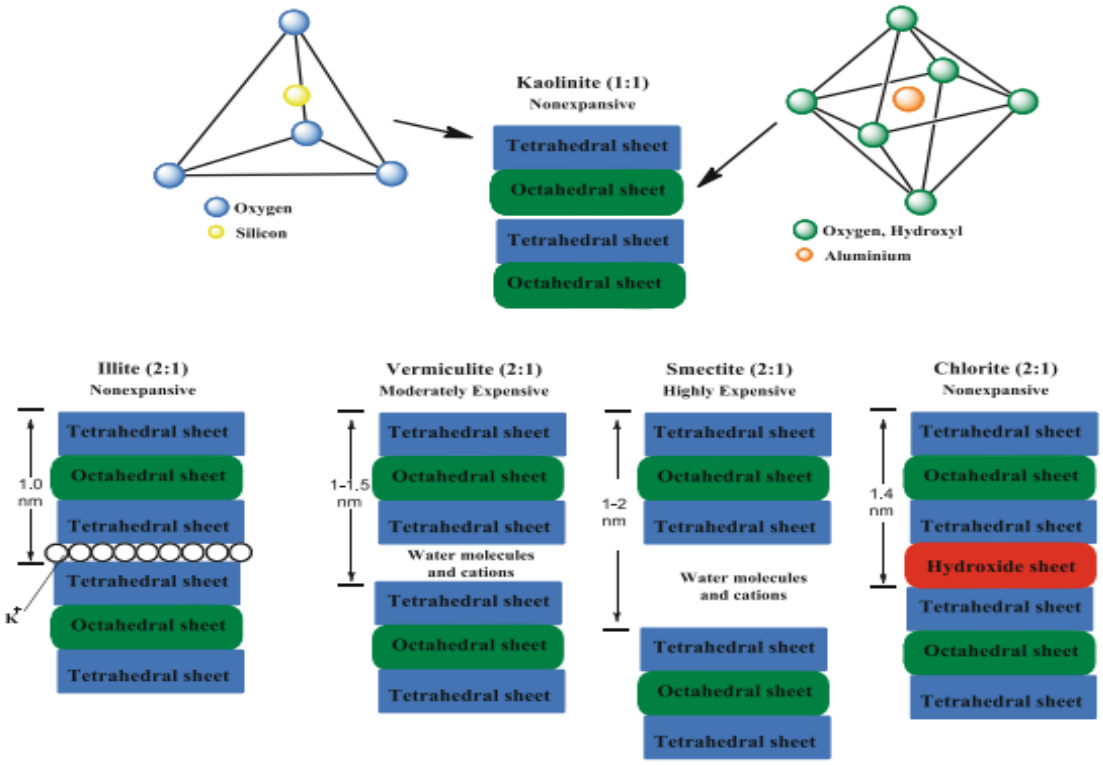

Figure 2.11: Typical structures of major clay minerals

Clay possesses two types of charges. The first one arises from the "broken edges" of clay due to the surface reactivity of clay and is pH-dependent. At a high pH (basic medium), the octahedral surface hydroxide group lost its H^+ ion by dissociation into the solution resulting in a negative surface charge. The second type is called permanent or structural charge, and it arises due to the substitution of Al^{3+}, Si^{4+}, Mg^{2+}, and Fe^{3+} ions. To balance the net charge, this substitution is normally complemented by the addition of alkaline metal or alkaline earth metals such as Na, K, Mg, and Ca in their interlayer space. Pure clays are not found in nature and are often a mixture of other clay minerals, and sediments and frequently contaminated with chemical impurities like oxides of arsenic, lead, chromium, and titanium (Ghadiri *et al.*, 2015). Table 2.3 illustrates some clay minerals and their various chemical formulas.

Table 2.3: Some clay minerals and their chemical formulas (Cohen and Ward, 1991; Uddin, 2018; Merabtene *et al.,* 2019).

The group name	Type	General chemical formula	Specific clay minerals
Kaolin group	1:1	$Al_2Si_2O_5(OH)_4$	Kaolinite, halloysite, dickite, nacrite
Serpentine	1:1	$Mg_3Si_2O_5(OH)_4$	Antigorite, chrysolite, lizardite
Illite	2:1	$K_xAl_4(Si_{8-x}Al_x)O_{20}(OH)_4$, where $x = 1.0 - 1.5$	Glauconite, hydromuscovite, K-deficient muscovite
Smectite	2:1	$(Na, Ca)_{0.33}(Al, Mg)_2(Si_4O_{10})(OH)_2 \cdot nH_2O$	Montmorillonite (bentonite), saponite, nontronite
Chlorite	2:1	$(Mg, Fe)_3(Si, Al)_4O_{10}(OH)_2 \cdot (Mg, Fe)_3(OH)_6$	Clinochlore, pennaclore, chamosite, sudoite
Vermiculite	2:1	$(Mg, Fe^{2+}, Fe^{3+})_3(Al, Si)_4O_{10}(OH)_2 \cdot 4H_2O$	
Talc	2:1	$Mg_3Si_4O_{10}(OH)_2$	
Pyrophyllite	2:1	$Al_2Si_4O_{10}(OH)_2$	

2.6.1.1 Kaolin

The Kaolin group are class of minerals that are white, soft plastic, and the least reactive clay. Clays or rocks with high kaolinite constituents are referred to as kaolin or china clay (Kausar *et al.*, 2018). Clay with less than 40% kaolinite content is characterized as a low-grade kaolin

type of clay whereas those between 40% and 60% are medium grade and above 70% of kaolinite is classified as high-grade kaolin clay (Cao *et al.*, 2021; Bediako and Valentini, 2022). There are Van der Waals attractive forces and hydrogen bonding between the oxygen atoms in the tetrahedral sheet of the kaolinite layer and the hydrogen atoms of the hydroxyl groups in the octahedral sheet. These strong forces hold the sheets of kaolinite together tightly and water cannot penetrate in-between them. As a result, kaolinite typically does not swell when in water (Chen and Peng, 2018). A clay mineral of the kaolin subgroup called halloysite is structurally and chemically similar to kaolinite. However, the two clay minerals have different morphology. Halloysite has a tubular or spheroidal shape, whereas kaolinite appears as hexagonal platelets with a book-like structure. Another key distinction is that, in contrast to kaolinite, where there are no water molecules in the interlayer region, halloysite has localized water molecules between 0 and 2 molecules per structural unit (Dedzo and Detellier, 2018). Kaolin clay is the clay mineral mostly used for the synthesis of zeolite types.

2.6.1.2 Illite

Illite clay mineral belongs to the mica family and has a grey-white to silvery-white, greenish-gray color. It has K^+ as the only interlayer cation (Marsh *et al.*, 2018). The potassium ions form a strong link between the layers of illite, thereby preventing water from entering the structure. Illite has a poor swelling potential as a result. It has varied layer structures and bonding forces that have a substantial impact on the characteristics of clay minerals, such as surface charge, ion exchangeability, and aggregation. These intrinsic properties lead to different behaviors of illite minerals in flotation (Chen and Peng, 2018).

2.6.1.3 Smectite-Montmorillonite

Montmorillonite clay mineral is a very soft phyllosilicate mineral belonging to the smectite family. Its layers are connected by weak van der Waals forces. The movement of water molecules within the interlayer space could displace the layers. As a result, montmorillonite is plastic and expands significantly, leading to significant stress even at a low concentration. As a result of isomorphic ion substitution at tetrahedral and octahedral structures, several types of smectite clays are formed, and this gives the layer a permanent negative charge (Chen and Peng, 2018; Kausar *et al.*, 2018). Mobile hydrated cations that are present in the large interlayer space balance out this charge defect. They have a higher cation exchange capacity, a larger surface area, and a swelling tendency, making them more reactive than 1:1 clay minerals (Dedzo and Detellier, 2018). Bentonite belongs to this class of clay mineral and it is made up of 98% of montmorillonite mineral.

2.6.1.4 Chlorite

Chlorites are occasionally categorized as a different category within the phyllosilicates and are not necessarily regarded as clay (Adeyemo *et al.*, 2017). Chlorite mineral is a member of the 2:1 silicate group and is typically monoclinic, which mostly consists of iron-magnesium silicates with some aluminum atoms. Because there is no water intake between the layers, its crystal does not expand. When magnesium ions occupy every octahedral position in chlorite, it is referred to as brucite. Similar to the magnesium-rich aluminum dioctahedral chlorites called sudoite, magnesium ions typically exchange some of the aluminum ions in the octahedral structure. In the octahedral sheets of Cookeite, a distinct form of dioctahedral chlorite, lithium replaces aluminum (Kumari and Mohan, 2021).

2.6.1.5 Vermiculite

Vermiculites are chemically intricate clay minerals and are generally formed as a result of the weathering of biotite and ferromagnesian minerals (iron and magnesium-rich rock or mineral). H. Webb, an American, first discovered it in 1824 in a mine near Vinsted, Massachusetts. Due to its ability to resist thermal expansion, it was given the name vermiculite in 1861, which translates to "worm-like" in English. Vermiculites that are high in magnesium content often contain two layers of water in the interlayer region. This results in an expansion of around 14 Å. K-rich vermiculites, on the other hand, do not have interlayer water and only have a basal spacing of around 10 Å (Bibi *et al.*, 2016; Wang and Wang, 2019).

Vermiculite has a substantial cation exchange potential, a great specific surface area, and a surface negative charge, all of which contribute to its exceptional ability to adsorb heavy metal ions. In addition, vermiculite has unique porosity, inter-layer spacing, and active groups on its surface that help it develop a greater affinity with dye molecules, pharmaceuticals or antibiotics, other organic molecules, and CO_2. Activated vermiculite has catalytic properties due to the presence of active Lewis acid and basic sites available in its structure. Vermiculite is often employed as a catalyst-supports for catalyzing the degradation of environmental contaminants as well as the catalyst synthesis and conversion of chemicals (Wang and Wang, 2019).

2.6.2 Applications of clay

Clay is utilized in several industrial processes such as the adsorption of harmful environmental substances, petroleum recovery, and refining of petroleum, among others. These applications are directly tied to their structure and compositions. Clay is used to make a variety of products, including cooking pots, decorative items, dishware, and even musical instruments like the

ocarina. Additionally, clay is utilized in several industrial processes, including those that produce paper, cement, ceramics, and chemical filters. Particle size, surface chemistry, particle shape, surface area, as well as other physical and chemical qualities peculiar to a certain application, are significant factors linked to clay mineral uses (Murray, 1991; Aboudi-Mana *et al.,* 2017; Awasthi *et al.,* 2019). Different types of clay minerals are used in biomedical applications such as the formulation of active molecules, controlled release of drugs and treatments, and in recent times are put on to protect against solar radiation (Moraes *et al.*, 2017). Furthermore, clays have a long history of application in chemical processes as catalysts and as catalyst supports. Clays and modified clays are used to catalyze several chemical reactions including condensation reactions, addition reactions, esterification, Friedel-Crafts, Diels-Alder reaction, isomerization, and oxidation reactions. The clay functions as both Lewis and Brønsted acids in catalysis (Nagendrappa, 2011).

2.6.3 Preparations of naturally occurring clay minerals for zeolite synthesis

Clay minerals can be converted into zeolites by carrying out several processes including quarrying of clay minerals, crushing, drying, grinding, sieving, and calcination followed by dealumination where needed and subsequent steps in hydrothermal treatment.

2.6.3.1 Thermal Activation of clay minerals by calcination

The SiO_4 tetrahedra sheets and $AlO_4(OH)_2$ octahedra sheets found in clay minerals existed in crystalline form, therefore stable and unreactive. This necessitates the activation of the clay structure, which turns the unreactive form into a reactive form (Adeniyi *et al.*, 2020).

The clay activation methods include mechanical, chemical, and thermal treatment. Amongst these, the thermal method is the most widely used to cause the reactivity of clay minerals due

to its efficiency. Thermal treatment, also known as calcination, requires heating the clay sample at an elevated temperature to trigger the octahedral structure to undergo dehydroxylation reaction and amorphization. Numerous variables, such as heating rate, calcination temperature and duration, environment (inert otherwise oxidizing), and cooling speed, affect the nature of the structural transformation. The selected temperature for efficient calcination for any particular clay mineral must be sufficient to cause dehydroxylation and amorphization, but not too high so that recrystallization takes place. Two major desired processes occurred during the calcination; i. dehydroxylation which is the release of the hydroxyl group (OH) from $AlO_4(OH)_2$ in the form of water and ii. amorphization which is the gradual transformation of the crystalline phase into a complete amorphous state. In certain conditions, dehydroxylation can also cause amorphization; however, there is no direct relationship between the two. Amorphization is beneficial for increasing clay reactivity. During calcination at elevated temperatures, the six-fold aluminum coordination in the octahedral sheet is reduced to 5-, 4-, or even 3-fold coordination at times. The resultant distorted and disordered structure with decreased Al atom coordination known as metaclay, is more reactive than the natural clay. The extent of reactivity of the meta-clay rest on the amorphous content. The temperature range at which each clay mineral undergoes dehydroxylation, amorphization, and recrystallization differs (see Figure 2.12). For example, the dehydroxylation temperature for halloysite, montmorillonite, and illite are in the range of 600-850 °C, 620-780 °C, and 520-650 °C respectively. When a clay material contains different clay minerals (such as natural clay deposits), it might be difficult to determine the optimum calcination temperature to achieve complete dehydroxylation and amorphization. Even more challenging is when the various clay minerals present dehydroxylate at different temperature ranges do not overlap (Khalifa *et al.*, 2020). In some cases, recrystallization of previously activated clay minerals forming stable and unreactive phases might happen at the time a second mineral is activated. It was noticeable that

recrystallization temperatures for various clay minerals were lower in a mixture of different clay minerals than the pure clay mineral. Optimum activation temperatures for natural clay range from 550 to 850 °C for varying holding times, however, the majority of the reported values are between 650 and 750 °C (Snellings *et al.*, 2012).

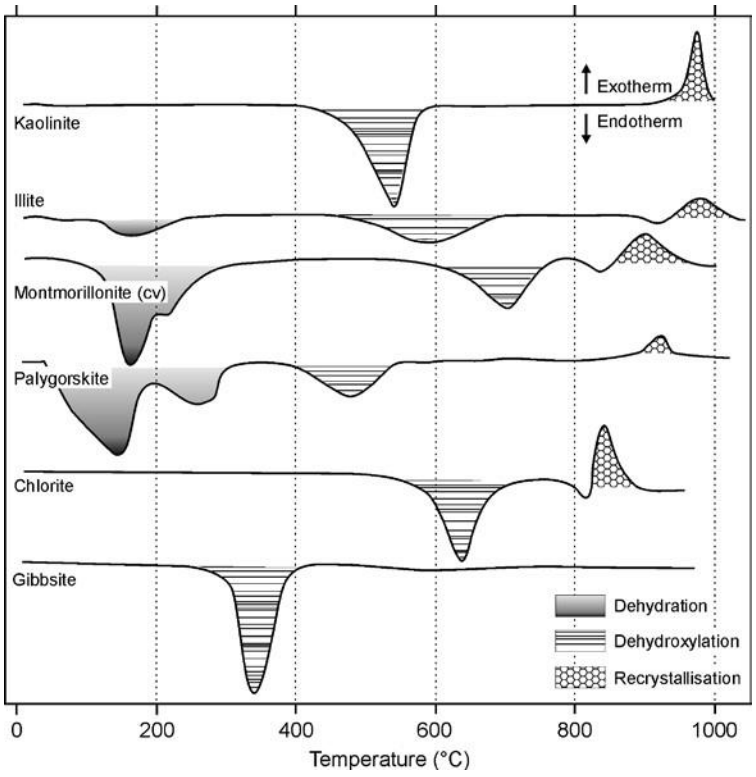

Figure 2.12: DTA curves illustrating the thermal behavior of some clay and clay-based minerals (Snellings *et al.*, 2012).

Equations (8a)-(8d) depict the dehydroxylation reaction of kaolinite clay minerals during calcination (Cheng *et al.*, 2019). Both the inner and inner-surface hydroxyl groups are denoted as H_2O in the kaolinite formula, $Al_2O_3 \cdot 2SiO_2 \cdot 2H_2O$.

Dehydroxylation reaction occurs between the temperature ranging from 450 ^oC to 900 ^oC and this resulted in the formation of metakaolin (see equation 8a).

$$Al_2O_3 \cdot 2SiO_2 \cdot 2H_2O \text{ (kaolinite)} \xrightarrow{\text{heat}} Al_2O_3 \cdot 2SiO_2 + 2H_2O \quad \ldots\ldots\ldots\ldots\ldots\ldots (8a)$$

Temperatures beyond 900 °C up to 925 °C further transformed the metakaolin into Al-Si spinel and amorphous silica product (see equation 8b).

$$2(Al_2O_3 \cdot 2SiO_2) \xrightarrow{\text{heat}} 2Al_2O_3 \cdot 3SiO_2 + SiO_2\ (\text{amorphous}) \ldots\ldots\ldots\ldots\ldots (8b)$$

The Si-Al spinel formed in the previous stage is converted to mullite and cristobalite phases at a temperature of 1050 °C (see equation 8c).

$$3(2Al_2O_3 \cdot 3SiO_2) \xrightarrow{\Delta} 2(3Al_2O_3 \cdot 2SiO_2) + 5SiO_2\ (\text{cristobalite}) \ldots\ldots\ldots (8c)$$

Recrystallization occurred at 1200 °C. The amorphous silica formed in equation 8b is subsequently transformed into a cristobalite crystal phase.

$$SiO_2(\text{amorphous}) \xrightarrow{\Delta} SiO_2\ (\text{cristobalite}) \ldots\ldots\ldots\ldots\ldots\ldots\ldots\ldots\ldots\ldots\ldots (8d)$$

2.7 Synthesis of ZSM-5 zeolite using clay as the raw material

Natural resources including kaolin, red mud, illite, rectorite, and diatomite have been used to create zeolite to lower production costs and also add to the economic worth of the minerals (Tehubijuluw *et al.*, 2021). Kaolin clay is the most widely clay mineral used in the production of ZSM-5. However, illite and palygorskite have also been reported. Two processes are required to transform clay minerals into zeolite: first, the clay (kaolin) must be thermally treated to create meta-clay (metakaolin), a metastable amorphous and highly reactive material. The second stage involves a hydrothermal process to convert metakaolin into zeolite in an alkaline aqueous media. To synthesize high SiO_2/Al_2O_3 molar ratios zeolite such as ZSM-5, it is necessary to increase the silica content of the metakaolin or partially remove the aluminum from the metakaolin. The first option suggests employing an extra silica source with high solubilities, such as sodium silicate. The second option, known as dealumination, is leaching the metakaolin in a solution of an inorganic acid such as HCl, H_2SO_4, or HNO_3 (Aguilar-

Mamani *et al.*, 2014). Table 2.4 displays some calcination conditions, dealumination conditions, and additional silica sources used for zeolite synthesis as reported in the literature.

Table 2.4: Some conditions of calcination and dealumination of clay minerals for ZSM-5 synthesis

ID	Source of Clay & Clay Mineral	Initial-treatment	Calcination Conditions	Acid Treatment Conditions	Additional Silica Source	References
1	Bangka kaolin	None	None	None	Ludox (Colloidal silica)	Iryani *et al*., 2020
2	Kaolin from China kaolin Company Ltd	None	800 °C for 2 h	6 M (1:5, g/mL) at 90 °C for 4 h	TEOS (Tetraethyl orthosilicate), Hexadecyltrimeth oxysilane	Xing *et al*., 2017
3	Qingha clay from Salt Lake in Qaidam Basin	Alkali fusion and ZSM-5 seed, NaOH:Clay (2:1)	500 °C for 2 h	None	Ludox	Feng *et al.*, 2017
4	Bangka Belitung kaolin	None	None	None	Ludox	Hartanto *et al*., 2019
5	Kaolin from Prosyanovsk	None	650 °C for 4 h	5 M sulfuric and citric acids solution (1:13, g/mL) at 80 °C for 2-6 h	*NM	Kuvatova *et al*., 2021
6	Kaolin from China Kaolin Company Ltd.	None	800 °C for 2 h	6 M HCl (1:5) at 90 °C for 4 h	*NM	Xing *et al*., 2017

7	Kaolin (Sigma-Aldrich)	None	750 °C for 2 h	36 wt% HCl (1:17, g/mL) at 115 ºC for 2.5 h	NM	Thakkar *et al.*, 2017
8	Kaolin from Caiçara, Rio Grande do Norte-Brazil	Sieved with 0.074mm mesh	700 °C for 2 h	NM	Silica sol	Silva *et al.*, 2013
9	Kaolin (Riedel de Haen, pro analysi)	None	750 °C for 2 h	3 M HCl (1:17, g/mL) at 115 °C for 150 min	NM	Aguilar *et al.*, 2014
10	Kaolin (Inner Mongolia, China)	None	800 ºC for 2 h	6 M HCl, (solid/liquid 1:5, g/mL)	NM	Pan *et al.*, 2014
11	Kaolin from Bangka Belitung, Indonesia	None	None	NM	Ludox	Qoniah *et al.*, 2015
12	Kaolin from China Kaolin Clay Company	None	300 - 900 ºC for 2 h	None	Silica sol, Water glass	Feng *et al.*, 2009
13	Bangka Belitung Kaolin	NM	NM	None	Ludox	Hartanto *et al.*, 2017
14	Kaolin from Makana Brick and Serina Trading, South Africa	NM	800 °C for 6 h	NM	Sodium silicate solution	Mohiuddin *et al.*, 2017
15	Indonesian kaolin from Bangka island	Sieved with 100 µm and flotation (1:3 w/v)	800 °C for 6 h	NM	Bayat natural zeolite	Faisal *et al.*, 2019
16	Illite collected from Changbai Mountain (Yanbian, China)	Flotation and ball milling	550, 650, and 800 °C for 2 h	6 M HCl at 170 °C for 5 h (1:6, g/mL)	NM	Han *et al.*, 2019

17	Kaolin (China kaolin company)	Mixed with water to make a slurry, sprayed, and dried	800 °C for 4 h	NM	Water glass, Silica	Chen *et al*., 2021
18	Kaolin from China (Zibo Hi-king Technology Co. Ltd.)	NM	980 °C for 2 h	NM	Silicic acid	Wang *et al*., 2013
19	Kaolin from China Kaolin Clay Company	NM	700 °C for 2 h	NM	Silica sol	Feng *et al*., 2009
20	Raw Jordanian kaolinite	Sieved with a 75 μm sieve	600 °C for 6 h	H_2SO_4 (1-3 M), 90 °C for 8 h (1:4, g/mL)	None	Al-hadi *et al*., 2015
21	Kaolin from Bangka Belitung, Indonesia	NM	NM	NM	Ludox	Qoniah *et al*., 2020
22	Raw kaolinite powders from Mongolia in China	NM	NM	NM	NM	Pan *et al*., 2014
23	Kaolin from Zonouze Co. Iran	NM	600 °C	NM	Silicic acid	Khatamian *et al*., 2009
24	Kaolinite from Georgia, USA	NM	600 °C for 24 h	2.5 M H_2SO_4 at 90 °C for 2 h		Madhusoodana *et al*., 2005
25	Illite minerals from Changbai Mountain, China	Purified by flotation	700 °C for 2 h	6 M H_2SO_4 at 170 °C for 6 h (1:5, g/mL)	NM	Li *et al*., 2021
26	Natural rectorite mineral from Hubei Celebrities Rectorite Company (Hubei Province, P. R.	NaOH and deionized water were kneaded and extruded	NM	NM	Water glass	Yue *et al*., 2020

	China)					
27	Illite minerals from Changbai Mountain (China)	Flotation process followed by ball milling	650 °C for 2 h	6 M HCl at 170 °C for 5.5 h (1:6, g/mL)	None	Liu *et al*., 2019
28	Palygorskite clay	NM	NM	3 M HCl at 80 °C for 48 h (1:20, g/mL)	None	Jiang *et al*., 2014
29	Kaolin from Kankara Mining, Katsina State Nigeria	NM	600 – 700 °C	NM	Silica gel	Abubakar *et al*., 2020
30	Kaolin from Inner Mongolia, China	NM	800 °C for 2 h	6 M HCl at 80 °C for 2 h, (1:5, g/mL)	NM	Pan *et al*., 2014
31	Kaolin from Bangka Belitung, Indonesia	Ref	NM	NM	Ludox	Hartanto *et al*., 2016
32	Kaolin from Makana Brick, Grahamstown, South Africa	Sieved to less than 200 µm, flotation	NM	NM	Sodium silicate solution	Mohiuddin *et al*., 2016
33	Kaolin from the Chinese Kaolin Company	Kaolin and NaOH were blended	980 °C for 2 h	NM	Sodium silicate	Sun *et al*., 2007
34	Commercial Perlite	NM	NM	NM	Sodium silicate	Wang *et al*., 2007
35	Commercial Kaolin	NM	850 °C for 3 h	NM	Sodium silicate	Wang *et al*., 2007
36	Kaolinite from Tabarka (Tunisia)	NM	700 °C for 2 h	3 M HCl (1:10, g/mL) at 90 °C	Ludox	Ghrib *et al*., 2017

				for 6, 12, 18 and 24 h		
37	Ahoko kaolin	NM	600 °C for 10 min	5 M H_2SO_4 (3:40, g/mL) at 80 °C for 1, 2, 4 and 8 h	None	Holmes *et al*., 2011
38	Kaolin from Bangka Belitung, Indonesian	NM	NM	NM	Colloidal silica	Nugraha *et al*., 2021

*NM: Not Mentioned

Table 2.5 displays some conditions for ZSM-5 synthesis as reported by some previous research, as well as their application.

Table 2.5: Hydrothermal syntheses conditions of ZSM-5 from clay and the zeolite applications

Aging Conditions	Crystallization		Reactants Molar ratios	Product	Applications	References
	Temperature	Time				
24 h	170 °C	48 h	SiO_2:Al_2O_3:TPAOH:NaOH:H_2O = 1:0.02:0.12:0.01:3	ZSM-5	Methanol aromatization	Xing *et al.*, 2017
24 h	165 °C	24 h	Na_2O/SiO_2 = 0.18, SiO_2/Al_2O_3 = 33, SiO_2/NBA = 7, and H_2O/SiO_2 = 30	ZSM-5	CO_2 capture from air	Thakkar *et al.*, 2017
24 h	165 °C	12 h	Na_2O/SiO_2 = 0.18; SiO_2/Al_2O_3 = 33; SiO_2/NBA = 7; H_2O/SiO_2 = 30	ZSM-5, Quartz	NM	Aguilar-Mamani *et al.*, 2014
No aging	150 °C	72 h	SiO_2/Al_2O_3 = 15, Na_2O/SiO_2 = 0.30, H_2O/Na_2O = 200	ZSM-5	Fluid Catalytic Cracking	Chen *et al.*, 2021

Stirred for 30 min	170 °C	2 d	SiO_2:Al_2O_3:TPABr:H_2O = 1.0:0.016:0.10:32.0	ZSM-5	Catalytic dehydration of 1-Phenylethanol	Al-hadi *et al.*, 2015
Stirred for 24 h	180 °C	48 h	3TPABr:43SiO_2:0.68Al_2O_3: 10Na_2O:4444H_2O	Quartz, Analcime zeolite		Jiang *et al.*, 2014
*NM	120–190 °C	24–96 h	SiO_2:Al_2O_3:Na_2O:TPABr:H_2O = 150:1:58.34:4.75:3375	ZSM-5, Quartz	Oligomerization of alkenes	Mohiuddin *et al.*, 2016

*NM: Not Mentioned

2.8 Characterization technique – X-ray diffraction

X-ray diffraction (XRD) is a non-destructive technique used in the characterization of crystallite materials. It is a useful tool in materials science, chemistry, physics, and geology. In principle, the X-ray interacts with the crystal lattice of a sample results in a diffraction pattern, and gives information about the crystal structure of the material. Synchrotron radiation or a high-energy X-ray tube are the two most common X-ray sources used in XRD. To generate X-rays, electrons are accelerated to extremely high energies and then collide with a target material, such as copper or molybdenum. The X-rays generated interact with the sample's crystal lattice, and the scattered X-rays create a diffraction pattern. The diffraction pattern is collected by a detector, which records the intensity and angle of the scattered X-rays. The positions and intensities of the diffraction peaks in an XRD pattern give valuable information on the crystallite structure. The crystal structure and phase, as well as to study of various properties such as crystal defects, crystallinity, and texture of the material can be determined by analyzing the positions and relative intensities of the diffraction peaks (Bunaciu *et al.*, 2015).

Bragg's Law describes the relation between the angle of incidence of X-rays on a crystal lattice and the resulting constructive interference of the scattered X-rays. It is expressed as:

$$n\lambda = 2d\sin(\theta) \quad \text{.....(9)}$$

where: n is the order of the diffraction peak, λ is the wavelength of the incident X-ray, d is the spacing between crystal lattice planes, and θ is the angle of incidence of the X-ray beam (Bunaciu *et al.*, 2015).

CHAPTER THREE

METHODOLOGY

3. Materials and Methods

3.1 Equipment

- Hot plate with a magnetic stirrer
- pH meter
- Oven
- Furnace
- Teflon-lined steel autoclave
- Reflux system
- Mortar and Pestle
- Electronic balance
- Map of deposit sites
- 1.0 L measuring cylinder
- Volumetric flask
- 200 mL conical flask
- Pycnometer
- Hydrometer
- 100 mL glass measuring cylinder
- Thermometer
- Glass rod
- BS test sieve 0.075 mm (75 microns)
- Stopwatch
- Stirring apparatus
- Wash bottle
- 500 mL Kjeldahl flask
- Steam distillation system unit (VELP Scientifica, UDK 129)
- Desiccator

3.2 Chemicals

Sodium hydroxide (98.0%, Park scientific limited, UK), hydrochloric acid (36.6% ACS, BDH VWR chemical, US), tetrapropylammonium bromide (99.0%, Lobal chemie Pvt Limited, India), ammonium nitrate (Xilong chemical co. limited, China), sodium hexametaphosphate

and sodium carbonate, potassium dichromate, sulphuric acid (>96%), orthophosphoric acid (85%), ferrous sulphate, diphenylamine, concentrated sulphuric acid (ammonia-free grade), boric acid, selenium, copper sulphate, potassium or sodium sulphate, bromosol green indicator, methyl red indicator, and zeolite ZSM-5 ammonium (SiO_2:Al_2O_3 = 30, Thermo Fisher Scientific Inc.) were purchased and used.

3.3 Collection and preparation of clay samples

Clay samples were collected from Anfoega (Volta region), Mfensi (Ashanti region), Teleku-Bokazo (Western region), and Tetegu (Greater Accra region). All the clay deposit sites are located in Ghana. The samples were sun-dried for about 7 days and oven dried for 6 h at 100 °C. The dried samples were pulverized into powder and sieved with 75 μm mesh to obtain fine particle size. The Anfoega, Mfensi, Teleku-Bokazo, and Tetegu clay were labeled as AFC, TBC, MFC, and TTC respectively.

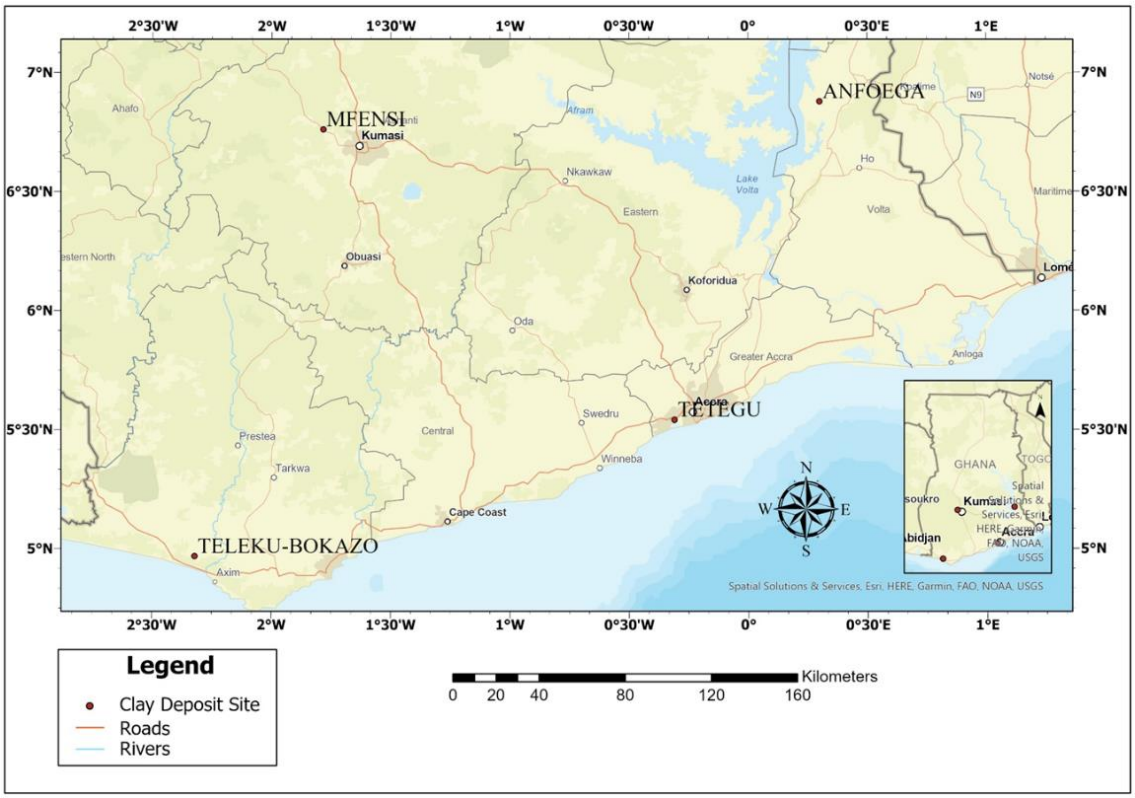

Figure 3.1: Map of Ghana illustrating various towns where the clay deposits are located

3.4 Determination of organic matter content of the raw clay samples

The organic carbon was carried out using the Walkley-black wet oxidation method which is based on the reduction of $Cr_2O_7^{2-}$ while the organic matter is being oxidized (Nelson and Sommers, 1983; Heanes, 1984).

About 1.0 g of each clay sample was weighed, and placed in a 500 mL Erlenmeyer flask. Exactly 10.0 mL of 1.0 N potassium dichromate ($K_2Cr_2O_7$) solution was added from a burette, followed by the addition of 20.0 mL concentrated sulphuric acid (H_2SO_4). The mixture was swirled thoroughly to ensure the solution was in contact with all the particles of the clay. The reaction mixture was allowed to stand for 30 min for the reaction to complete. The amount of $K_2Cr_2O_7$ reduced is equal to the amount of organic matter oxidized. The reaction was quenched by adding 200 mL of distilled water, followed by the addition of orthophosphoric acid. A volume of 2.0 mL of diphenylamine was added as an indicator, and the content was titrated against 1.0 N iron (II) sulphate ($FeSO_4$) solution until the color changed to dark blue and finally to green at the end-point. The experiment was done in triplicate and the titre values were recorded. The blank was taken through the same process without the addition of a clay sample. The %organic carbon was calculated using equation (1).

$$\%\text{Organic carbon} = \frac{\mathrm{M}\times(\mathrm{V_{bl}} - \mathrm{V_s}) \times 0.003 \times 1.33}{W_t} \times 100 \ldots\ldots\ldots\ldots\ldots(1)$$

where: M is the Molality of $FeSO_4$, V_{bl} is the volume of $FeSO_4$ titrated against the blank in mL, V_s is the volume of $FeSO_4$ titrated against the test sample measured in mL, and W_t is the mass of the clay sample weighed in grams. Milli-equivalent weight of organic carbon, C in grams is 0.003 (12/4000), and 1.33 (100/75) is a correction factor used to convert the wet combustion

C value to the true C value. This is because; the wet combustion method is about 75% efficient in estimating.

The organic matter content was determined by equation 2:

$$\text{Organic matter content} = \%\text{Organic carbon} \times 1.724 \quad \ldots\ldots\ldots\ldots\ldots\ldots\ldots\ldots\ldots\ldots \quad (2)$$

Van Bemellean factor is the 1.724

3.5 Determination of total nitrogen content of the clay samples

The percentage of the total nitrogen content of each of the clays was determined using the Kjeldahl method (Mulvaney, 1982).

A mass of 10.0 g of the clay sample was weighed into a 500 mL long-neck Kjeldahl flask, followed by the addition of 10.0 mL distilled water, and allowed to stand for 10 min to moisturize. About 5.0 g of Kjeldahl catalyst made up of 1.0 g of selenium, 10.0 g copper sulphate, and 100 g sodium sulphate was added. Followed by the addition of 30.0 mL of concentrated sulphuric acid (nitrogen-free grade). The reaction mixture was digested until a clear and colorless or light greenish was observed (about 1 h to 1:30 h) and the flask was cooled to room temperature. The sample was filtered into a 100 mL volumetric flask and was topped up to the mark with distilled water with several rinses from the digestion flask.

A volume of 10.0 mL of the aliquot was pipetted into a Kjeldahl distillation apparatus and followed by the addition of 20.0 mL of 40% sodium hydroxide. About 200 mL of the distillate was collected over 10.0 mL of 4% Boric acid and three (3) drops of mixed indicator (bromosol green and methyl red) in a 500 mL conical flask for 5 min. The presence of nitrogen gave a light blue color.

A volume of 100.0 mL of collected distillate was titrated with 0.1 N hydrochloric acid (HCl) till the blue color turned into a grey color and then quickly flashed to pink. The experiment was carried out in triplicate. A blank was carried out throughout all the steps without the clay sample.

The percentage nitrogen content of the sample was calculated using equation (3) below.

$$\%Nitrogen\ content = \frac{14.01\times(V-B)\times N\times R}{1000\times wt\ of\ sample} \times 100 \text{.....(3)}$$

where R is the ratio between the total volume of digest and digest volume (aliquot) for distillation. N represents the normality of HCl, which is 0.10 N. V denotes the volume of HCl titrated for the sample and B stands for the volume of HCl titrated for the blank.

3.6 Determination of specific gravity of the clay samples

The specific gravity for each of the four clay samples (AFC, TBC, MFC, and TTC) was determined using the pycnometer method. The clay sample was dried overnight at 105 ^{o}C to remove moisture content completely. An empty pycnometer was weighed and the mass was recorded as W_1. About 5 g of the clay sample was added to the pycnometer, weighed, and recorded as W_2. Distilled water was then added to the content and stirred to ensure complete mixing, and was allowed to stand overnight to expel the air bubbles. The pycnometer was then filled to the brim with distilled water, weighed, and recorded as W_3. Finally, the clean pycnometer was filled to the brim with only distilled water, weighed and the mass was recorded as W_4. The specific gravity was calculated using Equation 1.

$$Specific\ Gravity,\ Gs = \frac{W_2-W_1}{(W_4-W_1)-(W_3-W_2)} \text{.....(4)}$$

3.7 Particle size distribution analysis of the clay samples

Particle size distribution (PSD) analysis was performed on each clay sample by adapting the hydrometer test method, and it was carried out according to the standard protocol ASTM D422 (ASTM D422, 2007). All the samples were pre-conditioned by passing them through 75 microns mesh and drying overnight at 105 °C. A mass of 30 to 50 g of each pre-conditioned sample (AFC, TBC, MFC, and TTC) was weighed into the cup of the stirring apparatus, followed by the addition of 3.30 g of sodium hexametaphosphate and 0.70 g of sodium carbonate. Enough distilled water was added and stirred for 15 min for the complete dispersion of particles in the solution. The solution mixture was transferred into a 1000 mL glass measuring cylinder, topped up to the 1000 mL mark, and allowed to stand overnight. The solution was mixed thoroughly while putting a stopper on the mouth of the measuring cylinder and then placed on a level surface. A stopwatch was immediately started and a hydrometer was inserted into the measuring cylinder containing the solution mixture. The hydrometer readings corresponding to the upper meniscus at intervals of 30 sec, 1 min, and 2 min were taken. The hydrometer was then removed from the solution. The temperature of the solution was taken at each reading. The hydrometer reading was continued by inserting the hydrometer at intervals; 4, 8, 15, 30, 60, 120, 240, and 1440 min. The particle size (D) was determined using the formula:

$$D = M\sqrt{\frac{H_\theta}{t}} \quad \text{..... (5a)}$$

In which; $M = \left[\frac{0.3\eta}{g(Gs-1)\rho_w}\right]$..... (5b)

Where, η = viscosity of water in poise

Gs = Specific gravity of clay sample

t = time in minutes at which hydrometer reading was taken

g = 981cm/sec^2

H_θ = Actual depth

ρ_w = Density of water (mg/mL)

Percentage finer than size D is expressed by:

$$N = \left(\frac{G}{G-1}\right) \times \frac{R}{M_s} \times 100 \ldots\ldots\ldots\ldots\ldots\ldots\ldots\ldots\ldots\ldots\ldots\ldots (5c)$$

where R = corrected hydrometer reading

Ms = Mass of dry clay in 1000 mL suspension

A plot of percent passing (%) versus particle size (mm) was used to determine the sand, silt, and clay content of each clay sample.

3.8 Calcination of the clay samples

The samples were thermally activated at 800 °C for 2 h in a muffle furnace at a heating rate of 5 °C/min. The calcined Anfoega, Mfensi, Teleku-Bokazo, and Tetegu clay were labeled as CAFC, CTBC, CMFC, and CTTC respectively. The samples were placed in plastic containers for further work.

3.9 Dealumination of the calcined clay samples

Acid leaching was employed to reduce the aluminum content of the calcined clay samples. A mass of 10.0 g of the calcined sample was added to 50.0 mL (1:5, wt/vol) 6.0 M hydrochloric acid (HCl) and refluxed at 100 °C for 5 and 10 h with stirring. For CTBC, additional acid leaching conditions of 8.0 M HCl (1:5 wt/vol) for 10 h and 24 h were applied. At the end of the leaching, the sample was filtered with Whiteman No. 1 filter paper and washed until neutral

pH (pH = ~7). The sample was dried at 100 ^{o}C for 12 h to remove the water content. The leached calcined Anfoega, Mfensi, Teleku-Bokazo, and Tetegu clay were labeled as LCAFC, LCTBC, LCMFC, and LCTTC respectively. The samples were placed in separate plastic containers and used as a precursor for zeolite synthesis.

3.10 Synthesis of Zeolite using the dealuminated clay samples

For the synthesis of zeolite, 5.0 g of the dealuminated clay sample was uniformly mixed with 35.0 g of water (H_2O) followed by the addition of 0.10 g of sodium hydroxide (NaOH) as a mineralizing agent and 1.50 g of tetrapropylammonium bromide (TPABr) as structural directing. The reaction mixture was left to stand to age for 24 h at room temperature. The reaction mixture was transferred into a Teflon-lined autoclave and allowed to stand in a preheated oven at 190 °C for 24 h. The obtained product was washed with warm de-ionized water after crystallization to a pH below 8. It was dried in an oven at 100 °C for 12 h. The sample was then calcined at 550 °C for 6 h to remove the organic templates. The final product after calcined was stored in a desiccator to prevent re-absorption of moisture. X-ray diffraction (XRD) and Fourier transform infrared (FTIR) analysis were performed on the final products.

3.10.1 Determination of effects of synthesis parameters using Tetegu clay sample

For the optimization of synthesis parameters, the dealuminated Tetegu clay was uniformly mixed with water, NaOH, and TPABr in the molar ratio of $^{a}SiO_2$: Al_2O_3 : NaOH: TPABr: H_2O. The mixture was aged at varied ^{b}aging times at room temperature without stirring unless otherwise mentioned. The mixture was then transferred into a Teflon-lined autoclave and allowed to stand in a preheated oven at varied ^{c}temperatures and for varied ^{d}durations. The obtained product was washed with warm de-ionized water after crystallization and dried in an

oven at 100 °C for 12 h. The sample was then calcined at 550 °C for 6 h to remove the organic templates. The products were characterized with XRD.

[a]SiO_2	SiO_2/Al_2O_3	$NaOH/SiO_2$	$TPABr/SiO_2$	H_2O/SiO_2
1	41.44 – 150.53	0.016 – 0.161	0 – 0.072	7.00 – 50.00

[b]Aging Time	[c]Crystallization Temperature	[d]Crystallization Time
0 – 240 h	150 – 190 °C	6 – 36 h

3.11 Characterization of samples

Powder X-ray diffraction (XRD), Powder X-ray fluoresce (XRF), Fourier-transform infrared (FTIR) spectroscopy, and Thermogravimetric Analysis (TGA) coupled with Differential scanning calorimetry are instrumental techniques used in the characterization of the materials.

Powder XRD patterns of the raw clays, treated clays, and the final product obtained were recorded using a PANalytical X'pert diffractometer with Cu-Ka radiation (45kV and 40mA). The scanning was carried out in the range $2\theta = 5 – 100°$ with a step size of $2\theta = 0.1050$ and continuous scan type. The raw XRD data generated were analyzed using X'Pert High Score Plus software version 3.0 with Inorganic Crystal Structure Database (ICSD), Powder Diffraction File (PDF), and Crystallography Open Database (COD).

The characteristic bonds of the materials were measured using an FTIR spectrometer (Bruker) in the IR range of 400 – 4000 cm^{-1}. The chemical compositions of the samples were determined using an XRF spectrometer (Rigaku NEX CG XRF) from $_{11}Na$ to $_{92}U$. The thermal decomposition pattern of the raw clay samples was examined using the TGA-DSC and a temperature range of 25 – 1100 °C with a temperature ramp of 10 °C/min.

3.12 Statistical Analysis

All statistical analyses were performed using X'Pert High Score Plus software version 3.0, Excel (Microsoft office professional plus, 2016), and OriginPro version 8.5.0 SRI software.

3.12.1 Calculation of Activation Energy from TGA Data

The activation energy of TGA data was estimated using the Coats-Redfern method (Coats and Redfern, 1964).

$$\log\left[\frac{-\log(1-\alpha)}{T^2}\right] = \log\frac{AR}{\beta E_a}\left[1-\frac{2RT}{E_a}\right] - \frac{E_a}{2.303RT} \quad \text{.....(6a)}$$

where $\alpha = \frac{W_o - W_t}{W_o - W_f}$ .....(6b)

W_o is the weight of the sample before the thermal decomposition reaction

W_t is the weight of the sample at any given time

W_f is the final weight of the sample after the analysis

The plot of $\log\left[\frac{-\log(1-\alpha)}{T^2}\right]$ and $\frac{1000}{T}$ gives a slope $= \frac{-E_a}{2.303R}$

R is the ideal gas constant, which is equal to $8.314 \times 10^3\ JK^{-1}mol^{-1}$

3.12.2 Calculation of Enthalpy of Melting from DSC Data

The enthalpy of melting was estimated from DSC data by plotting $\frac{Heat\ flow\ (mJ/s)}{Weight\ (mg)}$ on the y-axis and time (s) on the x-axis. The enthalpy of melting (J/g) is equal to the integrated area under the downward peaks.

3.12.3 Calculation of Relative Crystallinity

The relative crystallinity (%) of the ZSM-5 zeolites phase was calculated from the characteristic peak area in the diffraction angles 2θ = 7-9° and 2θ = 22-25° using commercial HZSM-5 zeolite as the standard, where the degree of crystallinity of the standard was defined as 100% (Huang *et al.*, 2020; Zhang *et al.*, 2022).

$$Relative\ Crystallinity = \frac{Peak\ Area\ of\ Synthesized\ Sample}{Peak\ Area\ of\ Standard} \times 100 \ldots\ldots\ldots\ldots (7)$$

3.12.4 Calculation of Crystallite Sizes

Crystallite sizes for the as-synthesized zeolite ZSM-5 phase were determined using the Scherrer equation (Smail *et al.*, 2019).

$$D = \frac{K\lambda}{\beta COS\theta} \ldots\ldots\ldots\ldots\ldots\ldots\ldots\ldots\ldots\ldots\ldots\ldots\ldots\ldots\ldots\ldots\ldots\ldots (8)$$

where D is the average crystallite size (nm), K is the Sherrer constant, λ is the x-ray wavelength (CuK_α), β is the line broadening at FWHM in radians and θ is the Bragg's angle in degrees, half of 2θ.

CHAPTER FOUR

RESULTS AND DISCUSSIONS

4.1 Nitrogen, carbon, and organic matter content of the clay samples

Clays are obtained from different environments and their constituents determine whether they are suitable for zeolite synthesis or not. The presence of organic matter in clay can negatively influence clay quality for zeolite synthesis. Organic debris can obstruct the active sites on the clay minerals' surfaces that are necessary for the zeolitization process, which can hinder zeolite crystal formation. This might slow down zeolite production and result in an incomplete transformation of the clay minerals. Additionally, organic matter can be present in the final product as impurities, which can affect the characteristics and functionality of the synthesized zeolite (Elert *et al*., 2015).

Table 4.1: Nitrogen, carbon, and organic matter content of the clay samples after sieving

Sample	Total Nitrogen	Organic carbon	Organic matter
		%	
Anfoega clay	0.140	2.173	4.346
Mfensi clay	0.105	2.631	5.262
Teleku-Bokazo clay	0.105	0.279	0.482
Tetegu clay	0.140	0.559	0.963

Teleku-Bokazo and Tetegu clays contain low organic matters of 0.482% and 0.963, respectively (see Table 4.1). On the other hand, Anfoega and Mfensi clays contain an appropriable amount of organic matter of 4.346% and 5.262% respectively. Pre-treatment

processes such as floatation and calcination will be required to reduce or eliminate the organic matter content.

4.2 Particle size distribution of the raw clay samples

The particle size distribution of the clay sample was determined based on the principles of sedimentation with time. Sedimentation techniques are based on Stokes' law, which describes the relationship between the diameter of a spherical particle and settling velocity in a fluid at constant temperature (Karkanis *et al.*, 1991). The clay PSD has a close relationship with the amount of sand, silt, and clay contained in the sample. Sand is the largest soil particle, which ranges in size from 2.0 mm to 0.05 mm. Silt is intermediate in size, which has particle size ranges from 0.05 mm to 0.002 mm, and clay has the smallest particle size, which is less than 0.002 mm. The particles with a size larger than 2 mm are stones, pebbles, or gravel (Song *et al.*, 2015).

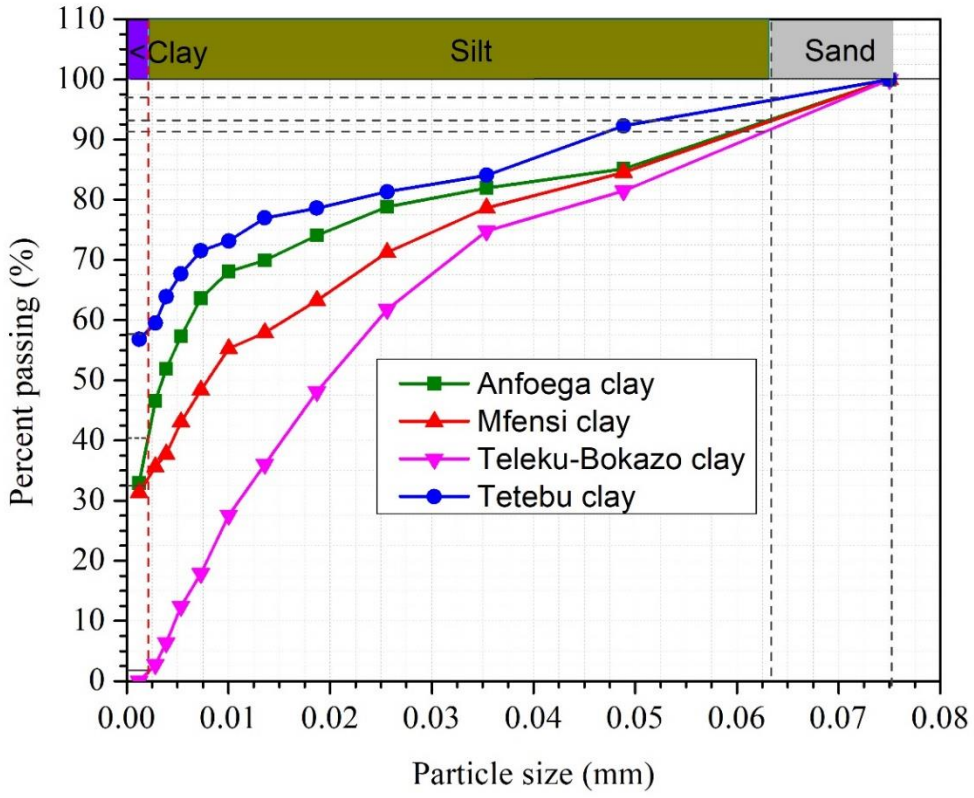

Figure 4.1: Particle size distribution of the raw Anfoega, Mfensi, Teleku-Bokazo, and Tetegu clay

Table 4.2: Clay, silt, and sand compositions of Anfoega, Mfensi, Teleku-Bokazo, and Tetegu clay

	Anfoega clay	Mfensi clay	Teleku-Bokazo clay	Tetegu clay
Specific Gravity	2.71	2.68	2.93	2.56
Clay content (%)	41.21	32.78	1.95	58.30
Silt content (%)	52.22	60.65	90.02	38.45
Sand content (%)	6.57	6.57	8.03	3.25

Anfoega clay has a composition of 41.21% particles smaller than 0.002 mm, 52.22% particles between 0.05 mm and 0.002 mm, and 6.57% particles size from 0.002 mm up to 2.0 mm (see Figure 4.1 and Table 4.2). In Mfensi clay, there are 32.78% of particles with a size less than 0.002mm, 60.65% of particles between 0.05 mm to 0.002 mm, and 6.57% of particles sizes from 0.05 mm up to 2.0 mm. The composition of Teleku-Bokazo clay is 2.93% particles smaller than 0.002 mm, 90.02% particles between 0.05 mm to 0.002 mm, and 8.03% particles size from 0.05 mm up to 2.0 mm. Tetegu clay has 58.30% of particles smaller than 0.002 mm, 38.45% of particles between 0.05 mm and 0.002 mm, and 3.25% of particles ranging in size from 0.05 mm to 2.0 mm (Table 4.2). The particle size distributions of the four clays are quite different from each other. These differences can have implications for their properties and potential uses.

The PSD translates to the percent constituent of clay, silt, and sand contained in each of the samples (see Table 4.2). The results show that Tetegu clay has the highest clay content (58.30%) compared with other samples. Both Anfoega and Mfensi clay have a high percentage of clay content. In contrast, the Teleku-Bokazo clay sample has a very low clay content (1.95%) and a very high percentage of silt (90.02%). This implies that the clay sample from Teleku-Bokazo is more silt than clay. Despite the fact that all of the samples have low sand levels, Teleku-Bokazo clay has the highest (8.03%) sand content. Tetegu clay has the least amount (3.25%) of sand content, which is more desirable since sand is not useful in zeolite synthesis. An earlier work by Amoanyi *et al.*, (2012) reported Mfensi clay to be greenish grey containing 37% clay, 43% silt, and 20% sand. The silt and sand content of Mfensi clay of this research differed from the earlier work, but the percent clay contents are similar (Amoanyi *et al*., 2012).

To the best of our knowledge, silt has not been reported in the literature for zeolite synthesis; therefore, it will be intriguing to investigate silt clay from Teleku-Bokazo for zeolite synthesis. The composition of silt clay can vary significantly depending on its origin and geological

history. However, silt clay usually contains a high amount of silica and alumina, which are the main components of zeolites. Therefore, silt clay could potentially be used as source material for zeolite synthesis.

4.3 Clay mineral compositions of the raw clay samples

The quantitative phase analysis was carried out using the Rietveld method. The Rietveld method of quantitative phase analysis is a potent tool for quantifying the quantity of each phase in a crystalline material. The Rietveld technique is based on the diffraction pattern of the sample and the least-squares refinement of the crystal structure model. The predicted diffraction pattern for each phase found in the sample is computed using the revised crystal structure model. The quantity of each phase in the sample is then calculated by comparing the theoretical and actual diffraction patterns. The pattern intensity of a phase varies depending on how much of it is present (Hill and Howard, 1987; Gualtieri *et al.*, 2019).

The quantitative phase analysis of clay samples could offer relevant information on the purity and composition of the starting materials used in the zeolite production process. By understanding the compositional variability of the starting materials, researchers can optimize the synthesis conditions to produce high-quality zeolites with the desired properties.

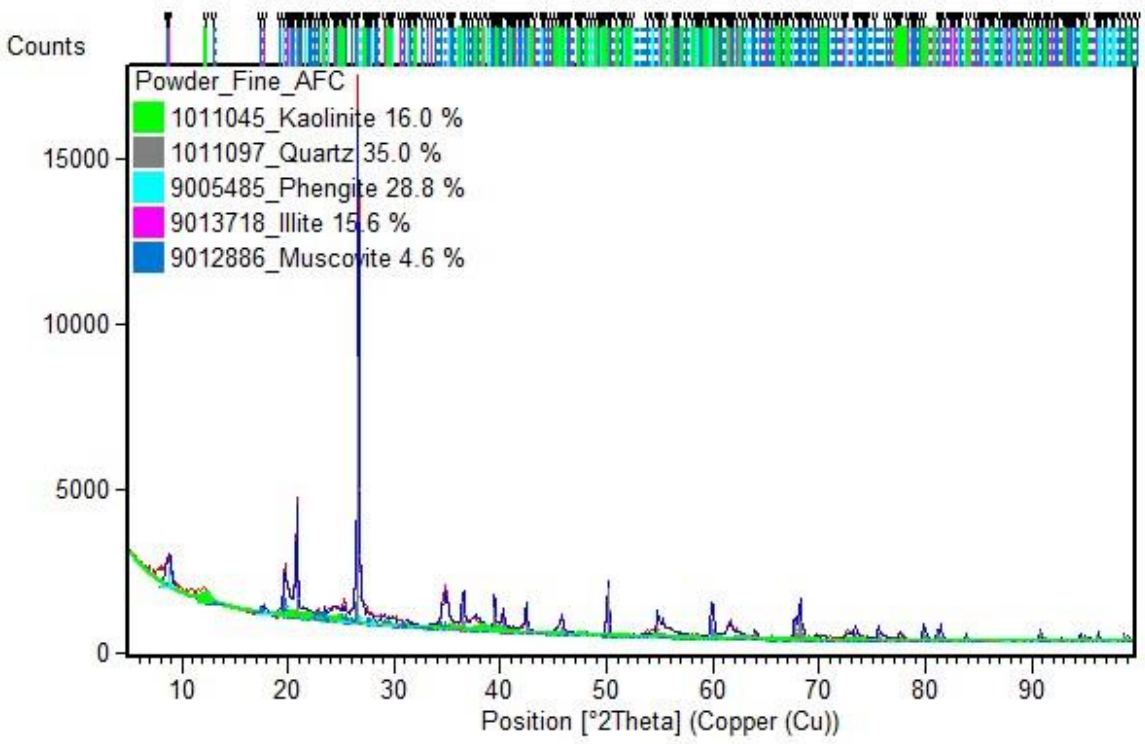

Figure 4.2: Mineral compositions of Anfoega clay

The raw Anfoega clay appears to contain a variety of mineral phases, including kaolinite (COD: 1011045), quartz low (COD: 1011097), muscovite (COD: 1011049), illite (COD: 9013718), and phengite (COD: 9005484), which are all common minerals in clays. Quantitative phase analysis using the Rietveld method shows the composition of 16.0% kaolinite, 35.0% quartz, 4.6% muscovite, 15.6% illite, and 28.8% Phengite (see Figure 4.2). The presence of aluminosilicate minerals in the sample is indicated by the presence of kaolinite, quartz, muscovite, illite, and phengite. These minerals could be valuable sources of alumina and silica for the production of zeolites. For instance, the clay minerals kaolinite and illite are commonly employed as sources of Al and Si in the synthesis of zeolites. Other minerals, such as quartz, muscovite, and phengite, can introduce impurities and change the conditions necessary for zeolite production. For instance, muscovite contains aluminum and silicon, but it also contains

potassium, which may not be desirable in some zeolite synthesis processes. In this case, adequate treatment is needed to eliminate the impurities.

Osei et al., reported that Anfoega clay to contain kaolinite, muscovite, montmorillonite, and quartz phases (Osei *et al.*, 2021). According to Kwakye-Awuah *et al*. (2018), the predominant phases present in Anfoega clay are 67.4% kaolinite and 32.4% quartz low (Kwakye-Awuah *et al.*, 2018). Kwakye-Awuah *et al*. (2021) also reported 45.3% kaolinite, 50.8% quartz, and 3.9% phengite compositions of Anfoega clay. The result obtained in this study has similarities with the previous studies.

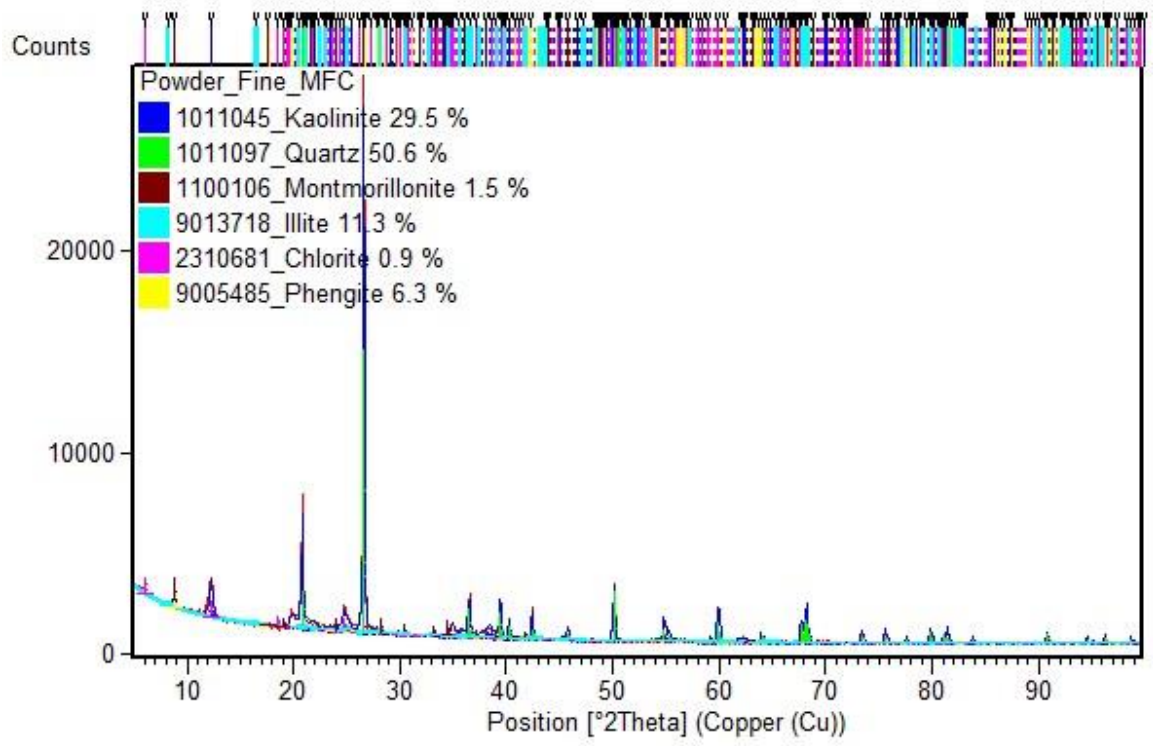

Figure 4.3: Mineral composition of Mfensi clay

The outcomes of quantitative phase analysis on Mfensi clay using the Rietveld method revealed the presence of six different minerals in the sample. The mineral quantities were estimated to be 29.5% kaolinite, 50.6% quartz low, 1.5% montmorillonite, 11.3% illite, 0.9% chlorite, and

6.3% Phengite (see Figure 4.3). This suggests that quartz and kaolinite are the dominant minerals, with montmorillonite, illite, chlorite, and Phengite present in smaller quantities. The presence of these minerals in Mfensi clay made it a potential source of silicon and aluminum for zeolite synthesis. However, the presence of chlorite and phengite may require additional treatment on the Mfensi clay to remove impurities like Fe before it can be a useful starting material. Previous research confirms the presence of kaolinite and quartz in the Mfensi clay (Endene *et al*., 2020).

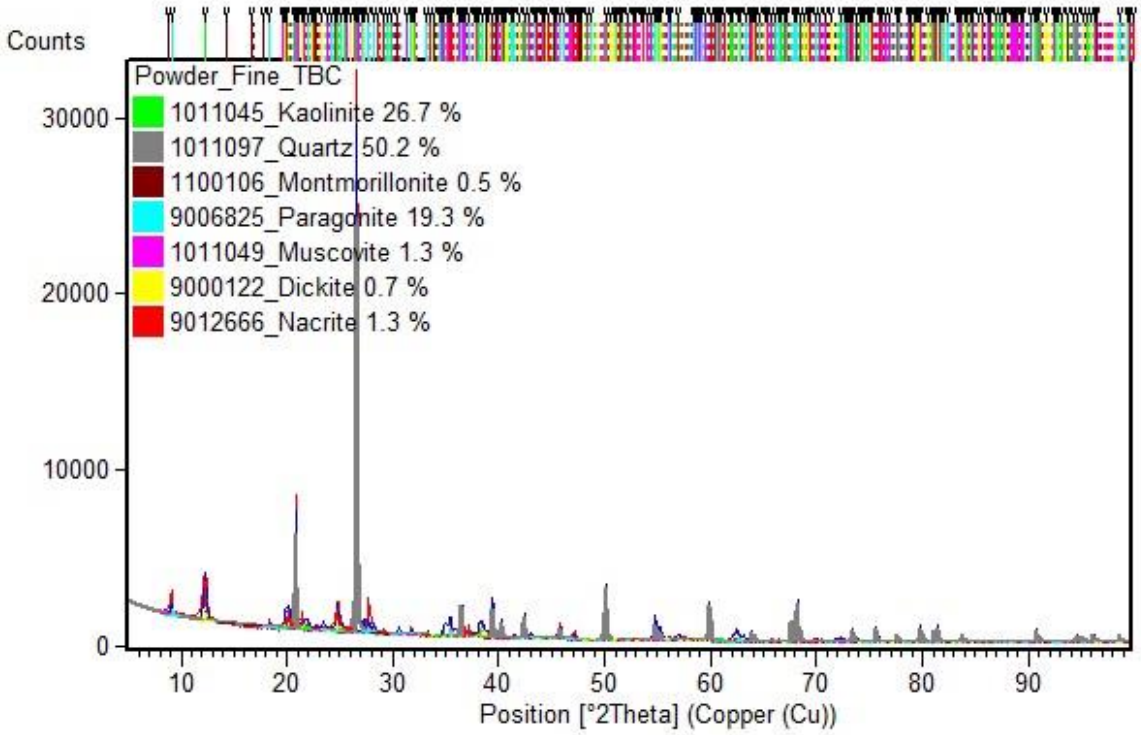

Figure 4.4: Mineral composition of Teleku-Bokazo clay

Kaolinite and quartz are the predominant mineral phases in Teleku-Bokazo clay, with kaolinite making up 26.7% and quartz making up 50.2% (see Figure 4.4). Kaolinite is a type of clay mineral that is rich in alumina and silica, which are important components required for zeolite

production. Quartz is composed of silicon dioxide and could serve as a source of silica for zeolite production.

Montmorillonite, paragonite, muscovite, dickite, and nacrite are also present in the clay sample, but in smaller percentages. Montmorillonite is a type of clay mineral that contains aluminum and silicon, but it can also contain impurities such as iron, calcium, and magnesium, which may not be desirable for zeolite synthesis. Paragonite and muscovite are also alumino-silicate minerals, which could be useful for zeolite synthesis. Dickite and nacrite are both polymorphs of kaolinite, and they are aluminum silicate minerals that may be useful minerals for zeolite synthesis. However, the high quartz content and the potential presence of impurities in some of the mineral phases may make Teleku-Bokazo clay less suitable as a starting material. Purification processes to reduce or eliminate these impurities may be required.

Marfo *et al*. (2020) also reported kaolinite, Illite, and quartz as the main crystalline phases present in Teleku-Bokazo clay.

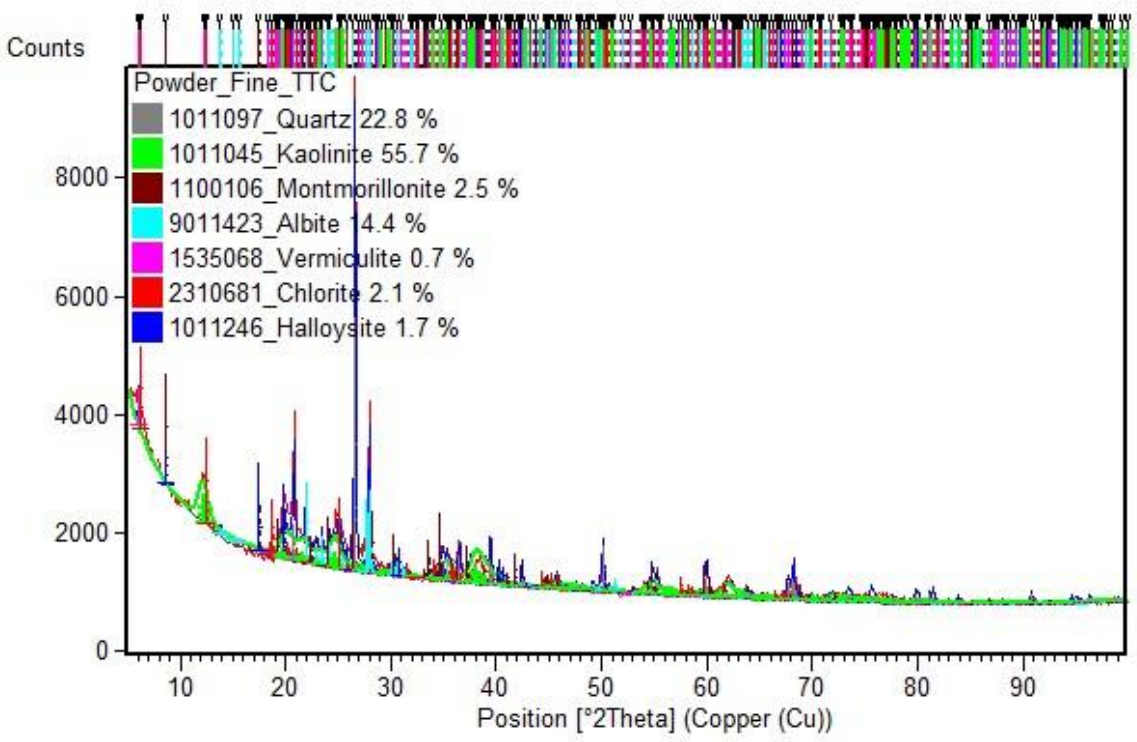

Figure 4.5: Mineral composition of Tetegu clay

Quantitative phase analysis of Tetegu clay shows 55.7% kaolinite, 1.7% halloysite, 22.8% quartz low, 2.5% montmorillonite, 14.4% Albite, 2.1% chlorite, and 0.7% vermiculite (see Figure 4.5). The high percentage of kaolinite in the clay indicates that it has a relatively high silica and alumina content, which is a key component in zeolite synthesis. Kaolinite is a common starting material for zeolite synthesis due to its high alumina content and relatively low levels of impurities. Therefore, the abundance of kaolinite in Tetegu clay makes it a potentially useful starting material for zeolite synthesis. Montmorillonite, vermiculite, and other clay minerals with high water content or high potassium content are not present in large amounts, which is desirable for zeolite synthesis. Chlorite is a phyllosilicate mineral that contains silicon, magnesium, iron, and aluminum, and it could contribute to the silica and alumina content of the clay. However, the iron and magnesium that may be present will lower the quality of this clay for zeolite synthesis.

The high percentage of kaolinite, the presence of other alumino-silicate minerals such as halloysite, montmorillonite, albite, and chlorite, and the relatively low levels of impurities in the Tetegu clay suggest that it has properties that make it potentially suitable for zeolite synthesis.

The Anfoega, Mfensi, and Teleku-Bokazo can be classified as low-grade kaolin clay, while Tetegu clay could be classified under medium-grade kaolin clay (Bediako and Valentini, 2022). The presence of the various mineral phases in Anfoega, Mfensi, Teleku-Bokazo, and Tetegu clay, particularly the alumino-silicate minerals, suggest that they have the potential to be used as a precursor for the synthesis of zeolites. However, the viability of the four clay samples for zeolite synthesis cannot be conclusively determined based solely on the quantitative phase analysis result. Therefore, further characterization of the clays was carried out to determine their suitability for zeolite synthesis.

4.4 FTIR spectroscopy analysis of the raw clay samples

Fourier transform infrared (FTIR) spectroscopy analysis is a powerful technique used to identify chemical functional groups present in a material by measuring the wavelengths of infrared radiation absorbed by the sample. The functional groups that are present in the clay can be inferred from the reported absorption bands that were observed. A typical clay shows absorption bands at 3695 cm^{-1}, 3620 cm^{-1}, 936 cm^{-1}, and 912 cm^{-1} that is ascribed to -OH stretching of inner surface hydroxyl groups in the interlayer, -OH stretching vibration of inner hydroxyl groups of Al octahedral structure, -OH bending modes of surface hydroxyl groups, and O-H bending of inner hydroxyl groups respectively. The internal vibration bands of T-O-T, where T stands for Al or Si, give absorption peaks at 1000, 690, and 470 cm^{-1}, respectively. The vibrations of the octahedral Al ion surroundings are attributed to the bands between 800

and 750 cm^{-1}. The H-O-H bending of physisorbed water has a distinctive band that has an absorption peak in the region of 1637 cm^{-1}. The Si-O-Al internal vibration band, which overlaps with the Si-O-Si absorptions, may give absorption peaks at 538 and 432 cm^{-1} (Djomgoue and Njopwouo, 2013; Yan *et al.*, 2017; Kumar and Lingfa, 2020).

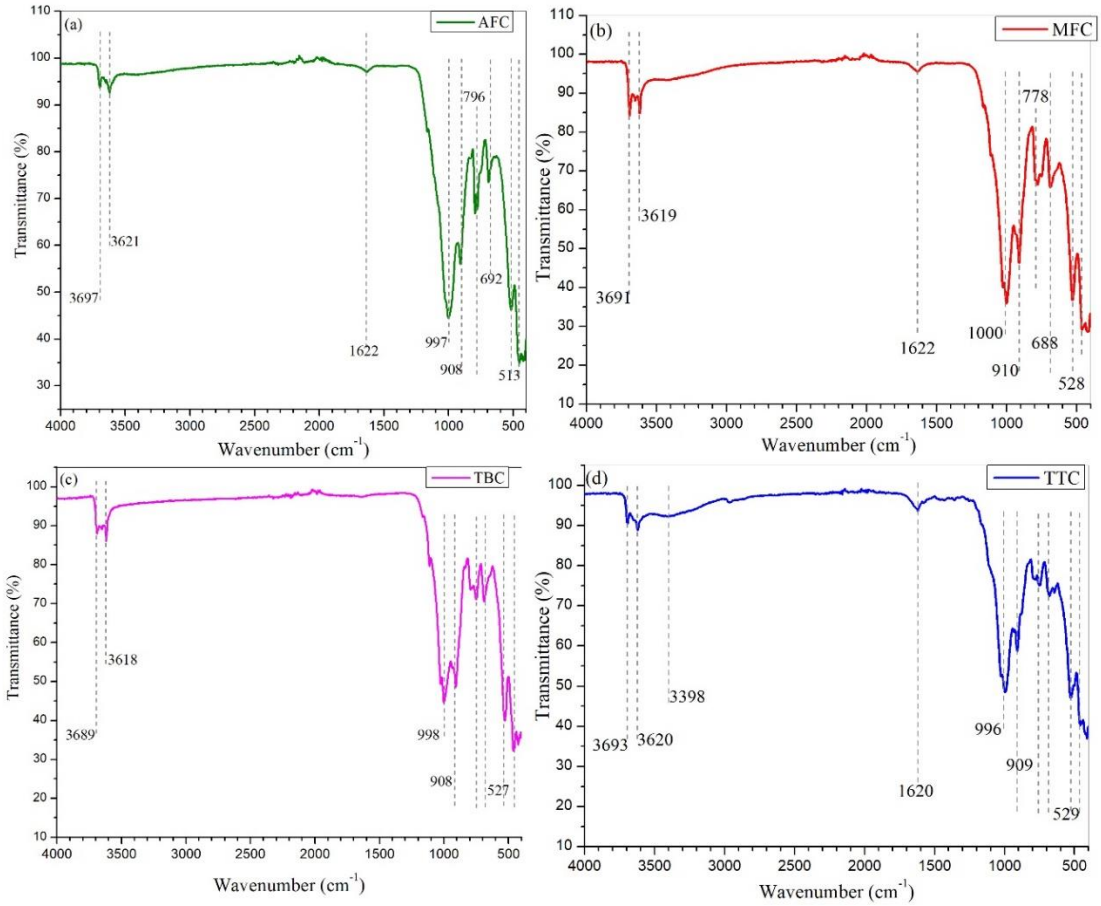

Figure 4.6: FTIR spectra of the raw (a) Anfoega, (b) Mfensi, (c) Teleku-Bokazo, and (d) Tetegu clay

FTIR analysis of Anfoega clay shows absorption bands at 3697, 3621, 1622, 997, 907, 796, 778, 692, 513, 446, and 417 cm^{-1} (see Figure 4.6). The observed absorption bands at 3697 cm^{-1} and 3621 cm^{-1} are characteristic stretching vibrations of the O-H bond indicating the presence of hydroxyl groups, which are typically found in clay minerals. The band at 1622 cm^{-1} corresponds to the bending vibration of water molecules or the presence of adsorbed water on

the clay surface. The band at 997 cm^{-1} is attributed to Si-O-Si stretching vibrations, which are also common in clay minerals. The bands at 907 cm^{-1}, 796 cm^{-1}, and 778 cm^{-1} are associated with Al-OH bending vibrations, while the band at 692 cm^{-1} is related to Si-O bending vibrations. The absorption bands at 513 cm^{-1} and 446 cm cm^{-1} correspond to Si-O deformation vibrations and Si-O-Al vibrations, respectively. Finally, the band at 417 cm^{-1} is attributed to the bending vibration of Al-O-Si groups, which is characteristic of kaolinite. These bands further confirm the presence of clay minerals in the clay sample. The doublet peaks at 796 and 778 cm^{-1} indicate the presence of quartz in the Anfoega clays (Król *et al.*, 2016).

FTIR analysis of Mfensi clay displays absorption bands at 3691, 3651, 3619, 1622, 1000, 910, 778, 688, 528, 459, and 421 cm^{-1}. The absorption bands at 3691, 3651, and 3619 cm^{-1} suggest the presence of the hydroxyl group, which is a characteristic stretching vibration of the O-H bond. The absorption band at 1622 cm^{-1} is characteristic of the bending vibration of the water molecule (H-O-H) in a clay mineral. The absorption bands at 1000 and 910 cm^{-1} suggest the presence of Si-O-Si stretching vibrations, which are characteristic of silicates. The absorption band at 778 cm^{-1} indicates the presence of the Si-O bending vibration, which is also characteristic of silicates. The absorption band at 688 cm^{-1} suggests the presence of the Al-O-Si bending vibration, which is another characteristic of aluminum silicate minerals. The absorption bands at 528, 459, and 421 cm^{-1} may be associated with the Al-O-Si stretching vibration, which is also characteristic of aluminum silicate minerals. The FTIR results suggest that Mfensi clay is primarily composed of hydrated aluminum and silicon minerals, which is consistent with the typical composition of clay minerals.

FTIR analysis of Teleku-Bokazo clay shows absorption bands at 3689, 3649, 3618, 1112, 1025, 998, 908, 787, 749, 689, 527, 458, and 427 cm^{-1}. The absorption bands at 3689, 3649, and 3618

cm^{-1} suggest the presence of the hydroxyl group and aluminum hydroxide (Al-OH), which is a characteristic stretching vibration of the O-H bonds. These three bands together suggest that the clay sample may contain hydrated minerals. The absorption bands at 1112, 1025, 998, and 908 cm^{-1} are associated with the stretching vibration of the Si-O-Si bond, indicating the presence of silicates in the clay sample. The absorption bands at 787, 749, 689, and 527 cm^{-1} indicate the presence of the bending vibration of the Si-O-Si bond, which is another characteristic of silicates. The absorption bands at 458 and 427 cm^{-1} suggest the presence of the Al-O-Si stretching vibration, which is another characteristic of aluminum silicate minerals. The FTIR results suggest that Teleku-Bokazo clay is primarily composed of hydrated aluminum and silicon minerals.

FTIR analysis of Tetegu clay shows absorption bands at 3693, 3620, 2967, 1620, 996, 909, 777, 748, 679, 643, 529, 459, and 411 cm^{-1}. The absorption bands at 3693 and 3620 cm^{-1} are associated with the stretching vibration of the hydroxyl group, which is a characteristic of hydrated minerals such as clay. The absorption band at 2967 cm^{-1} is associated with the stretching vibration of the C-H bond, which is indicative of organic impurities in the clay sample. The absorption band at 1620 cm^{-1} is associated with the bending vibration of the water molecule (H-O-H), which is common in hydrated minerals. The absorption bands at 996 and 909 cm^{-1} are associated with the stretching vibration of the Si-O-Si bonds, which is a characteristic absorption band of silicates. The absorption bands at 777 and 748 cm^{-1} indicate the presence of the Si-O bending vibration, which is also characteristic of silicates. The presence of silicates in the clay sample is a desirable property for certain applications, such as zeolite synthesis. The absorption bands at 679, 643, 529, 459, and 411 cm^{-1} suggest the presence of the Al-O-Si stretching vibration, which is characteristic of aluminum silicate minerals. This is a desirable property for zeolite synthesis, as aluminum is a key component of

the precursor material. The Tetegu clay appears to be a suitable precursor material for zeolite synthesis, as it contains the necessary components of alumino-silicate precursors.

4.5 TGA-DSC analysis of the raw clay samples

The sieved clay samples were further characterized by TGA-DSC and the results are illustrated in Figures 4.7 and 4.8. The thermal behavior of clays provides important information such as dehydroxylation temperature and the process of clay minerals constituents (Chin *et al.*, 2017). The dehydroxylated form of clay minerals is desirable for the synthesis of zeolites.

The Thermogravimetric Analysis curves (Figure 4.7a) represent the change in weight of the clay samples as they are heated.

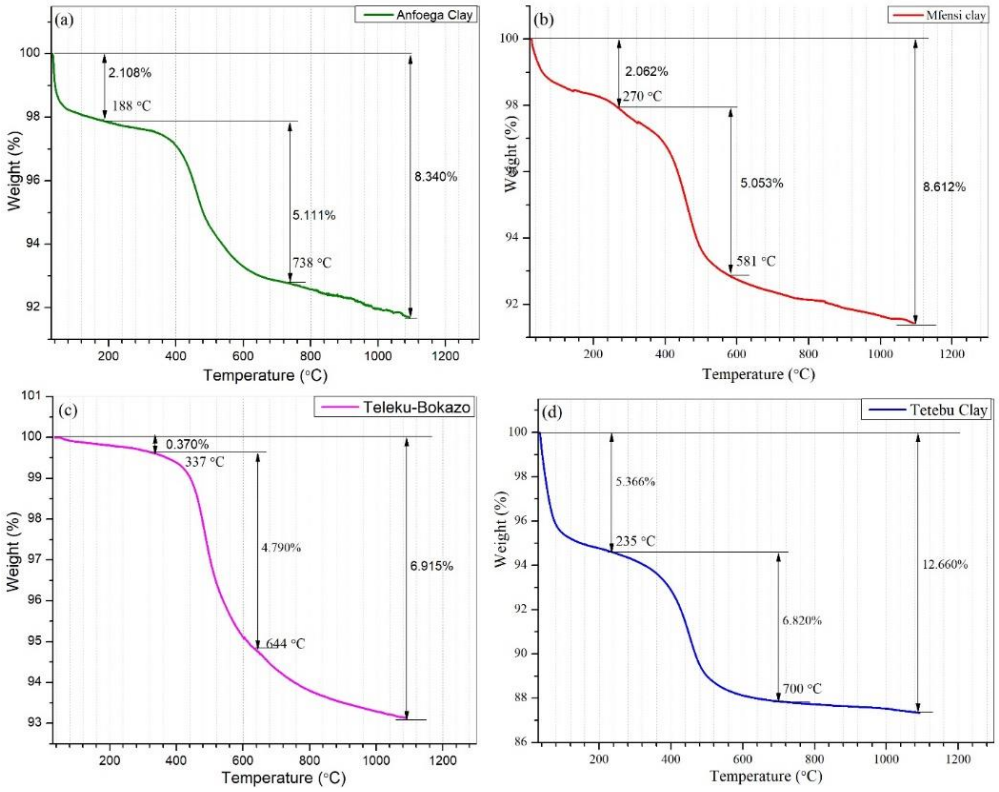

Figure 4.7: TGA curves of raw (a) Anfoega, (b) Mfensi, (c) Teleku-Bokazo, and (d) Tetegu clay

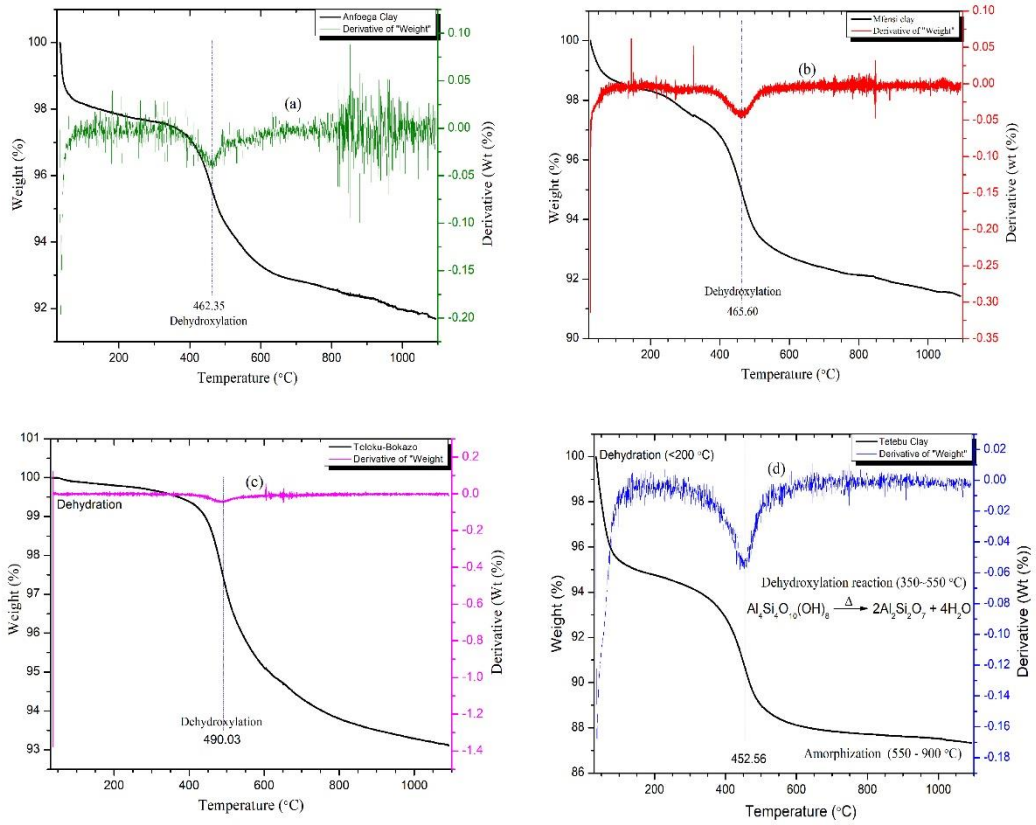

Figure 4.8: DTA curves of raw (a) Anfoega, (b) Mfensi, (c) Teleku-Bokazo, and (d) Tetegu clay

The TGA curve of Anfoega clay shows three main distinct weight losses: 2.11% weight loss from room temperature to 188 °C, 5.11% weight loss from 188 °C to 738 °C, and finally 1.12% weight loss from 738 °C to 1100 °C. The first weight loss is due to dehydration of the free physisorbed water present in the clay and other volatile components, as well as the decomposition of organic matter and the conversion of some minerals to their oxide forms. The second weight loss of 5.11% from 188 °C to 738 °C indicates the dehydroxylation of the clay minerals. Dehydroxylation is a process where hydroxyl groups that are chemically bound to the clay mineral structure are removed in the form of water molecules due to heating. During this process, crystalline water molecules that are a component of the clay structure are also

gotten rid of. The DTA curve (see Figure 4.8a) confirms the dehydroxylation reaction at a temperature of 462 °C (Yanu *et al.*, 2020; Messaoudi *et al.*, 2021).

The TGA curve of Mfensi clay displays three distinct weight loss stages, which can provide insights into the thermal behavior and composition of the clay. The first stage of weight loss in Mfensi clay occurs from room temperature to 188 °C, with a weight loss of 2.06%. This weight loss can be attributed to the evaporation of adsorbed water and volatile organic compounds from the surface of the clay mineral. The second stage of weight loss occurs from 188 °C to 738 °C and shows a weight loss of 5.05%. This stage can be attributed to the dehydroxylation of clay minerals, where hydroxyl groups are removed as water, resulting in the breakdown of the clay mineral structure. The third stage of weight loss occurs from 738 °C to 1100 °C, with a weight loss of 1.50%. This stage can be associated with the decomposition of the clay mineral structures.

The TGA curve of Teleku-Bokazo clay displays three distinct weight loss stages, each representing a different thermal event in the clay mineral structure. The first stage of weight loss in Teleku-Bokazo clay occurs from room temperature to 188 °C, with a weight loss of 0.37%. This weight loss can be attributed to the evaporation of adsorbed water from the surface of the clay mineral and the decomposition of volatile organic compounds from the clay material. The percent loss indicates less hydration ability of the clay and less organic matter content which agrees with the previous result (see Table 4.1). The second stage of weight loss occurs from 188 °C to 738 °C and shows a weight loss of 4.79%. This stage can be attributed to the dehydroxylation of clay minerals, where hydroxyl groups are removed as water, resulting in the breakdown of the clay mineral structure. The final stage of weight loss occurs from 738 °C to 1100 °C, with a weight loss of 1.76%. This stage can be attributed to the decomposition of residual clay minerals.

The TGA curve of Tetegu clay shows three main weight losses: 5.37% weight loss from room temperature to 188 °C, 6.82% weight loss from 188 °C to 738 °C, and finally 0.47% weight loss from 738 °C to 110 °C. Relatively high percent weight loss in the first stage signifies high physisorbed water content and organic compound content, which have been gotten rid of. The percent weight loss below a temperature of 188 °C revealed the high water-holding capacity of Tetegu clay. The second stage of weight loss can be ascribed to the dehydroxylation reaction of the clay minerals. The DTA curve confirmed the dehydroxylation reaction at 452 °C. There was 0.47% weight loss in the final stage of Tetegu clay, which probably correspond to the completion of the dehydroxylation of the clay minerals. A total of 12.66% (see Figure 4.8 d) of the clay content has been lost to ignition (Chin *et al.,* 2017; Yanu *et al.,* 2020; Aghris *et al.*, 2021).

Table 4.3: Calculated activation energy and enthalpy values from TGA-DSC data

	Anfoega clay	Mfensi clay	Teleku-Bokazo clay	Tetegu clay
Activation energy (kJ/mol)	39.72	40.52	39.51	39.65
Total Enthalpy Change (J/g)	-3540.03	-1256.59	-2360.15	-749.77

Activation energy is a term used in chemistry to describe the amount of energy required for a chemical reaction to take place. In the case of clay samples, activation energy can be used to describe the energy required for thermal reactions to take place in the clay mineral structure. The activation energy values provide information about the thermal stability of each clay sample. A higher activation energy value indicates that the clay sample is more thermally stable

and requires more thermal energy (heat) to undergo thermal reactions. Conversely, a lower activation energy value implies that the clay sample is less thermally stable and requires less energy to undergo thermal reactions. From the results (Table 4.8), Anfoega, Mfensi, Teleku-Bokazo, and Tetegu clay have activation energy values of 39.72, 40.52, 39.51, and 39.65 kJ/mol, respectively. These energies are required for thermal reactions such as calcination to occur in the clay mineral structure. The differences in activation energy values among the four samples are relatively small, indicating that they have similar thermal stabilities.

From the differential scanning calorimetry result, Anfoega clay exhibited three different enthalpy changes at the temperature ranges of 51.16 - 165.13 °C, 165.13 - 633.00 °C, and 633.00 – 991.59 °C. The corresponding enthalpies are -815.80 J/g, -1713.83 J/g, and -1010.40 J/g, respectively. The first temperature range (51.16 - 165.13 °C) is relatively low suggesting that this temperature range corresponds to simple processes such as dehydration reaction and decomposition of organic matter. The second temperature range (165.13 - 633.00 °C) corresponds to the dehydroxylation process, which involves the removal of water molecules from the clay structure and the decomposition of clay minerals. This temperature range requires more energy as evidenced by the more negative enthalpy change (-1713.83 J/g) observed. The magnitude of the enthalpy change during this temperature range suggests that the dehydroxylation process of clay minerals in Anfoega clay is highly energy-intensive. The highest temperature range (633.00 – 991.59 °C) can be associated with enthalpy change (-1010.40 J/g) due to the completion of the melting process and/or the formation of a new mineral phase.

Mfensi clay exhibits enthalpy changes at two different temperature ranges. The first temperature range is 86.22 -390.55 °C, and the second temperature range is 390.55 - 529.29 °C. The enthalpies corresponding to these temperature ranges are -1165.32 J/g and -91.27 J/g, respectively. The total enthalpy change at the temperature range 86.22 - 529.29 °C is -1256.15

kJ/mol corresponding to exothermic processes such as dehydration and dehydroxylation reaction.

The Teleku-Bokazo exhibits enthalpy changes at two different temperature ranges. The first temperature range is 278.40 – 978.56 °C, and the second temperature range is 978.56 – 1067.18 °C. The enthalpies corresponding to these temperature ranges are -2334.62 J/g and -25.53 J/g, respectively. The negative sign of the enthalpies indicates that the process is exothermic, meaning that heat is released as the clay undergoes these processes. The first temperature range corresponds to a process that releases a large amount of heat, with an enthalpy change of -2334.62 J/g. This could indicate a process such as Dehydroxylation and decomposition reactions, where the clay breaks down into its constituent components and releases energy in the form of heat. The second temperature range corresponds to a process that releases a smaller amount of heat, with an enthalpy change of -25.53 J/g. This could indicate a different process, such as a phase transition.

The Tetegu clay exhibits enthalpy changes at three different temperature ranges: 78.80-158.71 °C, 158.71 - 462.42 °C, and 462.42 - 613.95 °C. The corresponding enthalpies are -59.05 J/g, 582.60 J/g, and -108.11 J/g respectively. The first temperature range of 78.80 - 158.71 °C corresponds to a physical process such as dehydration, where water molecules are released from the clay structure as it is heated. The second temperature range of 158.71 - 462.42 °C corresponds to a significant process such as dehydroxylation reactions. The third temperature range of 462.42 - 613.95 °C corresponds to a negative enthalpy change of -108.11 J/g, which indicates that heat is being released during a process that occurs at this temperature range. This temperature range corresponds to further dehydroxylation of some clay minerals and decomposition changes in Tetegu clay.

These results provide important information about the thermal behavior of Anfoega clay, Mfensi, Teleku-Bokazo, and Tetegu, which can be useful for understanding and optimizing industrial processes that involve heating or processing the clay.

4.6 Chemical compositions of raw and dealuminated clay samples

X-ray fluorescence (XRF) analysis is an effective analytical method that is frequently used to ascertain the elemental composition of a variety of materials, including clay samples. The elemental compositions of the four clay samples both before and after acid leaching are shown in Tables 4.4 to 4.7 in their various oxide forms. ZSM-5 is known to have a minimum Si/Al molar ratio of 7, however, a Si/Al molar ratio of 10 to infinity is required in the starting material for its synthesis (Al-Jubouri *et al.,* 2021). For this reason, the calcined clays were acid leached to reduce the aluminum content thereby raising the silica to alumina molar ratio.

Table 4.4: Chemical composition of Anfoega clay before and after acid leaching

Composition (wt/wt%)	**Raw AFC**	**6 M HCl, 1:5 (w/v), 5 h**	**6 M HCl, 1:5 (w/v), 10 h**	**6 M HCl, 1:5 (w/v), 24 h**
SiO_2	69.700	90.900	94.100	97.500
Al_2O_3	20.100	5.380	3.680	0.842
Fe_2O_3	2.440	0.687	0.221	0.068
CaO	0.016	0.016	0.009	0.010
MgO	1.500	0.151	0.126	*ND

K_2O	4.530	1.390	0.508	0.277
Na_2O	*ND	*ND	*ND	*ND
TiO_2	1.020	1.180	1.060	1.150
ZrO_2	0.245	0.213	0.205	0.151
Others	0.449	0.083	0.091	0.002
% Al_2O_3 Extracted	-	73.234	81.692	95.812
SiO_2/Al_2O_3	**3.468**	**16.896**	**25.571**	**115.796**

*ND: Not Detected (Average mass% <0.0001)

The most abundant oxides in the raw Anfoega clay are silica (SiO_2) and alumina (Al_2O_3). The high silica-to-alumina ratio can be attributed to the presence of quartz in the clay as it was revealed by the XRD result (see Figure 4.2). Additionally, the presence of 2:1 phyllosilicates such as illite and phengite contributed to the high silica content. The presence of magnesium and iron can be associated with the phengite and illite content of the clay, respectively. The chemical constituent of the raw Anfoega clay as reported in Table 4.4 agreed with an earlier study (Kwakye-Awuah *et al.*, 2021).

To obtain a high SiO_2/Al_2O_3 ratio for ZSM-5 synthesis, dealumination by acid leaching was carried out on the calcined Anfoega clay using a 6 M HCl solution. The results show that the SiO_2/Al_2O_3 ratio increases as the time duration of the acid leaching increases. The SiO_2/Al_2O_3 ratio was found to be 16.896, 25.571, and 115.796 when the time duration was 5 h, 10 h, and 24 h respectively. A minimum of SiO_2/Al_2O_3 ratio = 10 is required for the synthesis of ZSM-5 zeolite. However, the higher the ratio, the higher the possibility of obtaining a ZSM-5 zeolite phase and higher crystallinity. The SiO_2/Al_2O_3 ratio was dramatically increased by acid leaching, which also markedly decreased the concentration of impurities like Fe, Mg, and K.

Table 4.5: Chemical composition of Mfensi clay before and after acid leaching

Composition (wt/wt%)	Raw MFC	6 M HCl, 1:5 (w/v), 5 h	6 M HCl, 1:5 (w/v), 10 h
SiO_2	71.300	93.200	94.800
Al_2O_3	21.200	3.960	2.870
Fe_2O_3	4.250	0.474	0.407
CaO	0.202	0.038	0.037
MgO	0.274	*ND	*ND
K_2O	1.080	0.773	0.348
Na_2O	*ND	*ND	*ND
TiO_2	1.190	1.260	1.250
ZrO_2	0.282	0.234	0.230
Others	0.222	0.061	0.058
% Al_2O_3 Extracted	-	81.321	86.46
SiO_2/Al_2O_3	**3.363**	**23.535**	**33.031**

*ND: Not Detected (Average mass% <0.0001)

The major oxide compositions of Mfensi clay are silica and alumina, and an appreciable amount of iron oxide (Fe_2O_3). The elemental constituents of Mfensi clay can be attributed to the presence of the clay minerals and quartz in this clay as confirmed by XRD analysis. The elemental constituent of the raw Mfensi clay as reported in Table 4.5 is similar to an earlier study, except for the presence of sodium in the previous study (Endene *et al.*, 2020).

Dealumination by acid leaching on calcined Mfensi clay raised the SiO_2/Al_2O_3 ratio to 23.535 and 33.031 over the time duration of 5 h and 10 h respectively. In addition, the concentration of some impurities such as Fe, Mg, K, and Ca have experienced a dramatic drop. The new elemental constituents of the leached samples are suitable for the synthesis of ZSM-5 zeolite.

Table 4.6: Chemical composition of Teleku-Bokazo clay before and after acid leaching

Composition (wt/wt%)	**Raw TBC**	**6 M HCl, 1:5 (w/v), 5 h**	**6 M HCl, 1:5 (w/v), 10 h**	**8 M HCl, 1:8 (w/v), 10 h**	**8 M HCl, 1:8 (w/v), 24 h**
SiO_2	68.500	85.400	86.900	90.900	96.200
Al_2O_3	26.300	11.300	10.400	7.190	2.770
Fe_2O_3	0.771	0.117	0.127	0.081	0.019
CaO	0.091	0.064	0.045	0.033	0.019
MgO	*ND	*ND	*ND	*ND	*ND
K_2O	0.820	0.681	0.372	0.231	0.064
Na_2O	3.000	2.030	1.730	1.230	0.617
TiO_2	0.147	0.160	0.171	0.151	0.146
ZrO_2	0.218	0.195	0.175	0.161	0.160
Others	0.153	0.053	0.080	0.023	0.005
% Al_2O_3 Extracted	-	57.034	60.456	72.662	89.468
SiO_2/Al_2O_3	**2.605**	**7.558**	**8.356**	**12.643**	**34.729**

*ND: Not Detected (Average mass% <0.0001)

The major metal oxide composition of the raw Teleku-Bokazo clay is silica and alumina, and an appreciable amount of sodium oxide (Na_2O). The relatively high sodium content confirmed the presence of paragonite, $NaAl_2(AlSi_3O_{10})(OH)_2$ as shown by the XRD result (see Figure 4.4). The low concentration of Fe, Ca, Mg, Ti, and Zr suggests the high purity of this clay, which is desirable for zeolite production. Additionally, the high concentration of silica and alumina suggests the suitability of this clay for zeolite synthesis.

Although Teleku-Bokazo clay seems to be suitable for zeolite synthesis, its low SiO_2/Al_2O_3 ratio (2.605) is not favorable for ZSM-5 zeolite synthesis, which is a high silica zeolite. To raise this ratio, the calcined Teleku-Bokazo clay is dealuminated by acid leaching techniques. The XRF analysis results show that the SiO_2/Al_2O_3 ratio was increased to 7.558 and 8.356 when the time duration of the acid leaching was 5 h and 10 h respectively, using a 6 M HCl solution. Since the SiO_2/Al_2O_3 ratio is still below 10, which is favorable for ZSM-5 zeolite synthesis, the concentration of the HCl solution was increased to 8 M. Using 8 M HCl solution resulted in SiO_2/Al_2O_3 ratio of 12.643 and 34.729, when the time durations were 10 h and 24 h respectively. The increase in the ratio was due to the removal of aluminum species from the calcined clay sample by dissolution in a hot concentrated HCl acid solution (Nnanwube and Onukwuli, 2023).

Table 4.7: Chemical composition of Tetegu clay before and after acid leaching

Composition (wt/wt%)	**Raw TTC**	**6 M HCl, 1:5 (w/v), 5 h**	**6 M HCl, 1:5 (w/v), 10 h**
SiO_2	60.700	92.300	93.400
Al_2O_3	23.500	3.780	3.050
Fe_2O_3	10.000	0.558	0.394
CaO	0.776	0.461	0.468
MgO	1.180	*ND	*ND
K_2O	1.210	0.648	0.588
Na_2O	0.279	0.303	0.292
TiO_2	1.420	1.620	1.540
ZrO_2	0.370	0.206	0.210
Others	0.565	0.124	0.058
% Al_2O_3 Extracted	-	83.915	87.021
SiO_2/Al_2O_3	**2.583**	**24.418**	**30.623**

*ND: Not Detected (Average mass% <0.0001)

Silica and alumina are the major components of the Tetegu clay, with SiO_2 accounting for 60.70% and Al_2O_3 accounting for 23.50%. These elements are commonly found in various minerals including clays, feldspars, and quartz, among others. Iron (Fe) is present in the sample at a concentration of 10.00%. The presence of iron could indicate the presence of iron oxides or iron-containing clay minerals such as chlorite and vermiculite. The presence of high iron

content in Tetegu clay as a starting material can inhibit the synthesis of certain types of zeolites, such as ZSM-5. It can slow the crystallization process, alter the morphology of zeolite obtained, and may influence the catalytic properties. The chemical composition of the raw Tetegu clay reported in this work is comparable to previous research (Dodoo-Arhin *et al.*, 2013).

To reduce the iron content of the clay and increase its SiO_2/Al_2O_3 ratio for ZSM-5 synthesis, the calcined Tetegu clay was acid-leached with a 6 M HCl solution. The SiO_2/Al_2O_3 ratio was found to be 24.418 and 30.623, which corresponds with 5 h and 10 h of acid leaching, respectively. In addition, the iron oxide concentration decreased dramatically to 0.558 and 0.394 for 5 h and 10 h acid leached, respectively. There was a significant decrease in other metal species such as Ca, Mg, and K. The high silica content and low impurity content of the acid-leached Tetegu clay make it a suitable precursor for ZSM-5 synthesis.

4.7 XRD patterns of the as-synthesized zeolites from the four clay samples

When natural clays become depolymerized when subjected to thermal activation by calcination and acid/alkali treatment, and they become sources of reactive silica and alumina for the synthesis of zeolites (Li, *et al*., 2023; Li *et al.*, 2021). The viability of the acid-leached clay samples from the four clay deposits was tested for ZSM-5 synthesis using the hydrothermal method of synthesis. The XRD results are presented in Figures 4.9 to 4.12.

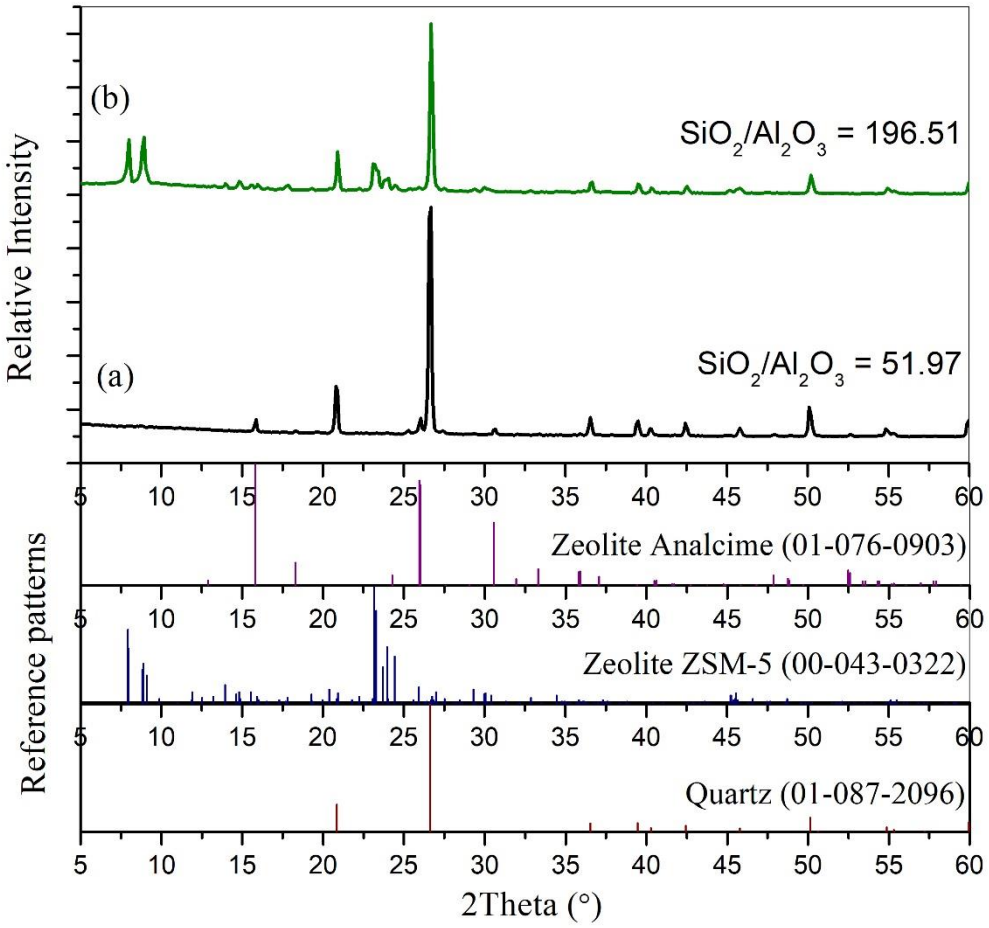

Figure 4.9: XRD patterns of zeolites synthesized from Anfoega clay after (a) acid-leaching for 10 h and (b) acid-leaching for 24 h

The acid-leached Anfoega clay for 10 h and 24 h gave SiO_2/Al_2O_3 molar ratios of 51.97 and 196.51 respectively. These samples were used for the synthesis of ZSM-5 zeolite and the XRD patterns for the obtained products are presented in Figure 4.9, (a) and (b), respectively. As shown in Figure 4.9a, the product obtained exhibited characteristic peaks of Analcime zeolite (PDF# 01-076-0903) at 2θ = 15.83°, 25.97°, and 30.56° (Bortolini *et al.*, 2020). The phase has a tetragonal crystal system with a corresponding space group of 141/acd and space group number 142. In Figure 4.9b, the product obtained exhibited characteristic peaks of ZSM-5 zeolite (PDF# 00-043-0322) at 2θ = 7-9° and 2θ = 22-25° (Al-Jubouri, Al-Batty and Holmes, 2021). However, both samples exhibited characteristic peaks of quartz low (PDF# 01-087-2096) at 2θ = 20.91°, 26.70°, and 50.22° (Wu *et al.*, 2020). Both samples contained quartz,

which was present in the starting materials. Kwakye-Awuah and co-workers successfully synthesized zeolite type A using Anfoega clay. They reported that the quartz phase was obtained along with the zeolite A, which showed no reactivity regardless of the variation of the synthesis parameters (Kwakye-Awuah *et al.*, 2021).

Analcime is a hydrated sodium aluminum silicate that exists in cubic crystals. The chemical formula of analcime is $NaAlSi_2O_6 \cdot H_2O$, with small amounts of potassium and calcium substituting sodium. Even though they are categorized as zeolites, their structure and chemical characteristics are more comparable to feldspathoids (Abdelmoneim *et al.*, 2020). The formation of analcime zeolite phase instead of ZSM-5 zeolite phase for the 10 h acid leached clay can be attributed to a high sodium concentration, a high pH, and/or low SiO_2/Al_2O_3 molar ratio (Wu *et al.*, 2020). Although the SiO_2/Al_2O_3 molar ratio of 51.97 should be acceptable for the synthesis, a significant amount might originate from the quartz contained in the starting material that is non-reactive and not accessible for the reaction. Analcime forms during zeolite formation rather than ZSM-5 because analcime is a low-silica zeolite while ZSM-5 is a high-silica zeolite. Therefore, sufficient time is needed for the acid-leaching process to significantly decrease the aluminum concentration before ZSM-5 zeolite can be synthesized from Anfoega clay. It is noteworthy that, this is the first time ZSM-5 has been synthesized using Anfoega clay, as far as I know.

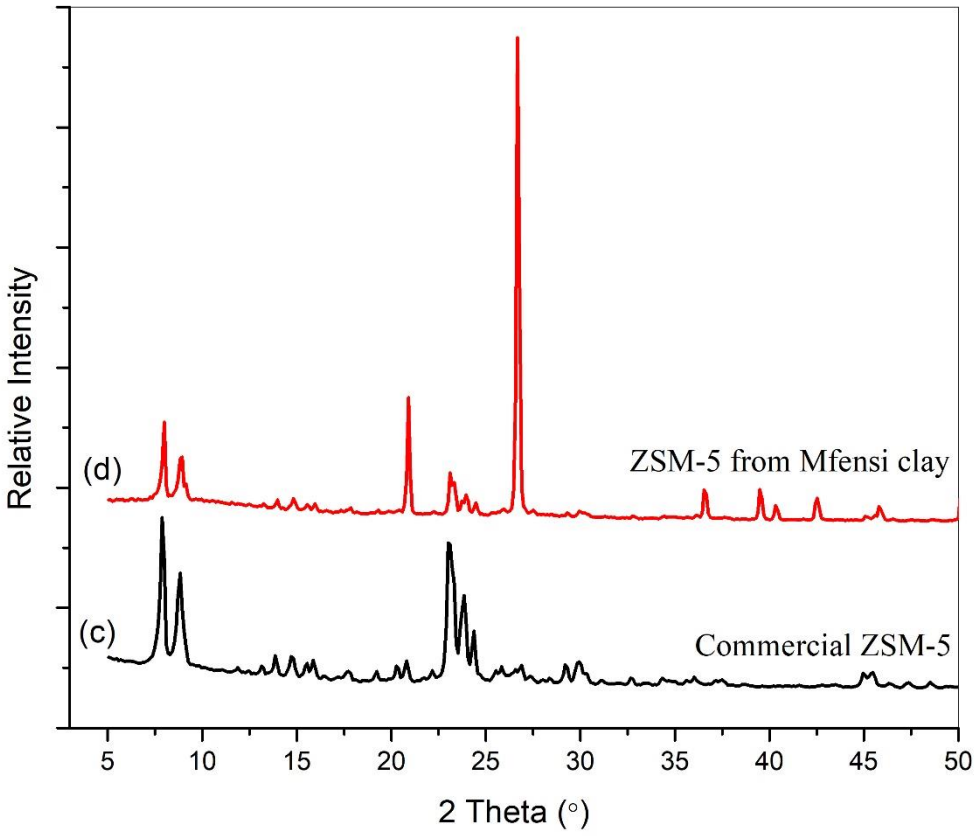

Figure 4.10: XRD pattern of (c) commercial ZSM-5 and (d) zeolite synthesized from Mfensi clay

The acid-leached Mfensi clay for 10 h after the calcination process was used as a precursor for the synthesis of ZSM-5 zeolite. The XRD pattern for the as-synthesized ZSM-5 zeolite is presented in Figure 4.10 (d). The presence of the ZSM-5 zeolite phase (PDF# 00-043-0322) is characterized by peaks at 2θ = 7-9° and 2θ = 22-25° (Al-Jubouri *et al.*, 2021). There is also a quartz phase (PDF# 01-087-2096) originating from the parent clay with characteristic peaks at 2θ = 20.90°, 26.69°, and 50.21° (Wu *et al.*, 2020). Quartz is an impurity that was not readily broken down in processes because it is thermally stable and stable in acidic/basic media (Otieno *et al.*, 2019). To the best of my knowledge, this is the first time Mfensi clay has been used in the synthesis of any form of zeolite, which is notable.

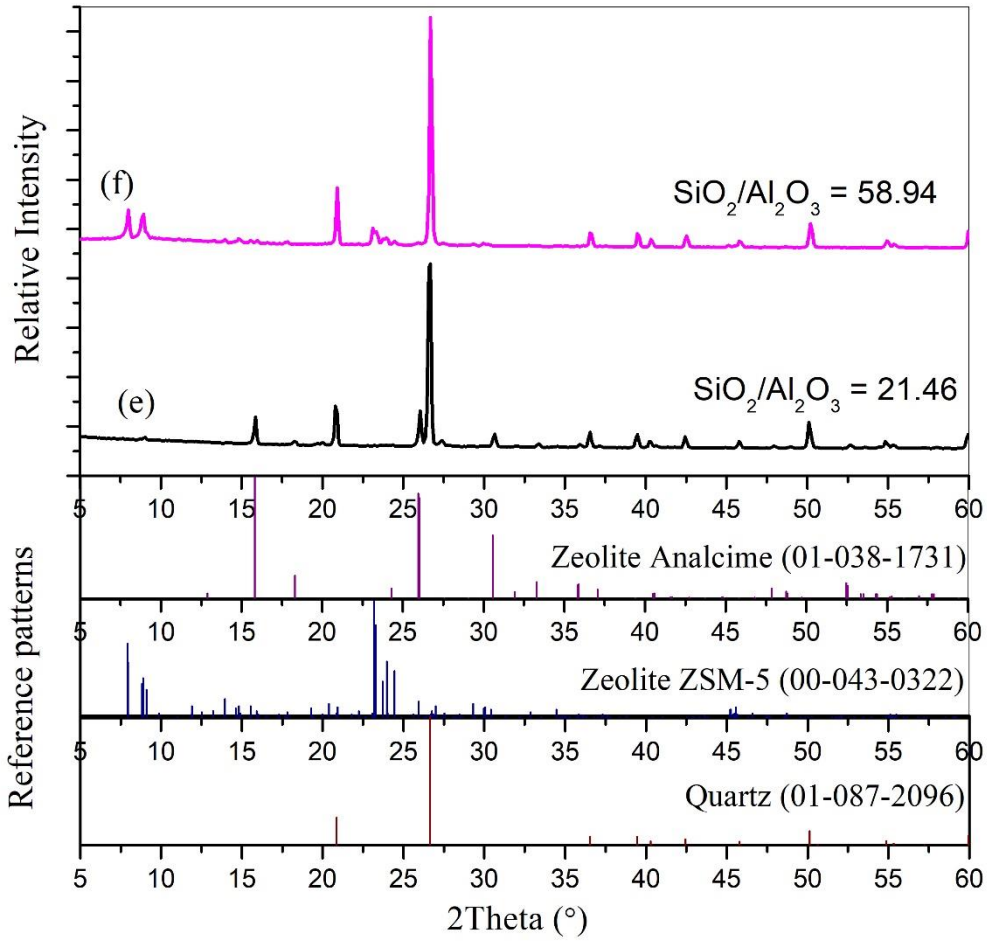

Figure 4.11: XRD patterns of zeolites synthesized from Teleku-Bokazo clay after acid for (e) 10 h and (f) 24 h using 8 M HCl solution

The calcined Teleku-Bokazo clay leached with 8 M HCl solution for 10 h and 24 h gave appropriate SiO_2/Al_2O_3 molar ratios, which are 21.46 and 58.94 respectively. These two clay samples were used for the synthesis of ZSM-5 zeolite, and the XRD patterns of the obtained product are presented in Figure 4.11 (e) and (f), respectively. The 10 h leached sample resulted in the formation of analcime zeolite phase (PDF# 01-083-1731) after the zeolitilization with characteristic peaks at 2θ = 15.82°, 25.99°, and 30.64° (Bortolini *et al.*, 2020). The sample leached for 24 h resulted in the formation of ZSM-5 zeolite phase after the zeolitilization with characteristic peaks at ZSM-5 zeolite (PDF# 00-043-0322) at 2θ = 7-9° and 2θ = 22-25° (Al-

Jubouri *et al.*, 2021). However, both samples exhibited characteristic peaks of quartz low (PDF# 01-087-2096) at 2θ = 20.90°, 26.69°, and 50.22° (Wu *et al.*, 2020). The presence of quartz in the products can be associated with the quartz constituent of the starting material. Tabil *et al.* (2021) reported the existence of residual alpha quartz in the zeolite Na-P1 that was produced after successfully synthesizing it from Teleku-Bokazo clay.

Analcime is a low silica (low Si/Al) zeolite with a chemical formula $Na_{16}Al_{16}Si_{32}O_{96}{\cdot}16H_2O$, with small amounts of potassium and calcium substituting sodium (Novembre and Gimeno, 2021b). While ZSM-5 is a high silica zeolite with a chemical formula $Na_xAl_xSi_{96-x}O_{192} \cdot 16H_2O$ $(0 < x, 27)$. Therefore, the formation of the analcime phase rather than the ZSM-5 zeolite phase for the 10 h acid-leached clay can be ascribed to the low SiO_2/Al_2O_3 molar ratio in the precursor (Wu *et al.*, 2020). Therefore, sufficient time is required for the acid-leaching procedure to drastically reduce the aluminum as well as calcium and potassium concentrations before ZSM-5 zeolite can be produced from Teleku-Bokazo clay.

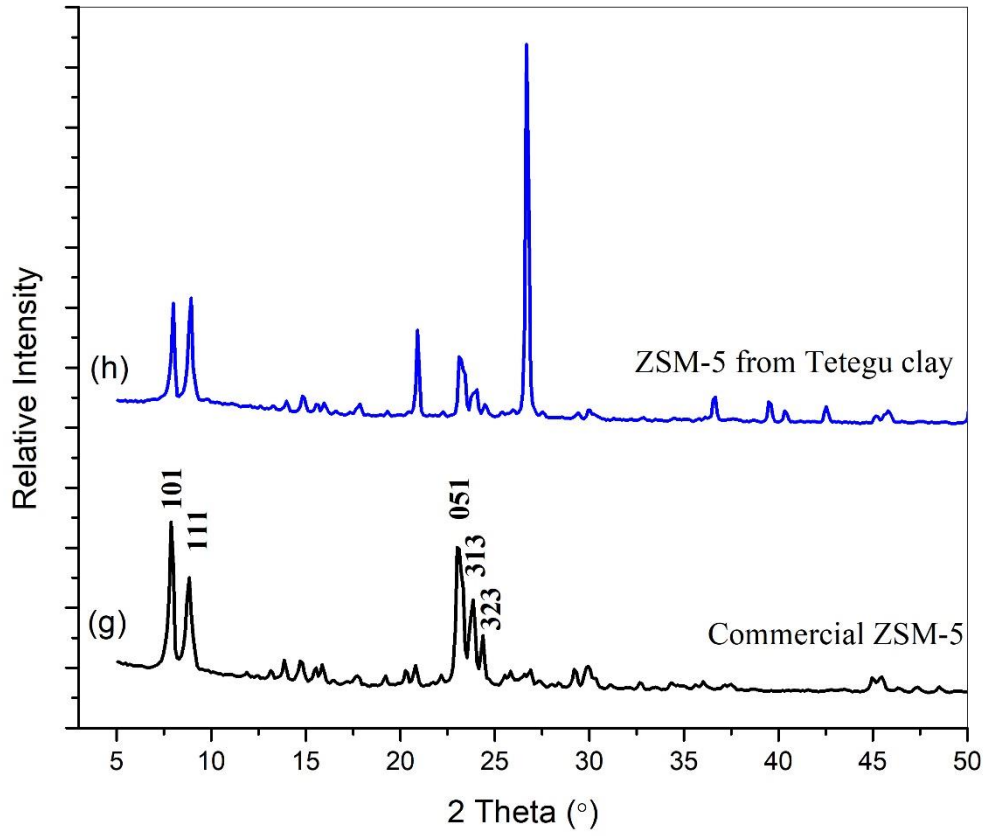

Figure 4.12: XRD patterns of (g) commercial ZSM-5 and (h) ZSM-5 zeolite synthesized from Tetegu clay

The acid-leached Tetegu clay for 10 h after the calcination process was used as a precursor for the synthesis of ZSM-5 zeolite. The XRD pattern for the as-synthesized ZSM-5 zeolite is presented in Figure 4.12 (h). The as-synthesized product exhibits the characteristic x-ray diffraction pattern of ZSM-5 zeolite (PDF# 00-044-0003) with the peaks at 2θ = 7.98°, 8.92°, 22.15°, 23.22° and 23.95° that associated with (101), (111), (051), (313) and (323) planes, respectively (Jesudoss *et al.*, 2018; Al-Jubouri *et al.*, 2021). The phase detected has an orthorhombic crystal system with the corresponding space group of Pnma and space group number 62. The diffraction peaks of the as-synthesized ZSM-5 zeolite match very well with that of the commercial ZSM-5. There is also a quartz phase (PDF# 01-087-2096) originating from the parent clay with characteristic peaks at 2θ = 20.94°, 26.71°, and 50.22° (Wu et al.,

2020). Quartz is an impurity that was not readily broken down in processes because it is thermally stable and stable in acidic/basic media (Otieno et al., 2019). It is worth noting this is the first time Tetegu clay is used in the synthesis of any zeolite type to the best of knowledge.

The presence of quartz in the as-synthesized ZSM-5 zeolites could have both positive and negative effects on their application, depending on the specific application and the concentration of the quartz. Quartz is typically inert and does not participate in catalytic reactions. It can act as a diluent when present in catalytic samples, reducing the overall concentration of active sites in the zeolite. This can lead to reduced catalytic activity most especially if the quartz content is high. Consequently, the performance of the catalyst may be compromised. The presence of quartz in the as-synthesized ZSM-5 zeolite can also be advantageous in some cases as it can help control the reaction rate and selectivity. It may prevent over-reaction or promote the desired products. Quartz is chemically stable and can withstand harsh operating conditions, providing structural support to the zeolite catalyst. This can enhance the zeolite's overall stability and longevity, which is important in continuous industrial processes (Mohiuddin *et al.,* 2018). The quartz content may need to be minimized or controlled to optimize performance depending on the targeted application. According to Mohiuddin et al. (2016), the quartz particle could serve as catalyst support for the ZSM-5 crystal, which is advantageous in catalysis. The presence of quartz was reported to enhance the catalytic conversion of toluene when using ZSM-5 and inhibit the formation of coke and carbonaceous deposits, which would otherwise deactivate the ZSM-5 zeolite.

Table 4.8: Relative crystallinity and crystallite sizes of ZSM-5 zeolite synthesized from (b) Anfoega clay, (d) Mfensi clay, (f) Teleku-Bokazo clay, and (h) Tetegu clay; (g) commercial ZSM-5 zeolite

	(b)	(d)	(f)	(d)	(g)
Relative crystallinity (%)	41.23	32.02	35.37	54.43	100.00
Crystallite size (nm)	36.08	35.53	34.75	29.74	29.42

The relative crystallinity and crystallite sizes were calculated from XRD data. Crystallinity refers to the degree of order in the arrangement of atoms or molecules within a crystal lattice. The crystallinity and crystallite size are parameters that can be used to determine the morphology and surface acidity of zeolite as a catalyst. Generally, higher crystallinity enhances the stability and selectivity of zeolite during catalysis. Notably, a smaller crystal size results in a larger surface area and an increased number of active acid sites (Phatai *et al.*, 2020). Therefore, high crystallinity and nano-crystallite size are desired in zeolite for catalytic activities. The relative crystallinity of the as-synthesized ZSM-5 zeolite phase for Anfoega, Mfensi, Teleku-Bokazo, and Tetegu clay are 41.23%, 32.02%, 35.37%, and 54.43%, respectively. The corresponding crystallite sizes are 36.08 nm, 35.53 nm, 34.75 nm, and 29.42 nm respectively (see Table 4.8). The crystal sizes of the as-synthesized zeolite range from 29.74 nm to 36.08 nm, which are all within the nano-range. Nanosized zeolites are of great importance for catalytic, adsorption, and separation applications. In comparison to zeolites with crystals of micrometer size, smaller zeolites will have a larger surface area and fewer diffusion restrictions (Sharma *et al.*, 2008). It is possible to infer from the result that, ZSM-5 obtained using Tetegu clay will possess better desirable catalytic properties than ZSM-5 obtained from

the other three clay sources. However, further characterization and testing would be necessary to fully understand the potential of these zeolites produced.

4.8 FTIR spectra of the as-synthesized zeolites

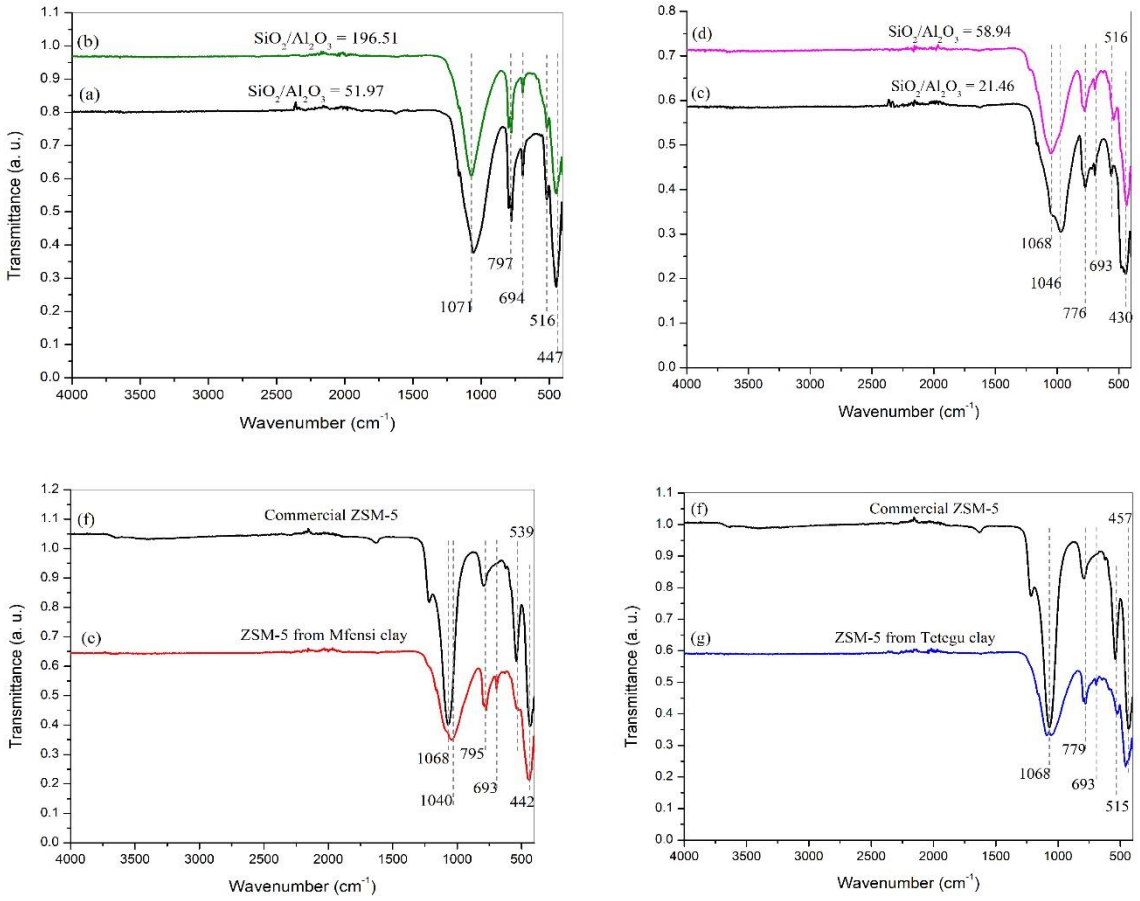

Figure 4.13: FTIR spectra for as-synthesized zeolites from (a) 10 h acid-leached CAFC (b) 24 h acid-leached CAFC (c) 10 h acid-leached CTBC (d) 24 h acid-leached CTBC (e) 10 h acid-leached CMFC, and (g) 10 h acid-leached CTTC. (f) FTIR spectrum of Commercial ZSM-5

As shown in Figure 4.13, the strong absorption band observed at 1080–1000 cm^{-1} can be ascribed to the tetrahedral T-O-T bond (T can be Si or Al) of symmetrical stretches. Absorption bands at 795-693 cm^{-1} can be assigned to the internal and external asymmetrical stretching of

the T-O tetrahedral linkage of the zeolite framework (Kumaran *et al.*, 2019). However, the absorption peaks around 976 cm^{-1} can also be associated with the Si-O bond stretching from quartz (Krivoshein *et al.*, 2020). The bands 516-515 cm^{-1} and 447-430 cm^{-1} are characteristic peaks of zeolites that are typical of O-Si-O bending mode in membered rings (Sabarish and Unnikrishnan, 2019).

4.9 FESEM micrographs of the as-synthesized zeolites

The morphological features of the as-synthesized zeolites were revealed by Field emission scanning electron microscopy (FESEM) and the results are present in Figure 4.14. Coffin-like shapes were observed for the ZSM-5 zeolite with some portions cracked and in addition to some irregular-shaped particles. Agglomeration of particles was observed in the four samples. All four samples exhibit crystal sizes of about 10 μm and had pores with different sizes which suggests its potential use as an industrial adsorbents and catalysts.

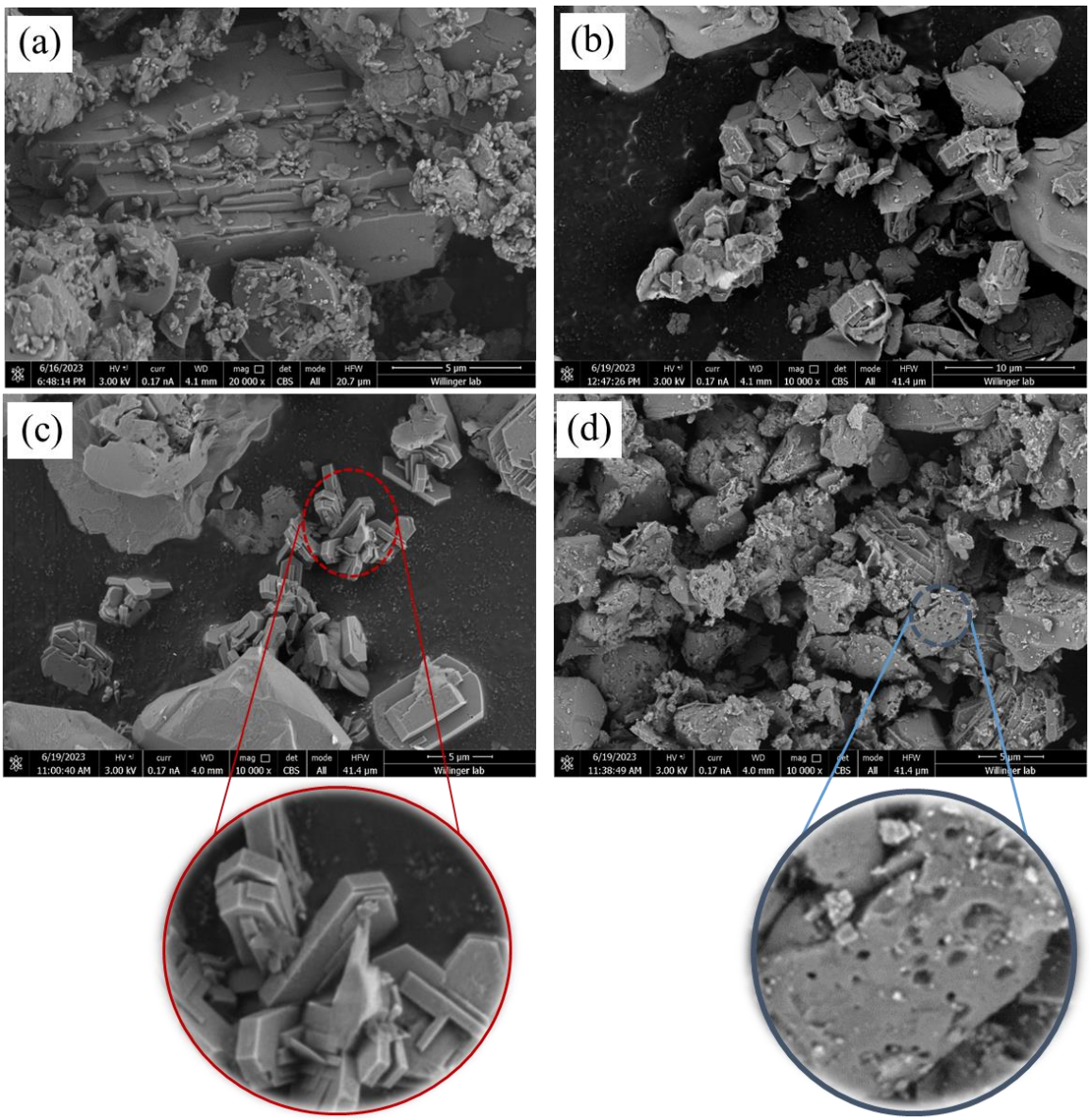

Figure 4.14: FESEM micrograms showing morphologies of as-synthesized ZSM-5 from (a) Anfoega (b) Mfensi (c) Teleku-Bokazo and (d) Tetegu clay

4.10 Effects of synthesis parameters on the ZSM-5 zeolite produced from Tetegu clay

Several synthesis parameters controlled the zeolite phase obtained and its characteristics such as crystallinity and morphology. Understanding the effects of these parameters is crucial for optimizing zeolite synthesis and achieving desired characteristics in terms of crystal structure, surface area, porosity, and catalytic activity. By manipulating these synthesis parameters,

researchers can tailor the properties of zeolites to suit specific applications (Sharma *et al.*, 2008). In this work, the optimal conditions for the synthesis of ZSM-5 from Tetegu clay were further investigated in more detail. The effects of key synthesis parameters including temperature, time, aging conditions, and reactant molar ratios were investigated.

4.10.1 Effects of crystallization temperature

The effects of crystallization temperature on the ZSM-5 phase were studied and the results are presented in Figure 4.15 and Table 4.9.

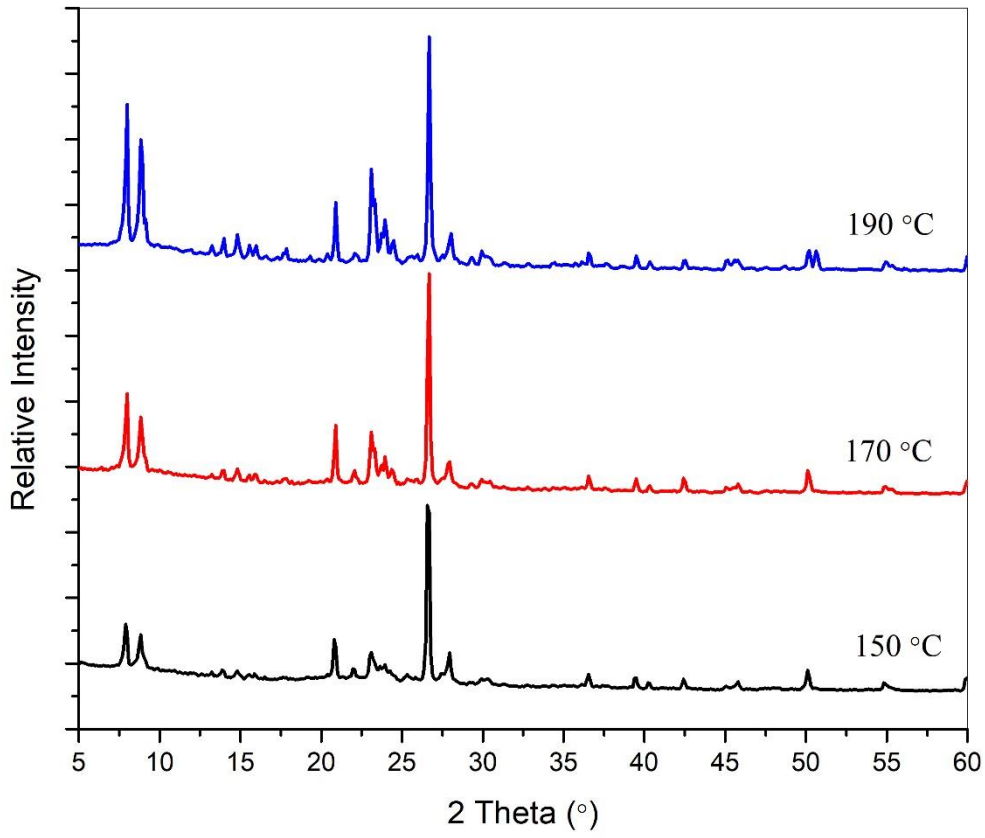

Figure 4.15: XRD patterns of as-synthesized products at different crystallization temperatures.

Table 4.9: Relative crystallinity and crystallite sizes of as-synthesized ZSM-5 phase at different crystallization temperatures.

Crystallization temperature	Relative crystallinity (%)	Crystallite size (nm)
190 °C	61.20	29.60
170 °C	35.04	28.38
150 °C	20.40	25.80

In this experiment, the crystallinity of the synthesized ZSM-5 zeolites was found to be 20.40%, 35.04%, and 61.20% at the crystallization temperatures of 150 °C, 170 °C, and 190 °C, respectively. Higher crystallinity indicates a more ordered structure, with better-defined channels and cages within the zeolite framework (Wuest, 2020). The increase in crystallinity with higher temperatures suggests that the growth and formation of ZSM-5 crystals become more favorable at elevated temperatures.

The crystal sizes were determined as 25.80 nm, 28.38 nm, and 29.60 nm for the ZSM-5 zeolites synthesized at 150 °C, 170 °C, and 190 °C, respectively. The observed trend of increasing crystalline size with increasing crystallization temperature is consistent with the Ostwald ripening phenomenon. Ostwald ripening occurs when smaller crystals dissolve and transfer their material to larger crystals, leading to an increase in average crystal size over time. At higher temperatures, the diffusion of precursor species or reactive intermediates becomes more rapid, leading to enhanced crystal nucleation and growth rates. This results in the formation of larger, more crystalline zeolite particles (Cabane *et al.*, 2005; Van *et al.*, 2018). The choice of crystallization temperature can, therefore, be tailored to control the crystallinity and crystal size

of ZSM-5 zeolites, optimizing their properties for specific applications such as catalysis, adsorption, or molecular sieving.

This result is consistent with another study by Pan *et al*., (2014), who also examined the effects of crystallization temperature on the synthesis of ZSM-5. They found out that crystallinity increases from 150 °C to 190 °C. However, higher temperatures favor the formation rate of quartz phase impurities (Pan *et al.*, 2014).

4.10.2 Effects of crystallization time

The effects of crystallization time on the ZSM-5 phase were studied and the results are presented in Figure 4.16 and Table 4.10.

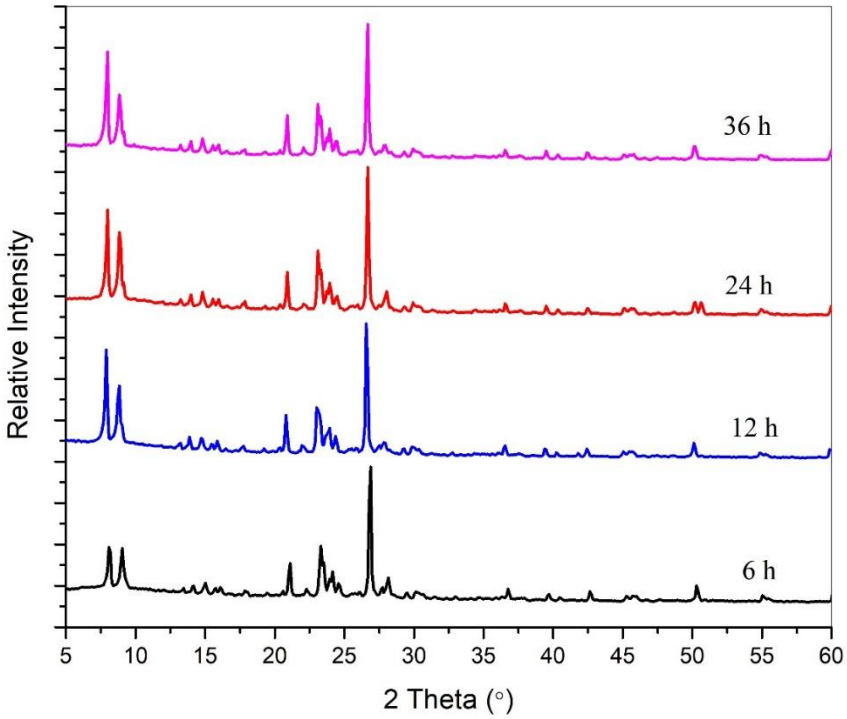

Figure 4.16: XRD patterns of as-synthesized products at different crystallization times.

Table 4.10: Relative crystallinity and crystallite sizes of as-synthesized ZSM-5 phase at different crystallization times.

Crystallization time	Relative crystallinity (%)	Crystallite size (nm)
36 h	56.49	30.70
24 h	61.20	29.60
12 h	56.25	30.43
6 h	43.00	30.36

In this experiment, the effects of crystallization time on the degree of crystallinity and crystal size were studied. The crystallinity values were found to be 43.00%, 56.25%, 61.20%, and 56.49% for the respective crystallization times of 6 h, 12 h, 24 h, and 36 h. The observed trend indicates that the crystallinity initially increases with longer crystallization times, reaching a peak at 24 h, and then decreasing slightly at 36 h. As the reaction progresses and more time is allowed for crystal growth, the crystallinity increases (Grand *et al.*, 2016).

Additionally, the crystal sizes were determined to be 30.36 nm, 30.43 nm, 29.60 nm, and 30.70 nm for the respective crystallization times of 6 h, 12 h, 24 h, and 36 h. The slight variation in crystal size observed in this experiment may be attributed to factors such as crystal growth rates, Ostwald ripening, and aggregation. It is worth noting that the differences in crystal size between the different time points are relatively small. However, the slight variations may be due to the specific reaction kinetics and the balance between crystal nucleation and crystal growth at different time intervals. The overall results suggest that longer crystallization times generally lead to higher crystallinity, indicating a more ordered ZSM-5 structure. However, longer times (36 h and above) may result in some reduction in crystallinity.

The finding in this research is similar to the observation reported by Hartanto *et al*., (2016). They investigated the influence of crystallization time on the crystallinity of ZSM-5 formation from 12 h to 72 h. They found that crystallinity increased from 12 h to 24 h, and decreased at 48 and 72 h (D. Hartanto *et al.*, 2016).

4.10.3 Effects of SiO_2/Al_2O_3 molar ratio

The Si/Al molar ratio is important in ZSM-5 zeolite synthesis due to its influence on the framework composition, crystal growth, acidity, catalytic activity, and stability. Understanding and controlling this ratio allows for the optimization and customization of ZSM-5 zeolite properties for specific applications in the fields of catalysis, adsorption, and molecular sieving (Ren *et al.*, 2019).

In this experiment, the effects of the SiO_2/Al_2O_3 molar ratio on the degree of crystallinity and crystal size of the as-synthesized ZSM-5 phase were investigated. The SiO_2/Al_2O_3 molar ratio of 41.44, 51.97, and 150.73 precursors were obtained from 5 h acid-leached CTTC, 10 h acid-leached CTTC, and 5.0 g of 10 h acid-leached CTTC and additional silica from sodium silicate solution. The results are presented in Figure 4.17 and Table 4.11.

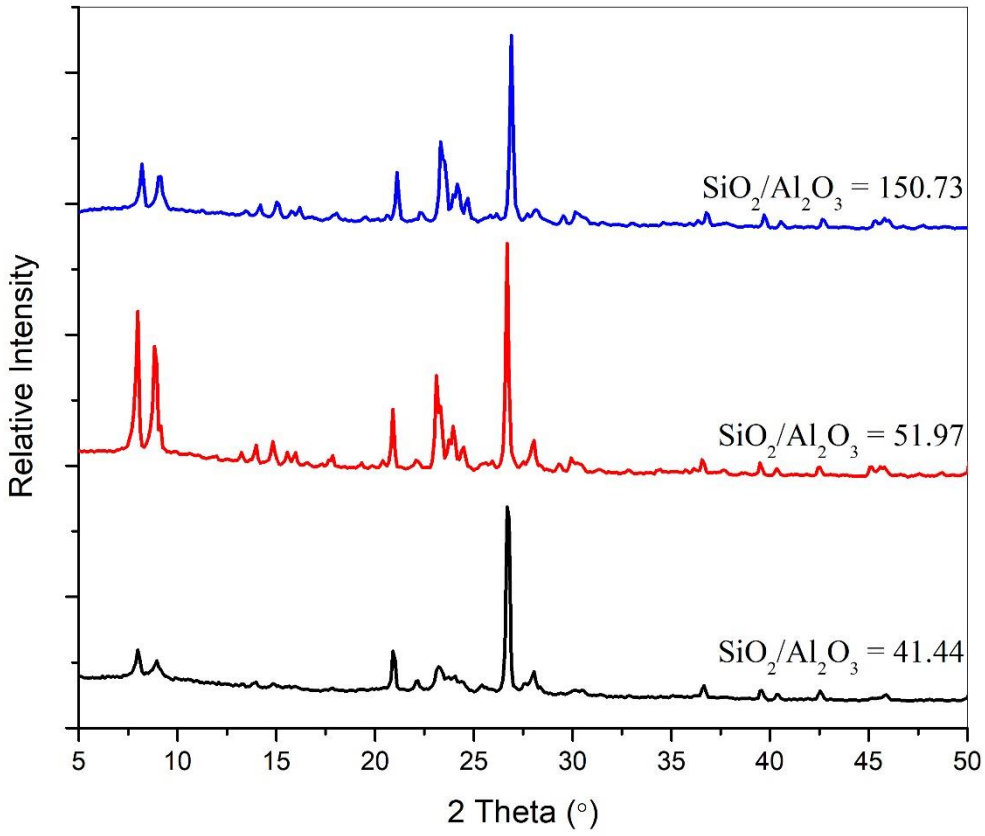

Figure 4.17: XRD patterns of as-synthesized products at different SiO_2/Al_2O_3 molar ratios.

Table 4.11: Relative crystallinity and crystallite sizes of as-synthesized ZSM-5 phase at different SiO_2/Al_2O_3 molar ratios.

	Relative crystallinity (%)	Crystallite size (nm)
SiO_2/Al_2O_3 = 41.44	20.26	19.76
SiO_2/Al_2O_3 = 51.97	61.20	29.60
SiO_2/Al_2O_3 = 150.73	38.18	29.88

The rate of ZSM-5 zeolite crystallization is influenced by the SiO_2/Al_2O_3 molar ratio. Generally, higher SiO_2/Al_2O_3 molar ratios lead to slower crystallization, while lower ratios promote faster crystal growth. A higher aluminum content, which corresponds to lower SiO_2/Al_2O_3 molar ratios, provides more nucleation sites and facilitates faster crystal growth. Higher SiO_2/Al_2O_3 molar ratios are associated with higher crystallinity but smaller crystal sizes, whereas lower SiO_2/Al_2O_3 molar ratios result in lower crystallinity but larger crystals (Shirazi *et al.,* 2008).

In this study, the zeolites synthesized at the SiO_2/Al_2O_3 molar ratios of 41.44, 51.97, and 150.73 exhibited crystallinity of 20.26%, 61.20%, and 38.18%, respectively. The zeolites synthesized at the SiO_2/Al_2O_3 molar ratios of 41.44, 51.97, and 150.73 exhibited crystal sizes of 17 nm, 29.60 nm, and 29.80 nm, respectively. It can be observed that the crystal sizes were smaller at lower molar ratios. A lower SiO_2/Al_2O_3 molar ratio results in a slower rate of crystallization, which produces smaller nanocrystals (Li *et al.*, 2017). This suggests that these conditions might favor the nucleation and growth of smaller crystals during the ZSM-5 synthesis process. In contrast, the higher molar ratio (150) resulted in a slightly larger crystal size, indicating a different growth mechanism or a slower crystal growth rate. The degree of crystallinity rises as the SiO_2/Al_2O_3 molar ratios rise from 41.44 to 51.97, and then fall at a higher ratio (150.73). The decrease in the degree of crystallization can be attributed to an excessively high Na_2O concentration in the reaction mixture (excess sodium contributed by the sodium silicate solution) leading to low crystallization or unreactive amorphous material.

Han *et al.* (2019) investigated the effects of SiO_2/Al_2O_3 ratio at 40, 50, 60, 70, and 80. They observed a gradual increase in crystallinity as the ratio increased, and the highest value of 95% when the ratio was 70 but decreased at the ratio of 80. The decrease was attributed to the fact that high SiO_2/Al_2O_3 ratios deteriorate the crystallinity and favor the growth of α–SiO_2 (Han *et al.*, 2019).

4.10.4 Effects of NaOH/SiO_2 molar ratio

The molar ratio of NaOH to SiO_2 is a crucial variable in the synthesis of ZSM-5 zeolite; NaOH is responsible for the alkalinity (high pH) of the reaction mixture, and the Na^+ cation functions as SDA as well as balance the net charge on the framework (Othman Ali *et al.*, 2011). In this experiment, the effects of the NaOH/SiO_2 molar ratios at 0.016, 0.032, and 0.161 were studied, and the results are displayed in Figure 4.18 and Table 4.12.

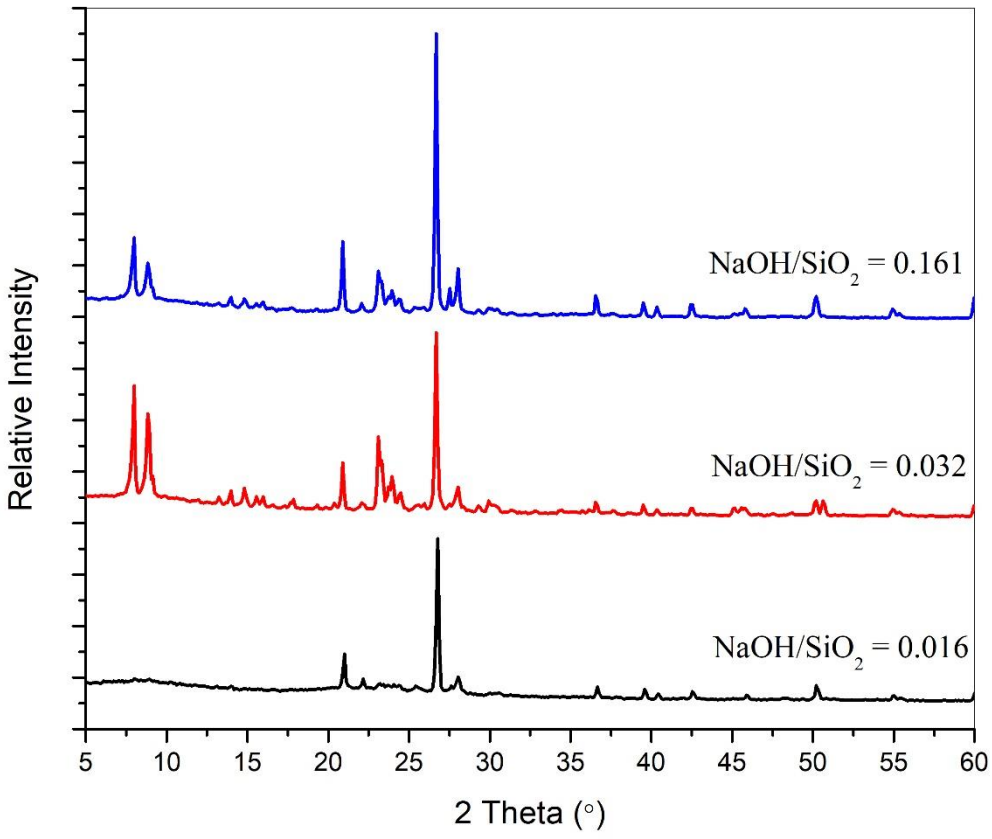

Figure 4.18: XRD patterns of as-synthesized products at different NaOH/SiO_2 molar ratios.

Table 4.12: Relative crystallinity and crystallite sizes of as-synthesized ZSM-5 phase at different $NaOH/SiO_2$ molar ratios.

	Relative crystallinity (%)	Crystallite size (nm)
$NaOH/SiO_2 = 0.016$	NA	NA
$NaOH/SiO_2 = 0.032$	61.20	29.60
$NaOH/SiO_2 = 0.161$	38.65	33.92

NA: Not Applicable (no ZSM-5 phase was detected in the product)

The ZSM-5 phase did not form when the $NaOH/SiO_2$ ratio was low (0.016). This implies that the amount of NaOH in the reaction mixture was insufficient to promote the formation of ZSM-5. Sodium hydroxide acts as a mineralizer in zeolite synthesis, facilitating the formation and stabilization of the desired zeolite structure. The crystallization of ZSM-5 will be hampered and the required phase may not form if there is insufficient NaOH concentration.

For the higher $NaOH/SiO_2$ ratios of 0.032 and 0.161, the ZSM-5 phase was successfully obtained. The resultant zeolites exhibited crystallinity values of 61.20% and 38.65% and crystal sizes of 29.60 nm and 33.92 nm, respectively. A higher $NaOH/SiO_2$ ratio provides a greater amount of NaOH, which aids in the formation and growth of ZSM-5 crystals. However, the low degree of crystallinity observed at high NaOH concentration ($NaOH/SiO_2 = 0.161$) can be attributed to high pH, which is less favorable for ZSM-5 crystallization. Notably, this extremely high pH favored the crystallization of the quartz phase, which is shown in the intensification of the peak at $2\theta = 26.71°$. This suggests that quartz is a competitive phase in the reaction process.

Previous research by Jiang *et al*. (2014) observed a decrease in the intensity of characteristics diffraction peaks of the ZSM-5 phase when Na_2O/SiO_2 was increased from 0.12 to 0.35 and

finally 0.47. Practically, the characteristic peaks disappeared at a ratio of 0.47. They also reported a decrease in ZSM-5 crystal sizes with higher Na_2O/SiO_2 molar ratios. They suggested that the low quality of the products at high NaOH concentration can be ascribed to the high dissolution of amorphous silica in the reaction mixture (Jiang *et al.*, 2014).

4.10.5 Effects of $TPABr/SiO_2$ molar ratio

The effects of TPABr concentration in the form of $TPABr/SiO_2$ on the ZSM-5 phase were studied and the results are presented in Figure 4.19 and Table 4.13.

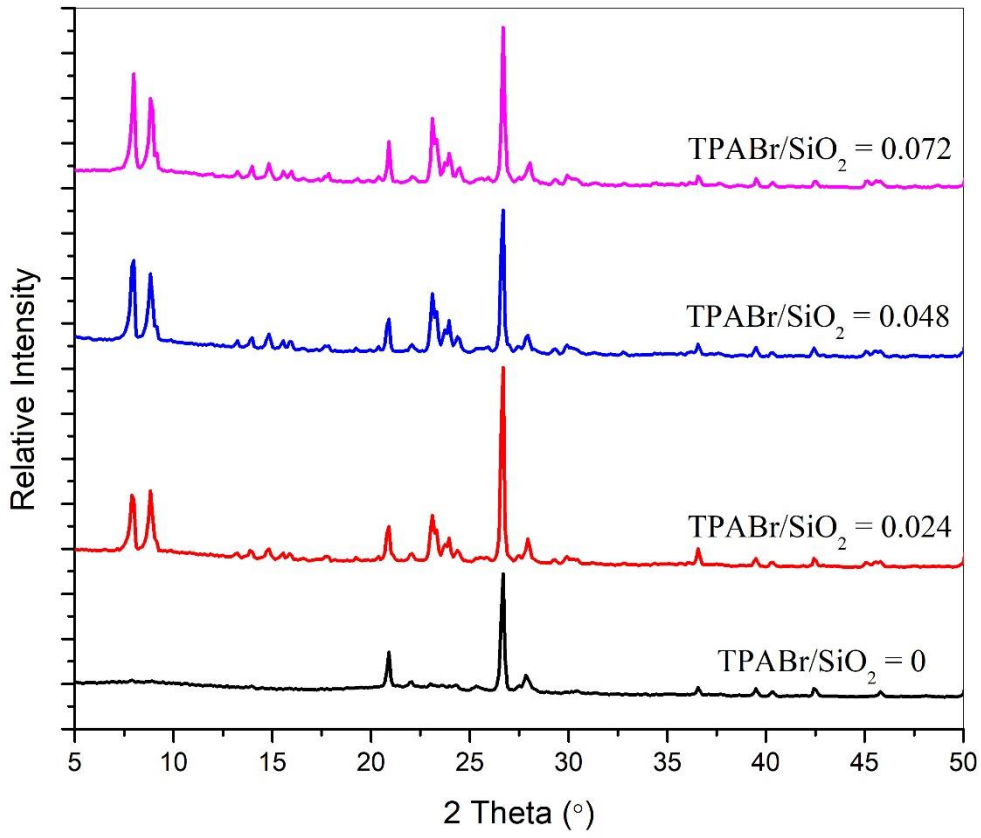

Figure 4.19: XRD patterns of as-synthesized products at different $TPABr/SiO_2$ molar ratios.

Table 4.13: Relative crystallinity and crystallite sizes of as-synthesized products at different $TPABr/SiO_2$ molar ratios.

	Relative crystallinity (%)	Crystallite size (nm)
$TPABr/SiO_2 = 0.000$	NA	NA
$TPABr/SiO_2 = 0.024$	46.06	31.26
$TPABr/SiO_2 = 0.048$	57.82	30.10
$TPABr/SiO_2 = 0.072$	61.20	29.60

NA: Not Applicable (no ZSM-5 phase was detected in the product)

The results show that a key factor in the production of ZSM-5 zeolite is the $TPABr/SiO_2$ molar ratio. ZSM-5 phase formation was not observed when TPABr was not present ($TPABr/SiO_2 = 0$). TPABr is required for the formation of the desired zeolite structure, which acts as a structure-directing agent. The zeolites synthesized with $TPABr/SiO_2$ ratios of 0.024, 0.048, and 0.072 exhibit increasing crystallinity values of 46%, 57%, and 61.20%, respectively. Raising the $TPABr/SiO_2$ molar ratio causes the degree of crystallinity to increase. This implies that higher concentrations of TPABr promote the formation of a well-crystallized ZSM-5 zeolite.

Additionally, as the $TPABr/SiO_2$ molar ratio increased, the size of the ZSM-5 zeolite crystals decreased. This finding implies that the production of smaller zeolite crystals is a result of higher TPABr concentrations. The crystal size values of 31.26 nm, 30.10 nm, and 29.60 nm indicate a trend towards finer particles as the molar ratio increased. This is because TPABr molecules control the nucleation and growth of the zeolite crystals. Higher TPABr concentrations can cause more nucleation events, slower crystal growth, and leading to smaller crystal sizes (Bozhilov *et al.*, 2021). Smaller crystal sizes can be desirable for various

applications, such as catalysts, as they provide a larger surface area for catalytic reactions, better accessibility for reactant molecules, and longer lifetimes (Zhang *et al.,* 2018).

It can also be observed from Figure 4.19 that, the crystallinity of the quartz phase decreases as the TPABr concentration increases ($TPABr/SiO_2$ = 0.024, 0.048, and 0.072), which is evidenced in the intensification of the peak at $2\theta = 26.71°$. However, for the four experiments, when the $TPABr/SiO_2 = 0.00$, the intensity of the peak at $2\theta = 26.71°$ is at its minimum. This suggests quartz is a competitive phase in the synthesis of ZSM-5 zeolite when using Tetegu clay. It is important to note that although the synthesis of ZSM-5 at high concentrations of TPABr is preferable, efforts are being made to decrease its use due to the pollution it generates when it is removed by calcination.

4.10.6 Effects of H_2O/SiO_2 molar ratio

Water is essential for the nucleation and crystal growth of ZSM-5 zeolite. Water acts as a solvent for the dissolution of silica and alumina sources, along with other additives or templates. The amount of water used determines the concentration of the reactants in the reaction medium can influence the kinetics, phase transformation, and crystallization of the zeolite. In this experiment, the effects of water content on the synthesis of ZSM-5 were investigated at H_2O/SiO_2 = 7.14, 25.00, and 50.00. The results are illustrated in Figure 4.20 and Table 4.14.

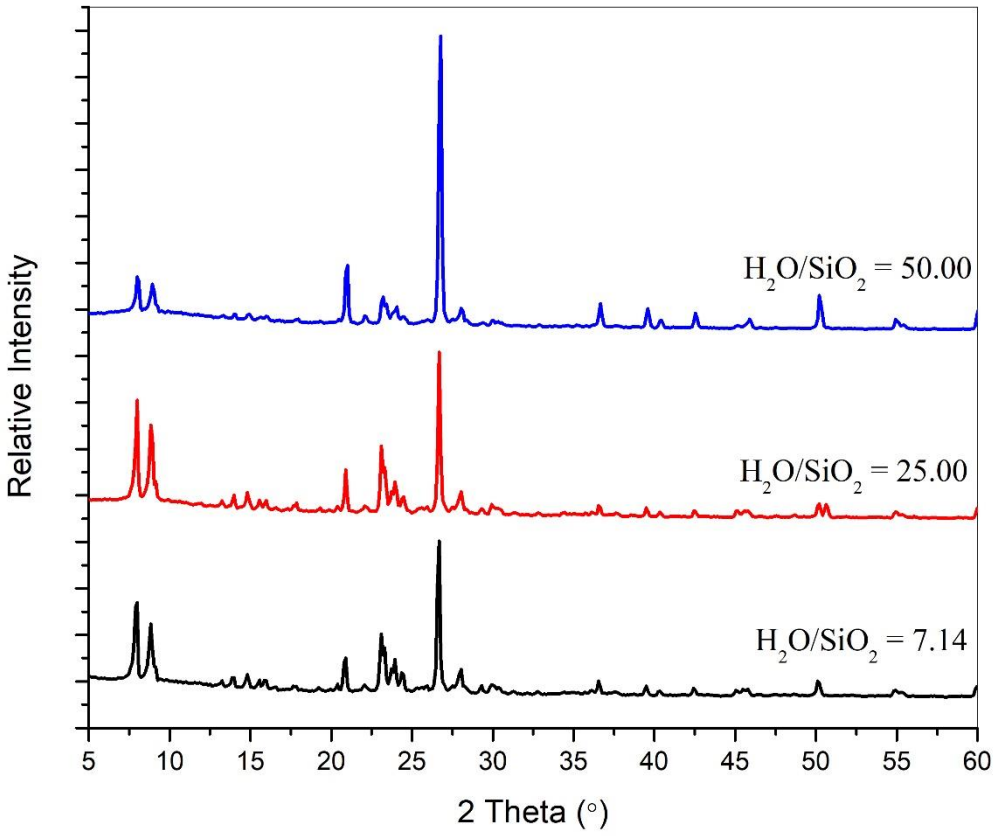

Figure 4.20: XRD patterns of as-synthesized products at different H_2O/SiO_2 molar ratios.

Table 4.14: Relative crystallinity and crystallite sizes of as-synthesized ZSM-5 phase at different H_2O/SiO_2 molar ratios.

	Relative crystallinity (%)	Crystallite size (nm)
H_2O/SiO_2 = 7.14	53.25	31.92
H_2O/SiO_2 = 25.00	61.20	29.60
H_2O/SiO_2 = 50.00	30.26	26.84

For the corresponding H_2O/SiO_2 molar ratios of 7.14, 25.00, and 50.00, the relative crystallinities were determined to be 53.25%, 61.20%, and 30.26%, respectively. The observed trend suggests that crystallinity increases from 7.14 to 25.00 in the H_2O/SiO_2 molar ratio before falling at a higher molar ratio of 50.0. This pattern suggests that, in comparison to the lower (7.14) and higher (50.0) molar ratios, the middle (25.00) molar ratio promotes better crystallinity. A small amount of water content means a concentrated system that provides a high degree of supersaturation that is favorable for nucleation and crystal growth. Conversely at high water content ($H_2O/SiO_2 = 50$), the concentration of reactants decreases which results in a low supersaturation and hinders the crystallinity process. Additionally, the pH of the reaction mixture has changed to an unfavorable pH due to the high water content. This excessively high molar ratio may have caused more dissolution and recrystallization, which could have decreased the overall crystallinity. On the contrary, this condition favors the crystallization of the competitive quartz phase. This is evidenced in the dramatic increase in the characteristic peak of quartz at $2\theta = 26.71°$.

For the given H_2O/SiO_2 molar ratios of 7.14, 25.00, and 50.0, the crystal sizes were 31.92 nm, 29.60 nm, and 26.84 nm respectively. The pattern shown indicates that the crystal size reduces with increasing H_2O/SiO_2 molar ratio. Excess water acts as a dispersing agent and promotes nucleation, preventing the agglomeration and growth of zeolite crystals during synthesis.

Hartanto *et al*., (2017) studied the effect of H_2O/SiO_2 molar ratios on the crystallinity and crystal sizes of ZSM-5. They reported an increase in crystallinity from 49.88% to 55.49% to 59.44% when the H_2O/SiO_2 molar ratios were 15, 25, and 30, respectively. However, the crystallinity fell to 8.52% when the ratio was increased to 35. These findings agreed with each other. They used SEM to further determine the crystal sizes, and they found that the crystal sizes grew to 2.684 μm, 3.562 μm, and 3.795 μm when the H_2O/SiO_2 molar ratios were 15, 25, and 30, respectively (Hartanto *et al.*, 2017).

4.10.7 Effects of aging conditions

Aging refers to the period during which the reaction mixture is allowed to stand before being subjected to hydrothermal treatment for crystallization to occur. Aging is a crucial step in the synthesis of ZSM-5, as its conditions influence the crystal size, morphology, and crystallinity of the resulting zeolite. The extent of precursor hydrolysis, depolymerization, and nucleation depends on the aging conditions. Longer aging times often result in larger crystal sizes and improved crystallinity. Mechanical stirring during aging can enhance the homogeneous nucleation and crystal growth process. Different aging conditions may result in different zeolite morphology such as different crystal shapes. In this experiment, the effects of mechanical stirring and aging for varying periods on the degree of crystallization and crystallite size of the ZSM-5 phase were studied. The results are illustrated in Figure 4.21 and Table 4.15.

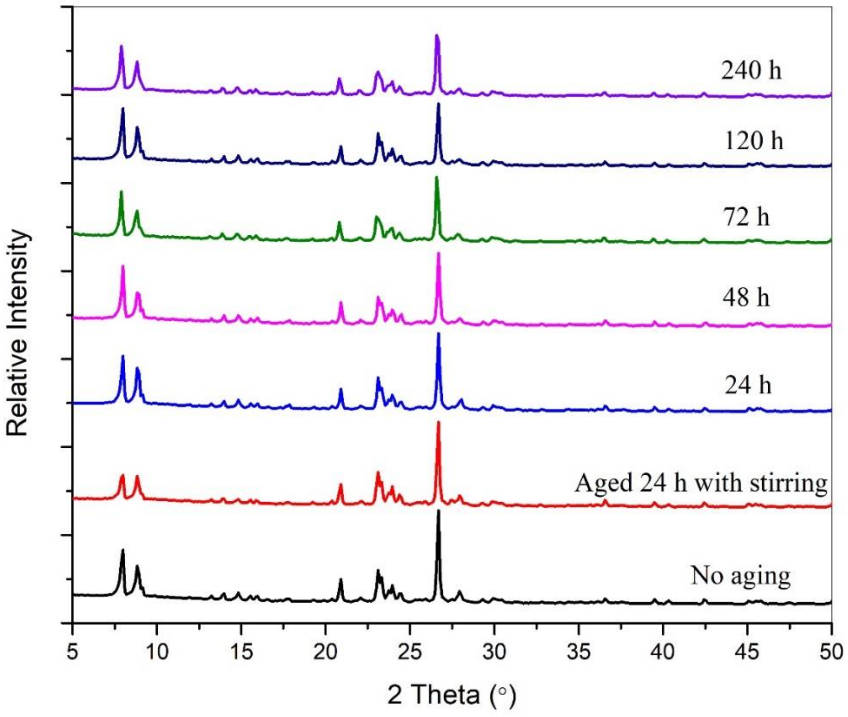

Figure 4.21: XRD patterns of as-synthesized products at different aging conditions.

Table 4.15: Relative crystallinity and crystallite sizes of as-synthesized ZSM-5 phase at different aging conditions.

Aging condition	Relative crystallinity (%)	Crystallite size (nm)
Aged for 24 h with stirring	48.32	32.42
0 h	60.35	32.00
24 h	61.20	29.60
48 h	58.47	35.65
72 h	51.67	34.16
120 h	62.39	33.42
240 h	54.16	35.90

The results (see Figure 4.21) show that the intensity of the characteristic of quartz at $2\theta = 26.71°$ decreases slightly with the aging period from 0 to 240 h. The prolonged aging time decreases the crystallinity of the quartz phase. This implies that the extended aging time influences the quartz phase formation, probably resulting in decreased crystallinity or the transformation of quartz into amorphous material.

In the study, crystallinity and crystal size were examined for two distinct aging conditions: aging with stirring and aging without stirring for 24 h. The results obtained show that as compared to aging with stirring (32.42%), aging without stirring produced greater crystallinity values (61.20%). For the aging process with stirring and aging without stirring, the crystallite sizes were found to be 29.60 nm and 32.42 nm, respectively. These imply that a higher degree

of crystallization and smaller crystal size is promoted in the ZSM-5 zeolite synthesis in the absence of stirring during aging.

The relative crystallinity values obtained for the different aging time durations without stirring are as follows: 60.35%, 61.20%, 58.47%, 51.67%, 62.39%, and 54.16% for aging times of 0, 24, 48, 72, 120, and 240 h, respectively. Regarding crystallite sizes, 32.00 nm, 29.60 nm, 35.65 nm, 34.16 nm, 33.42 nm, and 35.90 nm crystallite sizes were obtained for the aging time durations of 0, 24, 48, 72, 120, and 240 h, respectively. The ZSM-5 zeolite synthesized from clay exhibits varied crystallite sizes with different aging times. No clear trend is discernible in the data, indicating that the aging time does not consistently influence the crystallite sizes of the synthesized material. However, it is worth noting that the crystallite sizes generally range between 29.60 nm and 35.90 nm, suggesting a relatively uniform size distribution within the samples.

4.10.8 Effects of calcination after acid leaching

The quartz phase persisted in all the zeolite products obtained in the previous experiments. In this experiment, the impact of heat treatment of the acid-leached Tetegu clay at 800 °C on the zeolite product obtained after synthesis was studied. The results are illustrated in Figure 4.22 and Table 4.16.

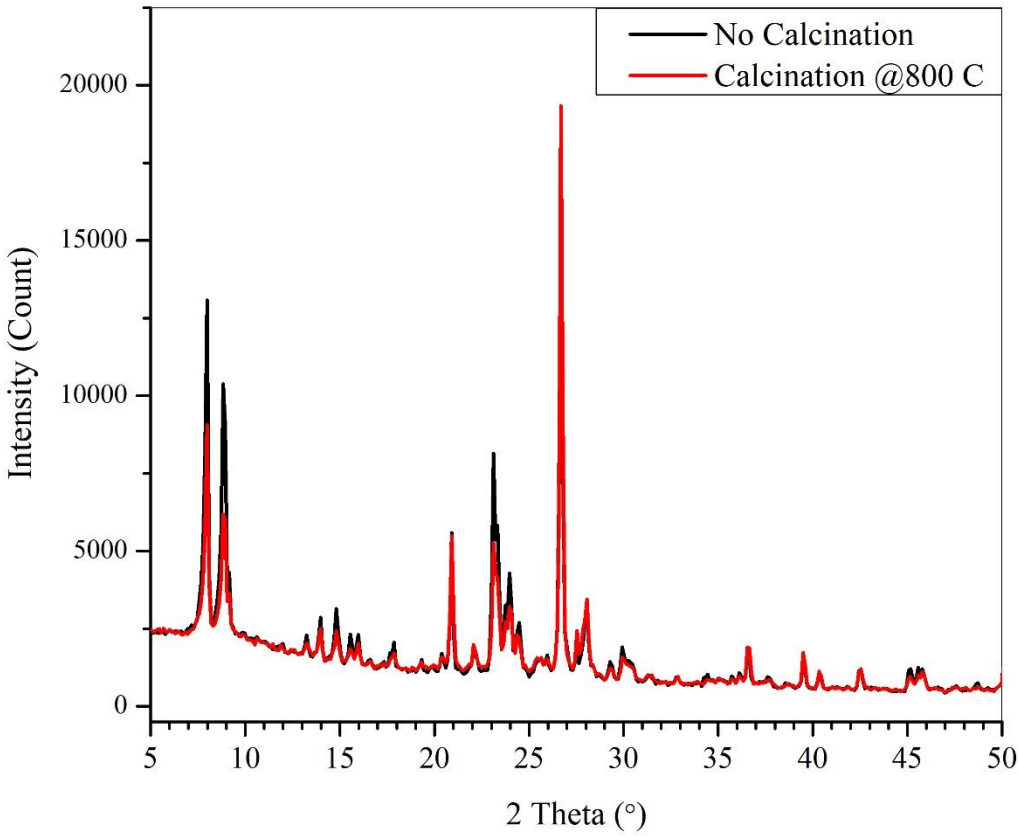

Figure 4.22: XRD diffraction patterns of as-synthesized products: without calcination (black) and with calcination (red) after dealumination.

Table 4.16: Relative crystallinity and crystallite sizes of as-synthesized ZSM-5 phase with and without calcination after dealumination.

	Relative crystallinity (%)	Crystallite size (nm)
No calcination	61.20	29.60
Calcination at 800 ^{o}C	39.69	31.12

The experimental results indicate that the calcined sample exhibited an increased crystallinity of the quartz phase compared to the non-calcined sample in the zeolite products. The observed increase in crystallinity of the quartz phase in the resulting product from the calcined sample suggests that the heat treatment at 800 °C affected the structural organization of the quartz crystals. It can be inferred that the heat facilitated the rearrangement of atoms within the crystal lattice, leading to a more ordered structure, which was stable during the synthesis.

The crystallinity of the ZSM phase obtained was 39.69% for the calcined sample and 61.20% for the non-calcined precursors. Additionally, the crystal size for the synthesized ZSM phase was determined as 31.12 nm for the calcined sample and 29.60 nm for the non-calcined sample. The result indicates that the calcination after the acid leaching is not a favorable process for the synthesis of ZSM-5 from Tetegu clay.

CHAPTER FIVE

CONCLUSIONS AND RECOMMENDATIONS

5.1 Conclusion

According to the results obtained, all four samples of clay - Anfoega, Mfensi, Teleku-Bokazo, and Tetegu - are rich in silica and alumina, which are desirable for the synthesis of zeolite. The dominant clay mineral is kaolinite, and Tetegu was found to contain the highest quantity of kaolinite among the four. Quartz is present in all four clay deposits in significant quantities and this reduces the quality of the clays for zeolite synthesis. The physical and chemical properties of each clay were discovered to vary, necessitating particular pretreatment procedures for ZSM-5 production. The results obtained showed that calcined Anfoega clay must be treated with 6 M HCl solution for 24 h to raise the SiO_2/Al_2O_3 ratio to a suitable ratio for ZSM-5 synthesis. On the other hand, Teleku-Bokazo clay needs 24 h of 8 M HCl treatment to raise the SiO_2/Al_2O_3 ratio to a desirable level for ZSM-5 production. Tetegu and Mfensi clay were made suitable for ZSM-5 production by calcination at 800 °C for 2 h, followed by 10 h of acid treatment. The Anfoega, Mfensi, Teleku-Bokazo, and Tetegu clay deposits have been shown by experimental results to be suitable sources of clay minerals for the production of nano-crystalline ZSM-5 zeolite. Notably, Tetegu clay has been demonstrated to be the most suitable clay among the four for the synthesis of ZSM-5 zeolite, primarily because of the substantial quantity of kaolinite in this clay. This work will pave the way for many other studies to improve the pre-treatment processes and the synthesis conditions of ZSM-5 zeolite using each of these clays.

The results obtained from the optimization of the synthesis conditions of ZSM-5 using Tetegu clay revealed that each parameter has a significant impact on the phase obtained. Higher crystallization temperature during ZSM-5 synthesis leads to higher crystallinity and larger

crystal sizes. Longer crystallization times generally lead to higher crystallinity, indicating a more ordered ZSM-5 structure. However, longer times (36 h and above) may result in some reduction in crystallinity. It was observed that NaOH is required to obtain the ZSM-5 phase, and low concentration hampers the formation of the desired phase. Higher $NaOH/SiO_2$ ratios promote the formation and growth of ZSM-5 crystals, resulting in increased crystallinity and larger crystal sizes. Another crucial parameter is TPABr concentration, which is required for the formation of the ZSM-5 zeolite framework. The findings show that both the crystallinity and crystal size of the produced ZSM-5 zeolite are considerably influenced by the $TPABr/SiO_2$ molar ratio. The development of well-crystallized zeolite structures with smaller crystal sizes is encouraged by higher TPABr concentrations. These findings highlight the role of TPABr as a structure-directing agent. It is noteworthy that, quartz is a competitive phase in the synthesis of ZSM-5 zeolite when using Tetegu clay that withstands all the synthesis conditions. The optimal conditions for the synthesis of nano-crystallite ZSM-5 zeolite from the Tetegu clay were found to be: a molar ratio of SiO_2/Al_2O_3 = 51.97, $NaOH/SiO_2$ = 0.032, $TPABr/SiO_2$ = 0.072, H_2O/SiO_2 = 25; crystallization temperature = 190 °C; crystallization time = 24 h, with aging at room temperature in a static condition for 24 h.

This study has established the viability of Anfoega, Mfensi, Teleku-Bokazo, and Tetegu clays as starting materials for the synthesis of ZSM-5 zeolite, and the appropriate optimal production conditions were established for Tetegu clay. Although this work has provided useful insight on this subject, further characterizations, and testing are required to completely understand the effects of the synthesis conditions on the morphology, and the catalytic potential of the as-synthesized zeolites.

5.2 Recommendations

Presented below are some future research recommended.

1. Further studies are recommended on how to remove quartz from the clay samples or get rid of it in the final products.
2. Additionally, more research should investigate the effects of synthesis conditions on Anfoega, Mfensi, and Teleku-Bokazo clays in detail, and finally optimize the conditions for ZSM-5 zeolite synthesis on an industrial scale.
3. The applications of these zeolites as catalysts, adsorbents, and ion exchangers should be studied and developed at the industrial level.
4. In particular, the application of these zeolites as solid acid catalysts for the catalytic conversion of plastic waste into fuel is strongly recommended.
5. In addition to these four clay deposits, Ghana is endowed with many other clay deposits across all regions and they should be explored for ZSM-5 zeolite production.

REFERENCES

Abdelmoneim, A. A., Abdul-Moneim, M., Geies, A. A., & Farghaly, S. O. (2020). Synthesis, characterization and application of analcime to control nitrate ions from the ground water samples from Wadi El-Assiuti – Egypt as a low-cost and locally available adsorbent. *IOP Conference Series: Materials Science and Engineering*, *975*(1), 012013. https://doi.org/10.1088/1757-899X/975/1/012013

Abdullahi, T., Harun, Z., & Othman, M. H. D. (2017). A review on sustainable synthesis of zeolite from kaolinite resources *via* hydrothermal process. *Advanced Powder Technology*, *28*(8), 1827–1840. https://doi.org/10.1016/j.apt.2017.04.028

Aboudi Mana, S. C., Hanafiah, M. M., & Chowdhury, A. J. K. (2017). Environmental characteristics of clay and clay-based minerals. *Geology, Ecology, and Landscapes*, *1*(3), 155–161. https://doi.org/10.1080/24749508.2017.1361128

Abubakar, A., & Abubakar, S. (2020). Synthesis and characterization of ZSM-5 zeolite using ethelinediammine as organic template: *via* hydrothermal process. *FUDMA Journal of Sciences (FJS)*, *4*(3), 476–480. https://doi.org/10.33003/fjs-2020-0403-338

Adeniyi, F. I., Ogundiran, M. B., Hemalatha, T., & Hanumantrai, B. B. (2020). Characterization of raw and thermally treated Nigerian kaolinite-containing clays using instrumental techniques. *SN Applied Sciences*, *2*(5), 821. https://doi.org/10.1007/s42452-020-2610-x

Adeyemo, A. A., Adeoye, I. O., & Bello, O. S. (2017). Adsorption of dyes using different types of clay: a review. *Applied Water Science*, *7*(2), 543–568. https://doi.org/10.1007/s13201-015-0322-y

Afridi, P., Siddiqui, F. A., Gonzalez-Cortes, S., & France, L. (2021). An innovative synthesis of Nano-ZSM-5 zeolite through interrupted ultrasound. *Journal of Ongoing Chemical*

Research, *6*(1), 15–23. https://doi.org/10.5281/zenodo.5564497

Aghris, S., Laghrib, F., Koumya, Y., El Kasmi, S., Azaitraoui, M., Farahi, A., Sajieddine, M., Bakasse, M., Lahrich, S., & El Mhammedi, M. A. (2021). Exploration of a new source of sustainable aluminosilicate clay minerals from Morocco: Mineralogical and physico-chemical characterizations for clear upcoming applications. *Journal of Inorganic and Organometallic Polymers and Materials*, *31*(7), 2925–2938. https://doi.org/10.1007/s10904-021-01950-1

Aguilar-Mamani, W., García, G., Hedlund, J., & Mouzon, J. (2014). Comparison between leached metakaolin and leached diatomaceous earth as raw materials for the synthesis of ZSM-5. *SpringerPlus*, *3*(1), 1–10. https://doi.org/10.1186/2193-1801-3-292

Al-Jubouri, S. M., Al-Batty, S. I., & Holmes, S. M. (2021). Using the ash of common water reeds as a silica source for producing high purity ZSM-5 zeolite microspheres. *Microporous and Mesoporous Materials*, *316*(January), 110953. https://doi.org/10.1016/j.micromeso.2021.110953

Alipour, S. M., Halladj, R., & Askari, S. (2014). Effects of the different synthetic parameters on the crystallinity and crystal size of nanosized ZSM-5 zeolite. *Reviews in Chemical Engineering*, *30*(3), 171315. https://doi.org/10.1515/revce-2014-0008

Althoff, R., Unger, K., & Schüth, F. (1994). Is the formation of a zeolite from a dry powder *via* a gas phase transport process possible? *Microporous Materials*, *2*(6), 557–562. https://doi.org/10.1016/0927-6513(94)E0027-R

Amoanyi, R., Kwawukume, P. S., & Momade, F. W. Y. (2012). Improving the strength properties of Afari and Mfensi clays by chemical stabilization. *International Journal of Engineering Research in Africa*, *8*(August), 1–15. https://doi.org/10.4028/www.scientific.net/JERA.8.1

Asamoah, R. B., Nyankson, E., Annan, E., Agyei-Tuffour, B., Efavi, J. K., Kan-Dapaah, K., Apalangya, V. A., Damoah, L. N. W., Dodoo-Arhin, D., Tiburu, E. K., Kwofie, S. K., Onwona-Agyeman, B., & Yaya, A. (2018). Industrial applications of clay materials from Ghana (a review). *Oriental Journal of Chemistry*, *34*(4), 1719–1734. https://doi.org/10.13005/ojc/340403

Asgar Pour, Z., & Sebakhy, K. O. (2022). A review on the effects of organic structure-directing agents on the hydrothermal synthesis and physicochemical properties of zeolites. *Chemistry*, *4*(2), 431–446. https://doi.org/10.3390/chemistry4020032

ASTM D422. (2007). *Standard test method for particle-size analysis of soils*. 1–8.

Awasthi, A., Jadhao, P., & Kumari, K. (2019). Clay nano-adsorbent: structures, applications and mechanism for water treatment. *SN Applied Sciences*, *1*(9), 1076. https://doi.org/10.1007/s42452-019-0858-9

Azizi, S. N., Alavi, D. A., & Abrishamkar, M. (2013). Phase transformation of zeolite P to Y and Analcime zeolites due to changing the time and temperature. *Journal of Spectroscopy*, *2013*(1), 1–5. https://doi.org/10.1155/2013/428216

Bacakova, L., Vandrovcova, M., Kopova, I., & Jirka, I. (2018). Applications of zeolites in biotechnology and medicine – a review. *Biomaterials Science*, *6*(5), 974–989. https://doi.org/10.1039/C8BM00028J

Baile, P., Fernández, E., Vidal, L., & Canals, A. (2019). Zeolites and zeolite-based materials in extraction and microextraction techniques. *The Analyst*, *144*(2), 366–387. https://doi.org/10.1039/C8AN01194J

Bayati, B., Babaluo, A. A., & Karimi, R. (2008). Hydrothermal synthesis of nanostructure NaA zeolite: The effect of synthesis parameters on zeolite seed size and crystallinity. *Journal*

of the European Ceramic Society, *28*(14), 2653–2657. https://doi.org/10.1016/j.jeurceramsoc.2008.03.033

Bediako, M., & Valentini, L. (2022). Strength performance and life cycle assessment of high-volume low-grade kaolin clay pozzolan concrete: A Ghanaian scenario. *Case Studies in Construction Materials*, *17*, e01679. https://doi.org/10.1016/j.cscm.2022.e01679

Belaabed, R., Elknidri, H., Elkhalfaouy, R., Addaou, A., Laajab, A., & Lahsini, A. (2017). Zeolite Y synthesis without organic template: The effect of synthesis parameters. *J. Mater. Environ. Sci*, *8*(10), 3550-3555.

Bibi, I., Icenhower, J., Niazi, N. K., Naz, T., Shahid, M., & Bashir, S. (2016). Clay Minerals. In *Environmental Materials and Waste* (pp. 543–567). Elsevier. https://doi.org/10.1016/B978-0-12-803837-6.00021-4

Bortolini, H. R., Lima, D. S., & Perez-Lopez, O. W. (2020). Hydrothermal synthesis of analcime without template. *Journal of Crystal Growth*, *532*(December 2019), 125424. https://doi.org/10.1016/j.jcrysgro.2019.125424

Bozhilov, K. N., Le, T. T., Qin, Z., Terlier, T., Palčić, A., Rimer, J. D., & Valtchev, V. (2021). Time-resolved dissolution elucidates the mechanism of zeolite MFI crystallization. *Science Advances*, *7*(25), 1–11. https://doi.org/10.1126/sciadv.abg0454

Bunaciu, A. A., Udriştioiu, E. gabriela, & Aboul-Enein, H. Y. (2015). X-ray diffraction: Instrumentation and applications. *Critical Reviews in Analytical Chemistry*, *45*(4), 289–299. https://doi.org/10.1080/10408347.2014.949616

Cabane, H., Laporte, D., & Provost, A. (2005). An experimental study of Ostwald ripening of olivine and plagioclase in silicate melts: implications for the growth and size of crystals in magmas. *Contributions to Mineralogy and Petrology*, *150*(1), 37–53.

https://doi.org/10.1007/s00410-005-0002-2

Cai, R., Liu, Y., Gu, S., & Yan, Y. (2010). Ambient pressure dry-del conversion method for zeolite MFI synthesis using ionic liquid and microwave heating. *Journal of the American Chemical Society*, *132*(37), 12776–12777. https://doi.org/10.1021/ja101649b

Cao, Y., Wang, Y., Zhang, Z., Ma, Y., & Wang, H. (2021). Turning sandstone clay into supplementary cementitious material: activation and pozzolanic reactivity evaluation. *Composites Part B: Engineering*, *223*(July), 109137. https://doi.org/10.1016/j.compositesb.2021.109137

Cataldo, E., Salvi, L., Paoli, F., Fucile, M., Masciandaro, G., Manzi, D., Masini, C. M., & Mattii, G. B. (2021). Application of zeolites in agriculture and other potential uses: A Review. *Agronomy*, *11*(8), 1547. https://doi.org/10.3390/agronomy11081547

Chawla, A., Li, R., Jain, R., Clark, R. J., Sutjianto, J. G., Palmer, J. C., & Rimer, J. D. (2018). Cooperative effects of inorganic and organic structure-directing agents in ZSM-5 crystallization. *Molecular Systems Design & Engineering*, *3*(1), 159–170. https://doi.org/10.1039/C7ME00097A

Chen, J., Ma, H., Liu, C., & Yuan, J. (2017). Synthesis of Analcime crystals and simultaneous potassium extraction from natrolite syenite. *Advances in Materials Science and Engineering*, *2017*, 1–9. https://doi.org/10.1155/2017/2617597

Chen, O., Liu, S. C., Zhang, P. Q., & Zheng, S. Q. (2021). Green synthesis and application of ZSM-5 zeolite. *Kemija u Industriji*, *70*(3–4), 121–127. https://doi.org/10.15255/kui.2020.041

Chen, X., & Peng, Y. (2018). Managing clay minerals in froth flotation—A critical review. *Mineral Processing and Extractive Metallurgy Review*, *39*(5), 289–307.

https://doi.org/10.1080/08827508.2018.1433175

Cheng, Xing, Bu, Zhang, Piao, Huang, Xie, & Wang. (2019). Dehydroxylation and structural distortion of kaolinite as a high-temperature sorbent in the furnace. *Minerals*, *9*(10), 587. https://doi.org/10.3390/min9100587

Cheng, Y., Liao, R. H., Li, J. S., Sun, X. Y., & Wang, L. J. (2008). Synthesis research of nanosized ZSM-5 zeolites in the absence of organic template. *Journal of Materials Processing Technology*, *206*(1–3), 445–452. https://doi.org/10.1016/j.jmatprotec.2007.12.054

Chin, C. L., Ahmad, Z. A., & Sow, S. S. (2017). Relationship between the thermal behaviour of the clays and their mineralogical and chemical composition: Example of Ipoh, Kuala Rompin and Mersing (Malaysia). *Applied Clay Science*, *143*(April 2016), 327–335. https://doi.org/10.1016/j.clay.2017.03.037

Coats, A. W., & Redfern, J. P. (1964). Kinetic parameters from thermogravimetric data. *Nature*, *201*(4914), 68–69. https://doi.org/10.1038/201068a0

Cocchi, M., Angelis, D. De, Mazzeo, L., Nardozi, P., Piemonte, V., Tuffi, R., & Vecchio Ciprioti, S. (2020). Catalytic pyrolysis of a residual plastic waste using zeolites produced by coal fly ash. *Catalysts*, *10*(10), 1113. https://doi.org/10.3390/catal10101113

Cohen, D., & Ward, C. R. (1991). Sednorm - A program to calculate a normative mineralogy for sedimentary rocks based. *Computers & Geosciences*, *17*(9), 1235–1253.

Collins, F., Rozhkovskaya, A., Outram, J. G., & Millar, G. J. (2020). A critical review of waste resources, synthesis, and applications for Zeolite LTA. *Microporous and Mesoporous Materials*, *291*(March 2019), 109667. https://doi.org/10.1016/j.micromeso.2019.109667

Cooper, E. R., Andrews, C. D., Wheatley, P. S., Webb, P. B., Wormald, P., & Morris, R. E.

(2004). Ionic liquids and eutectic mixtures as solvent and template in synthesis of zeolite analogues. *Nature*, *430*(7003), 1012–1016. https://doi.org/10.1038/nature02860

Csicsery, S. M. (1984). Shape-selective catalysis in zeolites. *Zeolites*, *4*(3), 202–213. https://doi.org/10.1016/0144-2449(84)90024-1

Cundy, C. S., & Cox, P. A. (2005). The hydrothermal synthesis of zeolites: Precursors, intermediates and reaction mechanism. *Microporous and Mesoporous Materials*, *82*(1–2), 1–78. https://doi.org/10.1016/j.micromeso.2005.02.016

Dai, C., Li, J., Zhang, A., Nie, C., Song, C., & Guo, X. (2017). Precise control of the size of zeolite B-ZSM-5 based on seed surface crystallization. *RSC Advances*, *7*(60), 37915–37922. https://doi.org/10.1039/C6RA28030G

Daligaux, V., Richard, R., & Manero, M.-H. (2021). Deactivation and regeneration of zeolite catalysts used in pyrolysis of plastic wastes—A process and analytical review. *Catalysts*, *11*(7), 770. https://doi.org/10.3390/catal11070770

Dapsens, P. Y., Mondelli, C., & Pérez-Ramírez, J. (2015). Design of Lewis-acid centres in zeolitic matrices for the conversion of renewables. *Chemical Society Reviews*, *44*(20), 7025–7043. https://doi.org/10.1039/C5CS00028A

Dedzo, G. K., & Detellier, C. (2018). Clay minerals-ionic liquids, nanoarchitectures, and applications. *Advanced Functional Materials*, *28*(27), 1703845. https://doi.org/10.1002/adfm.201703845

Derbe, T., Temesgen, S., & Bitew, M. (2021). A short review on synthesis, characterization, and applications of zeolites. *Advances in Materials Science and Engineering*, *2021*, 1–17. https://doi.org/10.1155/2021/6637898

Djomgoue, P., & Njopwouo, D. (2013). FTIR spectroscopy applied for surface clays

characterization. *Journal of Surface Engineered Materials and Advanced Technology*, *03*(04), 275–282. https://doi.org/10.4236/jsemat.2013.34037

Do Nascimento, G. M. (Ed.). (2021). *Clay and Clay Minerals*. BoD–Books on Demand.

Dodoo-Arhin, D., Dodoo-Arhin, D., Konadu, D. S., Annan, E., Buabeng, F. P., Yaya, A., & Agyei-Tuffour, B. (2013). Fabrication and characterisation of Ghanaian bauxite red mud-clay composite bricks for construction applications. *American Journal of M Aterials Science*, *2013*(5), 110–119. https://doi.org/10.5923/j.materials.20130305.02

Dos Santos, M. B., Vianna, K. C., Pastore, H. O., Andrade, H. M. C., & Mascarenhas, A. J. S. (2020). Studies on the synthesis of ZSM-5 by interzeolite transformation from zeolite Y without using organic structure directing agents. *Microporous and Mesoporous Materials*, *306*, 110413. https://doi.org/10.1016/j.micromeso.2020.110413

Elert, K., Sebastián Pardo, E., & Rodriguez-Navarro, C. (2015). Influence of organic matter on the reactivity of clay minerals in highly alkaline environments. *Applied Clay Science*, *111*, 27–36. https://doi.org/10.1016/j.clay.2015.03.006

Endene, E., Gidigasu, S. S. R., & Gawu, S. K. Y. (2020). Engineering geological evaluation of Mfensi and Afari clay deposits for liner application in municipal solid waste landfills. *SN Applied Sciences*, *2*(12), 2102. https://doi.org/10.1007/s42452-020-03887-5

Fadillah, G., Fatimah, I., Sahroni, I., Musawwa, M. M., Mahlia, T. M. I., & Muraza, O. (2021). Recent progress in low-cost catalysts for pyrolysis of plastic waste to fuels. *Catalysts*, *11*(7), 837. https://doi.org/10.3390/catal11070837

Faisal, M., Abdullah, I., & Krisnandi, Y. K. (2020). Hierarchical ZSM-5 synthesized from Bangka kaolin and Bayat natural zeolite for methane conversion catalysts. *IOP Conference Series: Materials Science and Engineering*, *902*(1), 0–9.

https://doi.org/10.1088/1757-899X/902/1/012045

Feliczak-Guzik, A. (2018). Hierarchical zeolites: Synthesis and catalytic properties. *Microporous and Mesoporous Materials*, *259*, 33–45. https://doi.org/10.1016/j.micromeso.2017.09.030

Feng, H., Li, C., & Shan, H. (2009a). Effect of calcination temperature of kaolin microspheres on the in situ synthesis of ZSM-5. *Catalysis Letters*, *129*(1–2), 71–78. https://doi.org/10.1007/s10562-008-9794-9

Feng, H., Li, C., & Shan, H. (2009b). In-situ synthesis and catalytic activity of ZSM-5 zeolite. *Applied Clay Science*, *42*(3–4), 439–445. https://doi.org/10.1016/j.clay.2008.05.004

Feng, K., Zhang, F., Li, S. F., & Sun, C. Y. (2017). The synthesis of ZSM-5 using natural clay of Qinghai Salt Lake and its Pb(II) adsorption. *IOP Conference Series: Earth and Environmental Science*, *81*(1), 0–6. https://doi.org/10.1088/1755-1315/81/1/012011

Fletcher, R. E., Ling, S., & Slater, B. (2017). Violations of Löwenstein's rule in zeolites. *Chem. Sci.*, *8*(11), 7483–7491. https://doi.org/10.1039/C7SC02531A

Gandhi, D., Bandyopadhyay, R., & Soni, B. (2021). Zeolite Y from kaolin clay of Kachchh, India: Synthesis, characterization and catalytic application. *Journal of the Indian Chemical Society*, *98*(12), 100246. https://doi.org/10.1016/j.jics.2021.100246

Garcia, G., Cardenas, E., Cabrera, S., & Hedlund, J. (2016). Microporous and mesoporous materials synthesis of zeolite Y from diatomite as silica source. *Microporous and Mesoporous Materials*, *219*, 29–37. https://doi.org/10.1016/j.micromeso.2015.07.015

Ghadiri, M., Chrzanowski, W., & Rohanizadeh, R. (2015). Biomedical applications of cationic clay minerals. *RSC Advances*, *5*(37), 29467–29481. https://doi.org/10.1039/C4RA16945J

Ghrib, Y., Frini-Srasra, N., & Srasra, E. (2017). Synthesis of ZSM-5 zeolite from

metakaolinite: Effects of the SiO_2/Al_2O_3 molar ratio, the initial precursor and the presence of organic template agent. *Surface Engineering and Applied Electrochemistry*, *53*(1), 64–70. https://doi.org/10.3103/S1068375517010057

Grand, J., Awala, H., & Mintova, S. (2016). Mechanism of zeolites crystal growth: new findings and open questions. *CrystEngComm*, *18*(5), 650–664. https://doi.org/10.1039/C5CE02286J

Gualtieri, A. F., Gatta, G. Di., Arletti, R., Artioli, G., Ballirano, P., Cruciani, G., Guagliardi, A., Malferrari, D., Masciocchi, N., & Scardi, P. (2019). Quantitative phase analysis using the Rietveld method: Towards a procedure for checking the reliability and quality of the results. *Periodico Di Mineralogia*, *88*(2), 147–151.

https://doi.org/https://doi.org/10.2451/2019PM870

Hammond, C., Padovan, D., & Tarantino, G. (2018). Porous metallosilicates for heterogeneous, liquid-phase catalysis: perspectives and pertaining challenges. *Royal Society Open Science*, *5*(2), 171315. https://doi.org/10.1098/rsos.171315

Han, L., Yan, X., Guo, L., Duan, Y., Wang, Z., Lu, T., Xu, J., Zhan, Y., & Wang, J. (2021). Ionothermal synthesis of triclinic SAPO-34 zeolites. *Catalysts*, *11*(5), 616. https://doi.org/10.3390/catal11050616

Han, S., Liu, Y., Yin, C., & Jiang, N. (2019). Fast synthesis of submicron ZSM-5 zeolite from leached illite clay using a seed-assisted method. *Microporous and Mesoporous Materials*, *275*(April 2018), 223–228. https://doi.org/10.1016/j.micromeso.2018.08.028

Hartanto, D., Iqbal, R. M., Shahbihi, W. E., Santoso, E., Fansuri, H., & Iryani, A. (2017). Effect of H_2O/SiO_2 molar ratio on direct synthesis of ZSM-5 from Bangka's Kaolin without pretreatment. *Malaysian Journal of Fundamental and Applied Sciences*, *13*(4), 817–820.

https://doi.org/10.11113/mjfas.v13n4.916

Hartanto, D., Pambudi, A. B., Cahyanti, D. N., & Utomo, W. P. (2019). On the synthesis of ZSM-5 directly from kaolin Bangka with aging time. *IOP Conference Series: Materials Science and Engineering*, *588*(1), 0–10. https://doi.org/10.1088/1757-899X/588/1/012039

Hartanto, D., Saputro, O., Utomo, W. P., Rosyidah, A., Sugiarso, D., Ersam, T., Nur, H., & Prasetyoko, D. (2016). Synthesis of ZSM-5 directly from kaolin without organic template: Part-1: Effect of crystallization time. *Asian Journal of Chemistry*, *28*(1), 211–215. https://doi.org/10.14233/ajchem.2016.19348

Hartanto, D., Sin, L., Mutia, S., Sugiarso, D., Kris, I., Ersam, T., Prasetyoko, D., & Nur, H. (2016). Can kaolin function as source of alumina in the synthesis of ZSM-5 without an organic template using a seeding technique? *Malaysian Journal of Fundamental and Applied Sciences*, *12*(2), 85–90.

Hartati, Prasetyoko, D., Santoso, M., Qoniah, I., Leaw, W. L., Firda, P. B. D., & Nur, H. (2020). A review on synthesis of kaolin-based zeolite and the effect of impurities. *Journal of the Chinese Chemical Society*, *67*(6), 911–936. https://doi.org/10.1002/jccs.201900047

He, Y., Tang, S., Yin, S., & Li, S. (2021). Research progress on green synthesis of various high-purity zeolites from natural material-kaolin. *Journal of Cleaner Production*, *306*, 127248. https://doi.org/10.1016/j.jclepro.2021.127248

Heanes, D. L. (1984). Determination of total organic-C in soils by an improved chromic acid digestion and spectrophotometric procedure. *Communications in Soil Science and Plant Analysis*, *15*(10), 1191–1213. https://doi.org/10.1080/00103628409367551

Hill, R. J., & Howard, C. J. (1987). Quantitative phase analysis from neutron powder

diffraction data using the Rietveld method. *Journal of Applied Crystallography*, *20*(6), 467–474. https://doi.org/10.1107/S0021889887086199

Holmes, S. M., Khoo, S. H., & Kovo, A. S. (2011). The direct conversion of impure natural kaolin into pure zeolite catalysts. *Green Chemistry*, *13*(5), 1152–1154. https://doi.org/10.1039/c1gc15099e

Hu, D. H., Chen, M. Q., Huang, Y. W., Wei, S. H., & Zhong, X. B. (2020). Evaluation on isothermal pyrolysis characteristics of typical technical solid wastes. *Thermochimica Acta*, *688*(April), 178604. https://doi.org/10.1016/j.tca.2020.178604

Hu, Y., Liu, C., Zhang, Y., Ren, N., & Tang, Y. (2009). Microporous and mesoporous materials microwave-assisted hydrothermal synthesis of nanozeolites with controllable size. *Microporous and Mesoporous Materials*, *119*(1–3), 306–314. https://doi.org/10.1016/j.micromeso.2008.11.005

Huang, Q., Li, R., Fu, G., & Jiang, J. (2020). Size effects of the crystallite of ZSM-5 zeolites on the direct catalytic conversion of L-Lactic acid to L, L-Lactide. *Crystals*, *10*(9), 781. https://doi.org/10.3390/cryst10090781

Inagaki, S., Tsuboi, Y., Nishita, Y., Syahylah, T., Wakihara, T., & Kubota, Y. (2013). Rapid synthesis of an aluminum-rich MSE-Type zeolite by the hydrothermal conversion of an FAU-type zeolite. *Chemistry - A European Journal*, *19*(24), 7780–7786. https://doi.org/10.1002/chem.201300125

Iryani, A., Nur, H., Santoso, M., & Hartanto, D. (2020). Adsorption study of rhodamine B and methylene blue dyes with ZSM-5 directly synthesized from Bangka Kaolin without organic template. *Indonesian Journal of Chemistry*, *20*(1), 130–140. https://doi.org/10.22146/ijc.41369

Javdani, A., Ahmadpour, J., & Yaripour, F. (2019). Nano-sized ZSM-5 zeolite synthesized *via* seeding technique for methanol conversions: A review. *Microporous and Mesoporous Materials*, *284*(January), 443–458. https://doi.org/10.1016/j.micromeso.2019.04.063

Jesudoss, S. K., Vijaya, J. J., Kaviyarasu, K., Kennedy, L. J., Jothi Ramalingam, R., & Al-Lohedan, H. A. (2018). Anti-cancer activity of hierarchical ZSM-5 zeolites synthesized from rice-based waste materials. *RSC Advances*, *8*(1), 481–490. https://doi.org/10.1039/C7RA11763A

Jha, B., & Singh, D. N. (2011). A review on synthesis, characterization and industrial applications of Flyash zeolites. *Journal of Materials Education*, *33*(1–2), 65–132.

Ji, Y., Wang, Y., Xie, B., & Xiao, F.-S. (2016). Zeolite seeds: Third type of structure directing agents in the synthesis of zeolites. *Comments on Inorganic Chemistry*, *36*(1), 1–16. https://doi.org/10.1080/02603594.2015.1031375

Jia, X., Jo, C., & Yip, A. C. K. (2021). Synthesis strategies for hierarchical zeolites. In *Heterogeneous Catalysts* (pp. 119–145). Wiley. https://doi.org/10.1002/9783527813599.ch7

Jia, X., Khan, W., Wu, Z., Choi, J., & Yip, A. C. K. (2019). Modern synthesis strategies for hierarchical zeolites: Bottom-up versus top-down strategies. *Advanced Powder Technology*, *30*(3), 467–484. https://doi.org/10.1016/j.apt.2018.12.014

Jiang, J., Duanmu, C., Yang, Y., Gu, X., & Chen, J. (2014). Synthesis and characterization of high siliceous ZSM-5 zeolite from acid-treated palygorskite. *Powder Technology*, *251*, 9–14. https://doi.org/10.1016/j.powtec.2013.10.020

Jin, Y., Sun, Q., Qi, G., Yang, C., Xu, J., Chen, F., Meng, X., Deng, F., & Xiao, F.-S. (2013). Solvent-free synthesis of silicoaluminophosphate zeolites. *Angewandte Chemie*

International Edition, *52*(35), 9172–9175. https://doi.org/10.1002/anie.201302672

Karimi, R., Bayati, B., Charchi Aghdam, N., Ejtemaee, M., & Babaluo, A. A. (2012). Studies of the effect of synthesis parameters on ZSM-5 nanocrystalline material during template-hydrothermal synthesis in the presence of chelating agent. *Powder Technology*, *229*, 229–236. https://doi.org/10.1016/j.powtec.2012.06.037

Karkanis, P. G., Au, K., & Schaalje, G. B. (1991). Comparison of four measurement schedules for determination of soil particle-size distribution by the hydrometer method. *Canadian Agricultural Engineering*, *33*(2), 211–215.

Kausar, A., Iqbal, M., Javed, A., Aftab, K., Nazli, Z., Bhatti, H. N., & Nouren, S. (2018). Dyes adsorption using clay and modified clay: A review. *Journal of Molecular Liquids*, *256*, 395–407. https://doi.org/10.1016/j.molliq.2018.02.034

Kerstens, D., Smeyers, B., Van Waeyenberg, J., Zhang, Q., Yu, J., & Sels, B. F. (2020). State of the art and perspectives of hierarchical zeolites: Practical overview of synthesis methods and use in catalysis. *Advanced Materials*, *32*(44), 2004690. https://doi.org/10.1002/adma.202004690

Khaleque, A., Alam, M. M., Hoque, M., Mondal, S., Haider, J. Bin, Xu, B., Johir, M. A. H., Karmakar, A. K., Zhou, J. L., Ahmed, M. B., & Moni, M. A. (2020). Zeolite synthesis from low-cost materials and environmental applications: A review. *Environmental Advances*, *2*(October), 100019. https://doi.org/10.1016/j.envadv.2020.100019

Khalifa, A. Z., Cizer, Ö., Pontikes, Y., Heath, A., Patureau, P., Bernal, S. A., & Marsh, A. T. M. (2020). Cement and concrete research advances in alkali-activation of clay minerals. *Cement and Concrete Research*, *132*(April), 106050. https://doi.org/10.1016/j.cemconres.2020.106050

Khatamian, M., & Irani, M. (2009). Preparation and characterization of nanosized ZSM-5 zeolite using kaolin and investigation of kaolin content, crystallization time and temperature changes on the size and crystallinity of products. *Journal of the Iranian Chemical Society*, *6*(1), 187–194. https://doi.org/10.1007/BF03246519

Kianfar, E. (2020). Zeolites: Properties, applications, modification and selectivity. *Zeolites: Advances in Research and Applications*, *3*(233), 2–20.

Knott, B. C., Nimlos, C. T., Robichaud, D. J., Nimlos, M. R., Kim, S., & Gounder, R. (2018). Consideration of the aluminum distribution in zeolites in theoretical and experimental catalysis research. *ACS Catalysis*, *8*(2), 770–784. https://doi.org/10.1021/acscatal.7b03676

Koohsaryan, E., & Anbia, M. (2016). Nanosized and hierarchical zeolites: A short review. *Chinese Journal of Catalysis*, *37*(4), 447–467. https://doi.org/10.1016/S1872-2067(15)61038-5

Kornas, A., Olszówka, J. E., Klein, P., & Pashkova, V. (2021). Milling activation for the solvent-free synthesis of zeolites. A practical guide. *Catalysts*, *11*(2), 246. https://doi.org/10.3390/catal11020246

Krivoshein, P. K., Volkov, D. S., Rogova, O. B., & Proskurnin, M. A. (2020). FTIR photoacoustic spectroscopy for identification and assessment of soil components: Chernozems and their size fractions. *Photoacoustics*, *18*(December 2019), 100162. https://doi.org/10.1016/j.pacs.2020.100162

Król, M., Minkiewicz, J., & Mozgawa, W. (2016). IR spectroscopy studies of zeolites in geopolymeric materials derived from kaolinite. *Journal of Molecular Structure*, *1126*, 200–206. https://doi.org/10.1016/j.molstruc.2016.02.027

Kumar, A., & Lingfa, P. (2020). Sodium bentonite and kaolin clays: Comparative study on their FTIR, XRF, and XRD. *Materials Today: Proceedings*, *22*(xxxx), 737–742. https://doi.org/10.1016/j.matpr.2019.10.037

Kumar, R., Verma, A., Shome, A., Sinha, R., Sinha, S., Jha, P. K., Kumar, R., Kumar, P., Shubham, Das, S., Sharma, P., & Vara Prasad, P. V. (2021). Impacts of plastic pollution on ecosystem services, sustainable development goals, and need to focus on circular economy and policy interventions. *Sustainability*, *13*(17), 9963. https://doi.org/10.3390/su13179963

Kumaran, S., Kamari, A., Abdulrasool, M. M., Wong, S. T. S., Jumadi, J., Yusoff, S. N. M., & Ishak, S. (2019). Synthesis, characterisation and mechanism of novel Ca-ZSM-5 zeolite nanocomposite from eggshell using simple co-precipitation method. *Journal of Physics: Conference Series*, *1397*(1), 012030. https://doi.org/10.1088/1742-6596/1397/1/012030

Kumari, N., & Mohan, C. (2021). Basics of clay minerals and their characteristic properties. In *Clay and Clay Minerals* (Vol. 33, p. 97672). IntechOpen. https://doi.org/10.5772/intechopen.97672

Kuvatova, R. Z., Travkina, O. S., & Kutepov, B. I. (2021). Synthesis of micro/mesoporous zeolite ZSM-5 using a natural aluminosilicate. *Catalysis in Industry*, *13*(2), 99–104. https://doi.org/10.1134/S2070050421020070

Kwakye-Awuah, B., Abavare, E. K. K., Sefa-Ntiri, B., Nkrumah, I., Von-Kiti, E., & Williams, C. (2021). Synthesis and characterization of geopolymer-zeolites from Ghanaian Kaolin samples by variation of two synthesis parameters. *Journal of Thermal Analysis and Calorimetry*, *146*(5), 1991–2003. https://doi.org/10.1007/s10973-021-10710-9

Kwakye-Awuah, B., Sefa-Ntiri, B., Von-Kiti, E., Nkrumah, I., & Williams, C. (2019). Adsorptive removal of iron and manganese from groundwater samples in Ghana by zeolite

y synthesized from bauxite and kaolin. *Water (Switzerland)*, *11*(9). https://doi.org/10.3390/w11091912

Kwakye-Awuah, B., Von-Kiti, E., Buamah, R., Nkrumah, I., & Williams, C. (2014). Effect of crystallization time on the hydrothermal synthesis of zeolites from kaolin and bauxite. *International Journal of Scientific and Engineering Research*, *5*(2).

Kwakye-Awuah, B., Von-kiti, E., Nkrumah, I., Sefa-Ntiri, B., & Williams, C. D. (2018). Synthesis of zeolites from bauxite and kaolin: Effect of synthesis parameters on competing phases. *World Academy of Science, Engineering and Technology, International Journal of Chemical and Materials Engineering, September 2019*.

Lafi, A. A. F., Matam, S. K., & Hodali, H. A. (2015). New Synthesis of ZSM-5 from High-Silica Kaolinite and Its Use in Vapor-Phase Conversion of 1-Phenylethanol to Styrene. *Industrial & Engineering Chemistry Research*, *54*(15), 3754–3760. https://doi.org/10.1021/ie505004k

Li, H., Wang, Y., Meng, F., Gao, F., Sun, C., Fan, C., Wang, X., & Wang, S. (2017). Controllable fabrication of single-crystalline, ultrafine and high-silica hierarchical ZSM-5 aggregates *via* solid-like state conversion. *RSC Advances*, *7*(41), 25605–25620. https://doi.org/10.1039/C7RA03962J

Li, S., Li, J., Dong, M., Fan, S., Zhao, T., Wang, J., & Fan, W. (2019). Strategies to control zeolite particle morphology. *Chemical Society Reviews*, *48*(3), 885–907. https://doi.org/10.1039/C8CS00774H

Li, X., Han, S., Guan, D., Jiang, N., Xu, J., & Park, S.-E. (2021). Rapid direct synthesis of nano-H-ZSM-5 from leached illite *via* solid-like-state conversion-based crystallization. *Applied Clay Science*, *203*, 106028. https://doi.org/10.1016/j.clay.2021.106028

Li, X., Han, S., Xu, J., & Jiang, N. (2023). Green synthesis of nano-H-ZSM-5 zeolite single-crystal aggregates *via* an in situ reconstruction of the topology of natural clay. *Microporous and Mesoporous Materials*, 112441. https://doi.org/10.1016/j.micromeso.2023.112441

Li, Y., Li, L., & Yu, J. (2017). Applications of Zeolites in Sustainable Chemistry. *Chem*, *3*(6), 928–949. https://doi.org/10.1016/j.chempr.2017.10.009

Lin, Z. S., & Huang, Y. (2016a). Tetraalkylammonium salt/alcohol mixtures as deep eutectic solvents for syntheses of high-silica zeolites. *Microporous and Mesoporous Materials*, *224*, 75–83. https://doi.org/10.1016/j.micromeso.2015.11.008

Lin, Z. S., & Huang, Y. (2016b). Syntheses of high-silica zeolites in urea/choline chloride deep eutectic solvent. *Canadian Journal of Chemistry*, *94*(6), 533–540. https://doi.org/10.1139/cjc-2016-0115

Liu, J., & Yu, J. (2016). Toward greener and designed synthesis of zeolite materials. In *Zeolites and Zeolite-Like Materials* (pp. 1–32). Elsevier. https://doi.org/10.1016/B978-0-444-63506-8.00001-X

Liu, Y., Han, S., Guan, D., Chen, S., Wu, Y., Yang, Y., & Jiang, N. (2019). Rapid green synthesis of ZSM-5 zeolite from leached illite clay. *Microporous and Mesoporous Materials*, *280*(February), 324–330. https://doi.org/10.1016/j.micromeso.2019.02.027

Lok, C. M., Van Doorn, J., & Aranda Almansa, G. (2019). Promoted ZSM-5 catalysts for the production of bio-aromatics, a review. *Renewable and Sustainable Energy Reviews*, *113*(June), 109248. https://doi.org/10.1016/j.rser.2019.109248

Louis, B., & Kiwi-Minsker, L. (2004). Synthesis of ZSM-5 zeolite in fluoride media: an innovative approach to tailor both crystal size and acidity. *Microporous and Mesoporous*

Materials, *74*(1–3), 171–178. https://doi.org/10.1016/j.micromeso.2004.06.016

Louis, B., Reuse, P., Kiwi-Minsker, L., & Renken, A. (2001). Synthesis of ZSM-5 coatings on stainless steel grids and their catalytic performance for partial oxidation of benzene by N2O. *Applied Catalysis A: General*, *210*(1–2), 103–109. https://doi.org/10.1016/S0926-860X(00)00788-2

Luo, W., Yang, X., Wang, Z., Huang, W., Chen, J., Jiang, W., Wang, L., Cheng, X., Deng, Y., & Zhao, D. (2017). Microporous and mesoporous materials synthesis of ZSM-5 aggregates made of zeolite nanocrystals through a simple solvent-free method. *Microporous and Mesoporous Materials*, *243*, 112–118. https://doi.org/10.1016/j.micromeso.2017.01.040

Madhusoodana, C. D., Das, R. N., Kameshima, Y., & Okada, K. (2005). Preparation of ZSM-5 zeolite honeycomb monoliths using microporous silica obtained from metakaolinite. *Journal of Porous Materials*, *12*(4), 273–280. https://doi.org/10.1007/s10934-005-3125-y

Maghfirah, A., Ilmi, M. M., Fajar, A. T. N., & Kadja, G. T. M. (2020). A review on the green synthesis of hierarchically porous zeolite. *Materials Today Chemistry*, *17*, 100348. https://doi.org/10.1016/j.mtchem.2020.100348

Marfo, K. K., Dodoo-Arhin, D., Agyei-Tuffou, B., Nyankson, E., Obada, D. O., Damoah, L. N. W., Annan, E., Yaya, A., Onwona-Agyeman, B., & Bediako, M. (2020). The physico-mechanical influence of dehydroxylized activated local kaolin: A supplementary cementitious material for construction applications. *Case Studies in Construction Materials*, *12*, e00306. https://doi.org/10.1016/j.cscm.2019.e00306

Marsh, A., Heath, A., Patureau, P., Evernden, M., & Walker, P. (2018). Alkali activation behaviour of un-calcined montmorillonite and illite clay minerals. *Applied Clay Science*,

166(September), 250–261. https://doi.org/10.1016/j.clay.2018.09.011

Mei, J., Duan, A., & Wang, X. (2021). A brief review on solvent-free synthesis of zeolites. *Materials*, *14*(4), 788. https://doi.org/10.3390/ma14040788

Meng, X., & Xiao, F.-S. (2014). Green routes for synthesis of zeolites. *Chemical Reviews*, *114*(2), 1521–1543. https://doi.org/10.1021/cr4001513

Merabtene, M., Kacimi, L., & Clastres, P. (2019). Elaboration of geopolymer binders from poor kaolin and dam sludge waste. *Heliyon*, *5*(6), e01938. https://doi.org/10.1016/j.heliyon.2019.e01938

Messaoudi, M., Tijani, N., Baya, S., Lahnafi, A., Ouallal, H., Moussout, H., & Messaoudi, L. (2021). Characterization of ceramic pieces shaped from clay intended for the development of filtration membranes. *South African Journal of Chemical Engineering*, *37*(April 2020), 1–11. https://doi.org/10.1016/j.sajce.2021.03.004

Miandad, R., Barakat, M. A., Aburiazaiza, A. S., Rehan, M., & Nizami, A. S. (2016). Catalytic pyrolysis of plastic waste: A review. *Process Safety and Environmental Protection*, *102*, 822–838. https://doi.org/10.1016/j.psep.2016.06.022

Miezah, K., Obiri-Danso, K., Kádár, Z., Fei-Baffoe, B., & Mensah, M. Y. (2015). Municipal solid waste characterization and quantification as a measure towards effective waste management in Ghana. *Waste Management*, *46*, 15–27. https://doi.org/10.1016/j.wasman.2015.09.009

Mohiuddin, E., Isa, Y. M., Mdleleni, M. M., & Key, D. (2017). Effect of kaolin chemical reactivity on the formation of ZSM-5 and its physicochemical properties. *Microporous and Mesoporous Materials*, *237*, 1–11. https://doi.org/10.1016/j.micromeso.2016.08.028

Mohiuddin, E., Makarfi Isa, Y., M. Mdleleni, M., & Key, D. (2020). Synthesis and Application

of Porous Kaolin-Based ZSM-5 in the Petrochemical Industry. *IntechOpen*. doi: 10.5772/intechopen.81375

Mohiuddin, E., Isa, Y. M., Mdleleni, M. M., Sincadu, N., Key, D., & Tshabalala, T. (2016). Synthesis of ZSM-5 from impure and beneficiated Grahamstown kaolin: Effect of kaolinite content, crystallisation temperatures and time. *Applied Clay Science, 119*, 213–221. https://doi.org/10.1016/j.clay.2015.10.008

Moliner, M., Rey, F., & Corma, A. (2013). Towards the rational design of efficient organic structure-directing agents for zeolite synthesis. *Angewandte Chemie International Edition*, *52*(52), 13880–13889. https://doi.org/10.1002/anie.201304713

Moraes, J. D. D., Bertolino, S. R. A., Cuffini, S. L., Ducart, D. F., Bretzke, P. E., & Leonardi, G. R. (2017). Clay minerals: Properties and applications to dermocosmetic products and perspectives of natural raw materials for therapeutic purposes—A review. *International Journal of Pharmaceutics*, *534*(1–2), 213–219. https://doi.org/10.1016/j.ijpharm.2017.10.031

Moshoeshoe, M., Silas Nadiye-Tabbiruka, M., & Obuseng, V. (2017). A review of the chemistry, structure, properties and applications of zeolites. *American Journal of Materials Science, 2017*(5), 196–221. https://doi.org/10.5923/j.materials.20170705.12

Mulvaney, B. J., & Page, A. L. (1982). Nitrogen-total. *Methods of soil analysis: Part, 2*, 595-624.

Murray, H. H. (1991). Overview — clay mineral applications. *Applied Clay Science*, *5*(5–6), 379–395. https://doi.org/10.1016/0169-1317(91)90014-Z

Nada, M. H., Gillan, E. G., & Larsen, S. C. (2019). Mechanochemical reaction pathways in solvent-free synthesis of ZSM-5. *Microporous and Mesoporous Materials*, *276*(July

2018), 23–28. https://doi.org/10.1016/j.micromeso.2018.09.009

Nagendrappa, G. (2011). Organic synthesis using clay and clay-supported catalysts. *Applied Clay Science*, *53*(2), 106–138. https://doi.org/10.1016/j.clay.2010.09.016

Narayanan, S., Tamizhdurai, P., Mangesh, V. L., Ragupathi, C., Santhana krishnan, P., & Ramesh, A. (2021). Recent advances in the synthesis and applications of mordenite zeolite – review. *RSC Advances*, *11*(1), 250–267. https://doi.org/10.1039/D0RA09434J

Nazir, L. S. M., Yeong, Y. F., & Chew, T. L. (2020). Methods and synthesis parameters affecting the formation of FAU type zeolite membrane and its separation performance: a review. *Journal of Asian Ceramic Societies*, *8*(3), 553–571. https://doi.org/10.1080/21870764.2020.1769816

Nelson, D. A., & Sommers, L. (1983). Total carbon, organic carbon, and organic matter. *Methods of soil analysis: Part 2 chemical and microbiological properties*, *9*, 539-579. https://doi.org/10.2134/agronmonogr9.2.2ed.c29

Nguyen, D. K., Dinh, V. P., Nguyen, H. Q., & Hung, N. T. (2023). Zeolite ZSM-5 synthesized from natural silica sources and its applications: a critical review. *Journal of Chemical Technology & Biotechnology*. https://doi.org/10.1002/jctb.7380

Nguyen, D. K., Dinh, V. P., Nguyen, H. Q., & Hung, N. T. (2023). Zeolite ZSM-5 synthesized from natural silica sources and its applications: a critical review. *Journal of Chemical Technology & Biotechnology*, *98*(6), 1339-1355. https://doi.org/10.1016/j.sajce.2022.09.014

Novembre, D., & Gimeno, D. (2021). Synthesis and characterization of analcime (ANA) zeolite using a kaolinitic rock. *Scientific Reports*, *0123456789*, 1–9. https://doi.org/10.1038/s41598-021-92862-0

Nugraha, R. E., Prasetyoko, D., Asikin-Mijan, N., Bahruji, H., Suprapto, S., Taufiq-Yap, Y. H., & Jalil, A. A. (2021). The effect of structure directing agents on micro/mesopore structures of aluminosilicates from Indonesian kaolin as deoxygenation catalysts. *Microporous and Mesoporous Materials*, *315*(October 2020), 110917. https://doi.org/10.1016/j.micromeso.2021.110917

Oleksiak, M. D., & Rimer, J. D. (2014). Synthesis of zeolites in the absence of organic structure-directing agents: factors governing crystal selection and polymorphism. *Reviews in Chemical Engineering*, *30*(1), 1–49. https://doi.org/10.1515/revce-2013-0020

Osei, G. K., Nzihou, A., Yaya, A., Minh, D. P., & Onwona-Agyeman, B. (2021). Catalytic pyrolysis of waste engine oil over Y zeolite synthesized from natural clay. *Waste and Biomass Valorization*, *12*(7), 4157–4170. https://doi.org/10.1007/s12649-020-01282-0

Othman Ali, I., Hassan, A. M., Shaaban, S. M., & Soliman, K. S. (2011). Synthesis and characterization of ZSM-5 zeolite from rice husk ash and their adsorption of Pb2+ onto unmodified and surfactant-modified zeolite. *Separation and Purification Technology*, *83*(1), 38–44. https://doi.org/10.1016/j.seppur.2011.08.034

Otieno, S. O., Kengara, F. O., Kemmegne-Mbouguen, J. C., Langmi, H. W., Kowenje, C. B. O., & Mokaya, R. (2019). The effects of metakaolinization and fused-metakaolinization on zeolites synthesized from quartz rich natural clays. *Microporous and Mesoporous Materials*, *290*(August), 109668. https://doi.org/10.1016/j.micromeso.2019.109668

Pan, F., Lu, X., Wang, Y., Chen, S., Wang, T., & Yan, Y. (2014). Synthesis and crystallization kinetics of ZSM-5 without organic template from coal-series kaolinite. *Microporous and Mesoporous Materials*, *184*, 134–140. https://doi.org/10.1016/j.micromeso.2013.10.013

Pan, F., Lu, X., Zhu, Q., Zhang, Z., Yan, Y., Wang, T., & Chen, S. (2015). Direct synthesis of HZSM-5 from natural clay. *Journal of Materials Chemistry A*, *3*(7), 4058–4066.

https://doi.org/10.1039/c4ta05791k

Pan, H., Pan, Q., Zhao, Y., Luo, Y., Shu, X., & He, M. (2010). A green and efficient synthesis of ZSM-5 using NaY as seed with mother liquid recycling and in the absence of organic template. *Industrial & Engineering Chemistry Research*, *49*(16), 7294–7302. https://doi.org/10.1021/ie100191a

Paquin, F., Rivnay, J., Salleo, A., Stingelin, N., & Silva, C. (2015). Multi-phase semicrystalline microstructures drive exciton dissociation in neat plastic semiconductors. *J. Mater. Chem. C*, *3*, 10715–10722. https://doi.org/10.1039/b000000x

Petrov, I., & Michalev, T. (2012). Synthesis of zeolite A: a review. *Научни Трудове На Русенския Университет*, *51*, 30-35.

Phatai, P., Loiha, S., Prayoonpokarach, S., & Wittayakun, J. (2020). Effect of crystallinity of zeolite beta on physicochemical properties and performance of cobalt catalysts. *Sains Malaysiana*, *49*(1), 75–84. https://doi.org/10.17576/jsm-2020-4901-09

Qin, Z., Lakiss, L., Tosheva, L., Gilson, J.-P., Vicente, A., Fernandez, C., & Valtchev, V. (2014). Comparative study of nano-ZSM-5 catalysts synthesized in OH − and F − media. *Advanced Functional Materials*, *24*(2), 257–264. https://doi.org/10.1002/adfm.201301541

Qoniah, I., Prasetyoko, D., Bahruji, H., Triwahyono, S., Jalil, A. A., Suprapto, Hartati, & Purbaningtias, T. E. (2015). Direct synthesis of mesoporous aluminosilicates from Indonesian kaolin clay without calcination. *Applied Clay Science*, *118*, 290–294. https://doi.org/10.1016/j.clay.2015.10.007

Qoniah, I., Prasetyoko, D., Hartati, & Nikmah, Y. L. (2020). Optimization of hydrothermal temperature and time parameters in the synthesis of hierarchical ZSM-5 from kaolin by

taguchi method. *Materials Science Forum*, *981 MSF*, 104–111. https://doi.org/10.4028/www.scientific.net/MSF.981.104

Qu, S., Liu, D., Shi, X., Wang, H., & Wang, X. (2019). Effects of ZSM-5 preparation conditions on textural properties and catalytic cracking of n-Hexane. *Journal of Petroleum Science and Technology*, *9*(4), 63–76. https://doi.org/10.22078/jpst.2019.3765.1595

Ramesh, K., Biswas, A. K., Somasundaram, J., & Rao, A. S. (2010). Nanoporous zeolites in farming: Current status and issues ahead. *Current Science*, *99*(6), 760–764. https://www.jstor.org/stable/24109603

Ren, X.-Y., Cao, J.-P., Zhao, X.-Y., Yang, Z., Wang, Y.-J., Chen, Q., Zhao, M., & Wei, X.-Y. (2019). Catalytic conversion of lignite pyrolysis volatiles to light aromatics over ZSM-5: SiO2/Al2O3 ratio effects and mechanism insights. *Journal of Analytical and Applied Pyrolysis*, *139*, 22–30. https://doi.org/10.1016/j.jaap.2019.01.003

Sabarish, R., & Unnikrishnan, G. (2019). Synthesis, characterization and evaluations of micro/mesoporous ZSM-5 zeolite using starch as bio template. *SN Applied Sciences*, *1*(9), 989. https://doi.org/10.1007/s42452-019-1036-9

Sang, S., Chang, F., Liu, Z., He, C., He, Y., & Xu, L. (2004). Difference of ZSM-5 zeolites synthesized with various templates. *Catalysis Today*, *93–95*, 729–734. https://doi.org/10.1016/j.cattod.2004.06.091

Schroeder, C., Siozios, V., Mück-Lichtenfeld, C., Hunger, M., Hansen, M. R., & Koller, H. (2020). Hydrogen bond formation of Brønsted acid sites in zeolites. *Chemistry of Materials*, *32*(4), 1564–1574. https://doi.org/10.1021/acs.chemmater.9b04714

Selvin, R., Hsu, H., Roselin, L. S., & Bououdina, M. (2011). Effect of aging on the precursor sol for the synthesis of nanocrystalline ZSM-5. *Synthesis and Reactivity in Inorganic,*

Metal-Organic, and Nano-Metal Chemistry, *41*(8), 1028–1032. https://doi.org/10.1080/15533174.2011.591339

Seo, Y., Lee, K., & Shin, D. (2003). Investigation of catalytic degradation of high- density polyethylene by hydrocarbon group type analysis. *J. Anal. Appl. Pyrolysis*, *70*.

Serati-Nouri, H., Jafari, A., Roshangar, L., Dadashpour, M., Pilehvar-Soltanahmadi, Y., & Zarghami, N. (2020). Biomedical applications of zeolite-based materials: A review. *Materials Science and Engineering: C*, *116*(February), 111225. https://doi.org/10.1016/j.msec.2020.111225

Servatan, M., Zarrintaj, P., Mahmodi, G., Kim, S.-J., Ganjali, M. R., Saeb, M. R., & Mozafari, M. (2020). Zeolites in drug delivery: Progress, challenges and opportunities. *Drug Discovery Today*, *25*(4), 642–656. https://doi.org/10.1016/j.drudis.2020.02.005

Sharbini Kamaluddin, H., Gong, X., Ma, P., Narasimharao, K., Dutta Chowdhury, A., & Mokhtar, M. (2022). Influence of zeolite ZSM-5 synthesis protocols and physicochemical properties in the methanol-to-olefin process. *Materials Today Chemistry*, *26*, 101061. https://doi.org/10.1016/j.mtchem.2022.101061

Sharma, P., Rajaram, P., & Tomar, R. (2008). Synthesis and morphological studies of nanocrystalline MOR type zeolite material. *Journal of Colloid and Interface Science*, *325*(2), 547–557. https://doi.org/10.1016/j.jcis.2008.05.058

Shirazi, L., Jamshidi, E., & Ghasemi, M. R. (2008). The effect of Si/Al ratio of ZSM-5 zeolite on its morphology, acidity and crystal size. *Crystal Research and Technology*, *43*(12), 1300–1306. https://doi.org/10.1002/crat.200800149

Silva, V. J., Rodrigues, J. J., Soares, R. R., Napolitano, M. N., & Rodrigues, M. G. F. (2013). Cobalt supported on ZSM-5 zeolite using kaolin as silicon and aluminun sources for

Fischer-Tropsch synthesis. *Brazilian Journal of Petroleum and Gas*, *7*(2), 83–94. https://doi.org/10.5419/bjpg2013-0007

Sipra, A. T., Gao, N., & Sarwar, H. (2018). Municipal solid waste (MSW) pyrolysis for bio-fuel production: A review of effects of MSW components and catalysts. *Fuel Processing Technology*, *175*(February), 131–147. https://doi.org/10.1016/j.fuproc.2018.02.012

Smail, H., Rehan, M., Shareef, K., Ramli, Z., Nizami, A.-S., & Gardy, J. (2019). Synthesis of uniform mesoporous zeolite ZSM-5 catalyst for Friedel-Crafts acylation. *ChemEngineering*, *3*(2), 35. https://doi.org/10.3390/chemengineering3020035

Smit, B., & Maesen, T. L. M. (2008). Towards a molecular understanding of shape selectivity. *Nature*, *451*(7179), 671–678. https://doi.org/10.1038/nature06552

Snellings, R., Mertens, G., & Elsen, J. (2012). Supplementary cementitious materials. *Reviews in Mineralogy and Geochemistry*, *74*(1), 211–278. https://doi.org/10.2138/rmg.2012.74.6

Song, W., Justice, R. E., Jones, C. A., Grassian, V. H., & Larsen, S. C. (2004). Size-dependent properties of nanocrystalline silicalite synthesized with systematically varied crystal sizes. *Langmuir*, *20*(11), 4696–4702. https://doi.org/10.1021/la049817m

Song, Z., Zhang, C., Liu, G., Qu, D., & Xue, S. (2015). Fractal feature of particle-size distribution in the rhizospheres and bulk soils during natural recovery on the Loess Plateau, China. *PLOS ONE*, *10*(9), e0138057. https://doi.org/10.1371/journal.pone.0138057

Subsadsana, M., Sangdara, P., & Ruangviriyachai, C. (2017). Effect of bimetallic NiW modified crystalline ZSM-5 zeolite on catalytic conversion of crude palm oil and identification of biofuel products. In *Asia-Pacific Journal of Chemical Engineering* (Vol. 12, Issue 1, pp. 147–158). https://doi.org/10.1002/apj.2061

Sumari, S., Fajaroh, F., Yahmin, Sholihah, N., Santoso, A., & Budianto, A. (2019). Effect of temperature synthesis on structural behaviours of NaY zeolite ysing local sand as a silica source. *IOP Conference Series: Materials Science and Engineering*, *515*(7), 012036. https://doi.org/10.1088/1757-899X/515/1/012036

Sun, S.-H., Ma, J.-T., & Gao, X.-H. (2007). Synthesis of ZSM-5 on kaolin microspheres in the absence of an organic amine template. *Clay Minerals*, *42*(2), 203–211. https://doi.org/10.1180/claymin.2007.042.2.06

Szerement, J., Szatanik-Kloc, A., Jarosz, R., Bajda, T., & Mierzwa-Hersztek, M. (2021). Contemporary applications of natural and synthetic zeolites from fly ash in agriculture and environmental protection. *Journal of Cleaner Production*, *311*(October 2020), 127461. https://doi.org/10.1016/j.jclepro.2021.127461

Tabi, R. N., Agyemang, F. O., Mensah-Darkwa, K., Arthur, E. K., Gikunoo, E., & Momade, F. (2021). Zeolite synthesis and its application in water defluorination. *Materials Chemistry and Physics*, *261*, 124229. https://doi.org/10.1016/j.matchemphys.2021.124229

Tan, C., Liu, Z., Yonezawa, Y., Sukenaga, S., Ando, M., Shibata, H., Sasaki, Y., Okubo, T., & Wakihara, T. (2020). Unique crystallization behavior in zeolite synthesis under external high pressures. *Chemical Communications*, *56*(18), 2811–2814. https://doi.org/10.1039/C9CC09966B

Taufiqurrahmi, N., Mohamed, A. R., & Bhatia, S. (2011). Nanocrystalline zeolite Y: Synthesis and characterization. *IOP Conference Series: Materials Science and Engineering*, *17*(1), 012030. https://doi.org/10.1088/1757-899X/17/1/012030

Tehubijuluw, H., Subagyo, R., Yulita, M. F., Nugraha, R. E., Kusumawati, Y., Bahruji, H., Jalil, A. A., Hartati, H., & Prasetyoko, D. (2021). Utilization of red mud waste into

mesoporous ZSM-5 for methylene blue adsorption-desorption studies. *Environmental Science and Pollution Research*, *28*(28), 37354–37370. https://doi.org/10.1007/s11356-021-13285-y

Thakkar, H., Issa, A., Rownaghi, A. A., & Rezaei, F. (2017). CO2 Capture from air using amine-functionalized kaolin-based zeolites. *Chemical Engineering & Technology*, *40*(11), 1999–2007. https://doi.org/10.1002/ceat.201700188

Tran-Nguyen, P. L., Ly, K.-P., Thanh, L. H. V., Angkawijaya, A. E., Santoso, S. P., Tran, N.-P.-D., Tsai, M.-L., & Ju, Y.-H. (2021). Facile synthesis of zeolite NaX using rice husk ash without pretreatment. *Journal of the Taiwan Institute of Chemical Engineers*, *123*, 338–345. https://doi.org/10.1016/j.jtice.2021.05.009

Tulashie, S. K., Boadu, E. K., & Dapaah, S. (2019). Plastic waste to fuel *via* pyrolysis: A key way to solving the severe plastic waste problem in Ghana. *Thermal Science and Engineering Progress*, *11*(March), 417–424. https://doi.org/10.1016/j.tsep.2019.05.002

Uddin, F. (2018). Montmorillonite: An introduction to properties and utilization. *Current Topics in the Utilization of Clay in Industrial and Medical Applications*, 3–24. https://doi.org/10.5772/intechopen.77987

Van Westen, T., & Groot, R. D. (2018). Effect of temperature cycling on Ostwald ripening. *Crystal Growth & Design*, *18*(9), 4952–4962. https://doi.org/10.1021/acs.cgd.8b00267

Verdoliva, V., Saviano, M., & De Luca, S. (2019). Zeolites as acid/basic solid catalysts: Recent synthetic developments. *Catalysts*, *9*(3), 248. https://doi.org/10.3390/catal9030248

Wakihara, T., Sasaki, Y., Kato, H., Ikuhara, Y., & Okubo, T. (2005). Investigation of the surface structure of zeolite A. *Physical Chemistry Chemical Physics*, *7*(19), 3416. https://doi.org/10.1039/b509263a

Wang, P., Shen, B., Shen, D., Peng, T., & Gao, J. (2007). Synthesis of ZSM-5 zeolite from expanded perlite/kaolin and its catalytic performance for FCC naphtha aromatization. *Catalysis Communications*, *8*(10), 1452–1456. https://doi.org/10.1016/j.catcom.2006.12.018

Wang, W., & Wang, A. (2019). Vermiculite nanomaterials: Structure, properties, and potential applications. In *Nanomaterials from Clay Minerals*. Elsevier Inc. https://doi.org/10.1016/B978-0-12-814533-3.00009-0

Wang, Y., Feng, R., Li, X., Liu, X., & Yan, Z. (2013). In situ synthesis, characterization and catalytic activity of ZSM-5 zeolites on kaolin microspheres from amine-free system. *Journal of Porous Materials*, *20*(1), 137–141. https://doi.org/10.1007/s10934-012-9582-1

Weisz, P. B., & Frilette, V. J. (1960). Intracrystalline and molecular-shape-selective catalysis by zeolite salts. *The Journal of Physical Chemistry*, *64*(3), 382–382. https://doi.org/10.1021/j100832a513

Wen, H., Zhou, Y., Xie, J., Long, Z., Zhang, W., & Wang, J. (2014). Pure-silica ZSM-22 zeolite rapidly synthesized by novel ionic liquid-directed dry-gel conversion. *RSC Adv.*, *4*(91), 49647–49654. https://doi.org/10.1039/C4RA07627C

Wheatley, P. S., Allan, P. K., Teat, S. J., Ashbrook, S. E., & Morris, R. E. (2010). Task specific ionic liquids for the ionothermal synthesis of siliceous zeolites. *Chemical Science*, *1*(4), 483. https://doi.org/10.1039/c0sc00178c

Widayat, W., & Annisa, A. N. (2017). Synthesis and characterization of ZSM-5 catalyst at different temperatures. *IOP Conference Series: Materials Science and Engineering*, *214*, 012032. https://doi.org/10.1088/1757-899X/214/1/012032

Wilson, M. J. (2004). Weathering of the primary rock-forming minerals: processes, products and rates. *Clay Minerals*, *39*(3), 233–266. https://doi.org/10.1180/0009855043930133

Wu, M., Jiang, W., Jiang, J., Zou, Y., Zhang, P., Mao, P., XU, Y., & Shi, Y. (2020). Synthesis of ZSM-5 zeolites using palygorskite as raw material under solvent-free conditions. *Bulletin of Materials Science*, *43*(1), 289. https://doi.org/10.1007/s12034-020-02263-8

Wu, Q., Hong, X., Zhu, L., Meng, X., Han, S., Zhang, J., Liu, X., Jin, C., & Xiao, F.-S. (2019). Generalized ionothermal synthesis of silica-based zeolites. *Microporous and Mesoporous Materials*, *286*(February), 163–168. https://doi.org/10.1016/j.micromeso.2019.05.017

Wu, Q., Liu, X., Zhu, L., Ding, L., Gao, P., Wang, X., Pan, S., Bian, C., Meng, X., Xu, J., Deng, F., Maurer, S., Müller, U., & Xiao, F.-S. (2015). Solvent-free synthesis of zeolites from anhydrous starting raw solids. *Journal of the American Chemical Society*, *137*(3), 1052–1055. https://doi.org/10.1021/ja5124013

Wu, Q., Meng, X., Gao, X., & Xiao, F.-S. (2018). Solvent-free synthesis of zeolites: Mechanism and utility. *Accounts of Chemical Research*, *51*(6), 1396–1403. https://doi.org/10.1021/acs.accounts.8b00057

Wu, Q., Wang, X., Qi, G., Guo, Q., Pan, S., Meng, X., Xu, J., Deng, F., Fan, F., Feng, Z., Li, C., Maurer, S., Müller, U., & Xiao, F. S. (2014). Sustainable synthesis of zeolites without addition of both organotemplates and solvents. *Journal of the American Chemical Society*, *136*(10), 4019–4025. https://doi.org/10.1021/ja500098j

Wuest, J. D. (2020). Atoms and the void: modular construction of ordered porous solids. *Nature Communications*, *11*(1), 4652. https://doi.org/10.1038/s41467-020-18419-3

Xie, D. (2021). Rational design and targeted synthesis of small-pore zeolites with the assistance of molecular modeling, structural analysis, and synthetic chemistry. *Industrial &*

Engineering Chemistry Research, *60*(43), 15403–15415. https://doi.org/10.1021/acs.iecr.1c02878

Xing, L., Wei, Z., Wen, Z., & Zhu, X. (2017). Catalytic study for methanol aromatization over hierarchical ZSM-5 zeolite synthesized by kaolin. *Petroleum Science and Technology*, *35*(24), 2235–2240. https://doi.org/10.1080/10916466.2017.1381712

Xu, W., Dong, J., Li, J., Li, J., & Wu, F. (1990). A novel method for the preparation of zeolite ZSM-5. *Journal of the Chemical Society, Chemical Communications*, *2*(10), 755. https://doi.org/10.1039/c39900000755

Yan, K., Guo, Y., Fang, L., Cui, L., Cheng, F., & Li, T. (2017). Decomposition and phase transformation mechanism of kaolinite calcined with sodium carbonate. *Applied Clay Science*, *147*(February), 90–96. https://doi.org/10.1016/j.clay.2017.07.010

Yanu, C. A., Sieliechi, J. M., & Ngassoum, M. B. (2020). Optimization of ceramic paste viscosity use for the elaboration of tubular membrane support by extrusion and its application. *Journal of Materials Science and Chemical Engineering*, *08*(03), 1–22. https://doi.org/10.4236/msce.2020.83001

Yoldi, M., Korili, S. A., & Gil, A. (2019). Zeolite synthesis from industrial wastes. *Microporous and Mesoporous Materials*, *287*(March), 183–191. https://doi.org/10.1016/j.micromeso.2019.06.009

Yuan, D., He, D., Xu, S., Song, Z., Zhang, M., Wei, Y., He, Y., Xu, S., Liu, Z., & Xu, Y. (2015). Imidazolium-based ionic liquids as novel organic SDA to synthesize high-silica Y zeolite. *Microporous and Mesoporous Materials*, *204*(C), 1–7. https://doi.org/10.1016/j.micromeso.2014.10.049

Yue, Y., Hu, Y., Dong, P., Li, X., Liu, H., Bao, J., Wang, T., Bi, X., Zhu, H., Yuan, P., Bai, Z.,

& Bao, X. (2020). Mesoscale depolymerization of natural rectorite mineral *via* a quasi-solid-phase approach for zeolite synthesis. *Chemical Engineering Science*, *220*, 115635. https://doi.org/10.1016/j.ces.2020.115635

Zhang, J., Li, X., Liu, J., & Wang, C. (2018). A comparative study of MFI zeolite derived from different silica sources: synthesis, characterization and catalytic performance. *Catalysts*, *9*(1), 13. https://doi.org/10.3390/catal9010013

Zhang, K., Fernandez, S., O'Brien, J. T., Pilyugina, T., Kobaslija, S., & Ostraat, M. L. (2018). Organotemplate-free synthesis of hierarchical beta zeolites. *Catalysis Today*, *316*(2017), 26–30. https://doi.org/10.1016/j.cattod.2017.11.033

Zhang, Y., Ji, G., Ma, D., Chen, C., Wang, Y., Wang, W., & Li, A. (2020). Exergy and energy analysis of pyrolysis of plastic wastes in rotary kiln with heat carrier. *Process Safety and Environmental Protection*, *142*, 203–211. https://doi.org/10.1016/j.psep.2020.06.021

Zhang, Y., Liu, Y., & Li, J. (2022). In situ synthesis of metal-containing ZSM-5 and its catalytic performance in aromatization of methanol. *ACS Omega*, *7*(28), 24241–24248. https://doi.org/10.1021/acsomega.2c01442

Zhang, Y., Qu, Y., & Wang, J. (2018). Effect of crystal size on the catalytic performance of HZSM-5 Zeolite in the methanol to aromatics reaction. *Petroleum Science and Technology*, *36*(12), 898–903. https://doi.org/10.1080/10916466.2018.1451889

Zhou, C. H., & Keeling, J. (2013). Fundamental and applied research on clay minerals: From climate and environment to nanotechnology. *Applied Clay Science*, *74*, 3–9. https://doi.org/10.1016/j.clay.2013.02.013

Zhou, J., Liu, Z., Wang, Y., Kong, D., & Xie, Z. (2018). Shape selective catalysis in methylation of toluene: Development, challenges and perspectives. *Frontiers of Chemical*

Science and Engineering, *12*(1), 103–112. https://doi.org/10.1007/s11705-017-1671-x

Zhou, N., Dai, L., Lv, Y., Li, H., Deng, W., Guo, F., Chen, P., Lei, H., & Ruan, R. (2021). Catalytic pyrolysis of plastic wastes in a continuous microwave assisted pyrolysis system for fuel production. *Chemical Engineering Journal*, *418*(December 2020), 129412. https://doi.org/10.1016/j.cej.2021.129412

Zou, Y., Hu, Y., Shen, Z., Yao, L., Tang, D., Zhang, S., Wang, S., Hu, B., Zhao, G., & Wang, X. (2022). Application of aluminosilicate clay mineral-based composites in photocatalysis. *Journal of Environmental Sciences*, *115*, 190–214. https://doi.org/10.1016/j.jes.2021.07.015

Zoubida, L., & Hichem, B. (2018). The nanostructure zeolites MFI-type ZSM5. In *Nanocrystals and Nanostructures*. InTech. https://doi.org/10.5772/intechopen.77020

APPENDICES

Appendix 1: Pictures of the fine powdered raw, calcined, acid-leached clay samples and zeolites obtained.

Anfoega clay	**Teleku-Bokazo clay**	**Mfensi clay**	**Tetegu clay**
Raw clay 	Raw clay 	Raw clay 	Raw clay 
Calcined clay 	Calcined clay 	Calcined clay 	Calcined clay 
Acid leached clay 	Acid leached clay 	Acid leached clay 	Acid leached clay 
Synthesized zeolite 	Synthesized zeolite 	Synthesized zeolite 	Synthesized zeolite 

Appendix 2: Determination Activation Energy value from TGA data for (a) Anfoega, (b) Mfensi, (c) Teleku-Bokazo, and (d) Tetegu clay

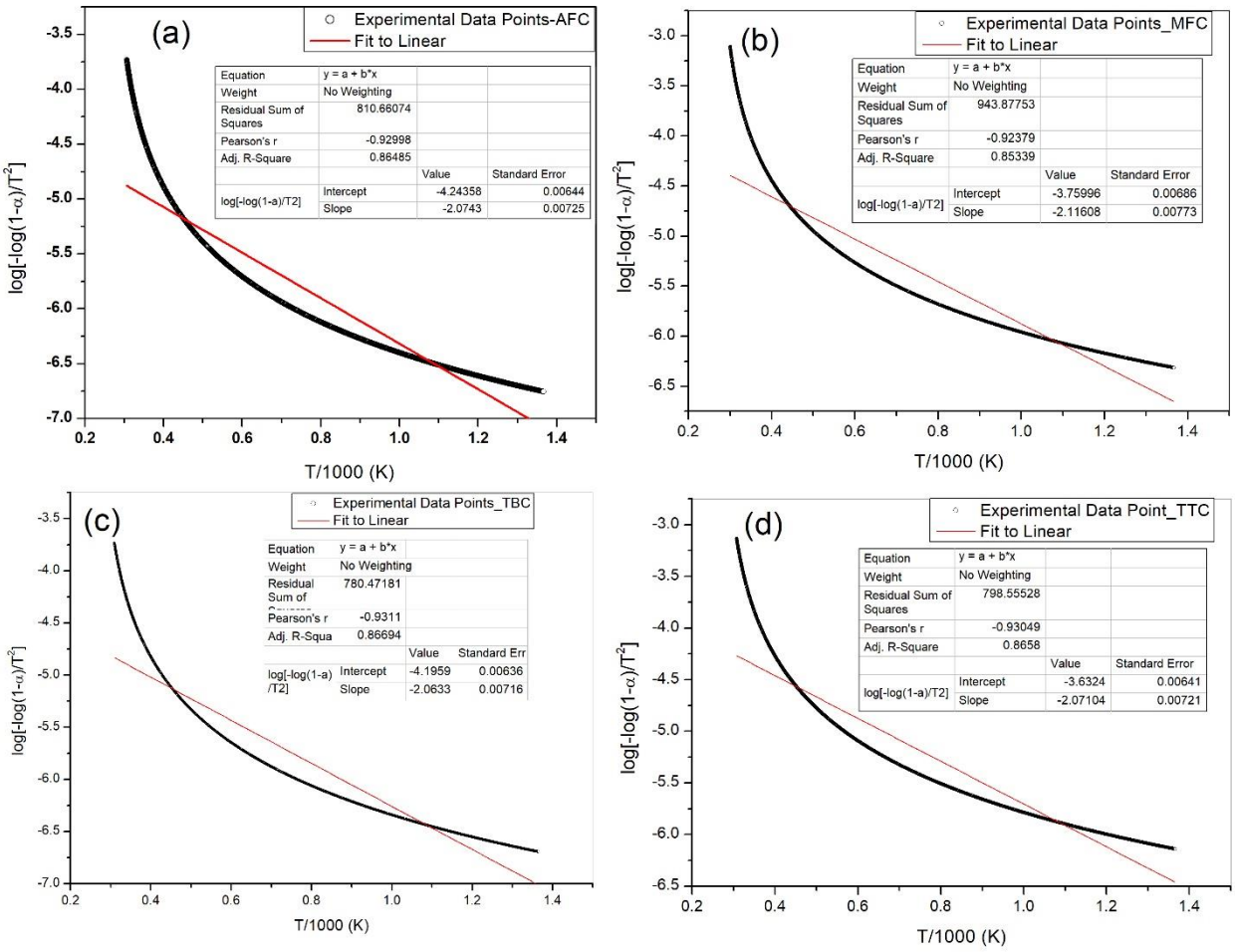

Appendix 3a: Determination of Enthalpy value from DSC data for Anfoega clay

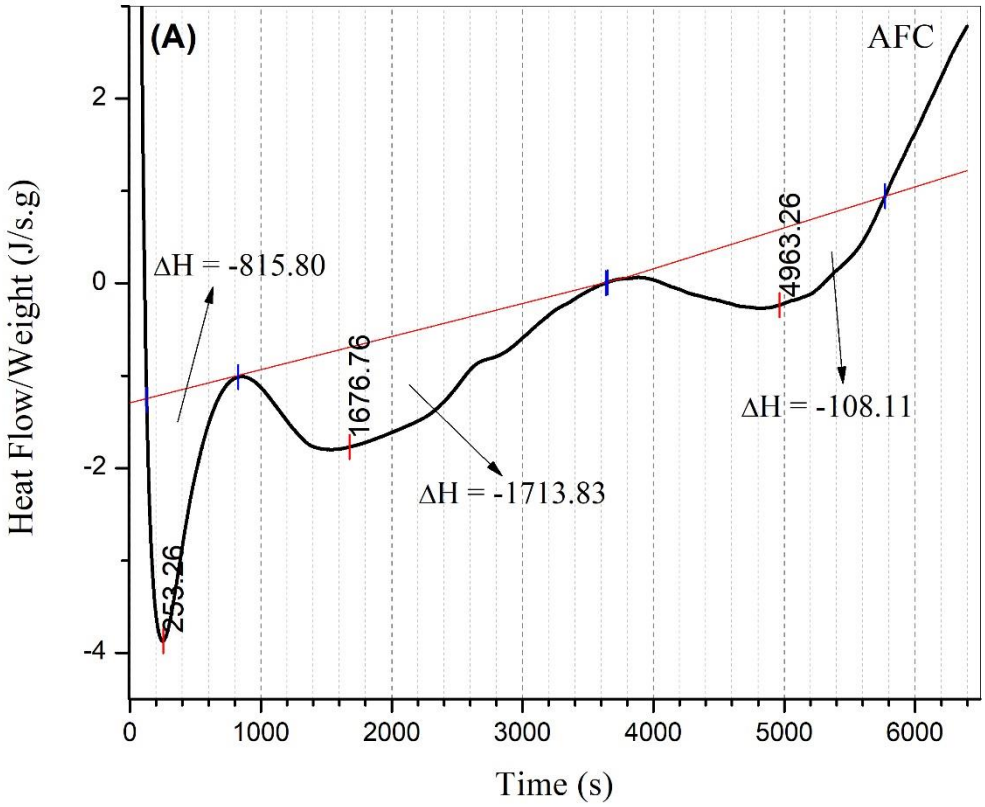

Appendix 3b: Determination of Enthalpy value from DSC data for Mfensi clay

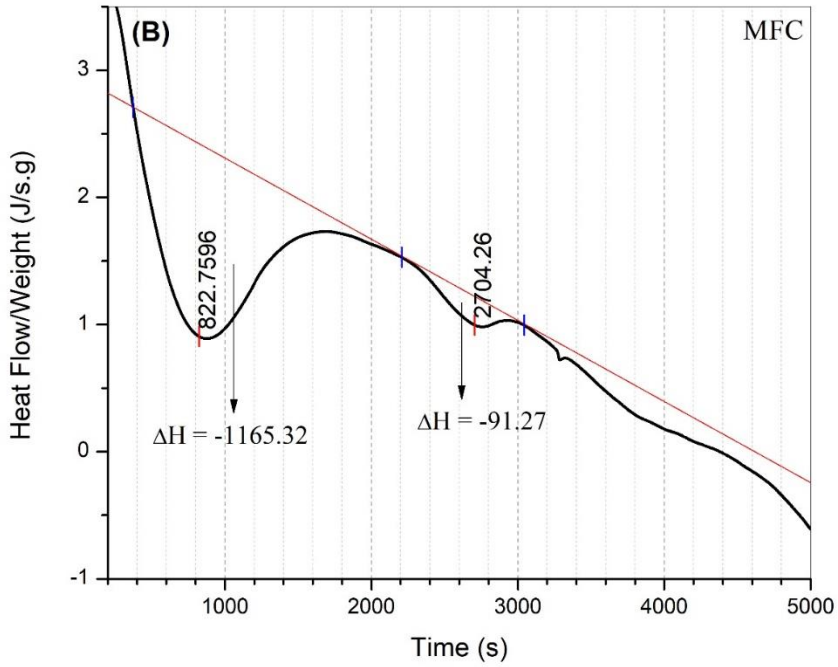

Appendix 3c: Determination of Enthalpy value from DSC data for Teleku-Bokazo clay

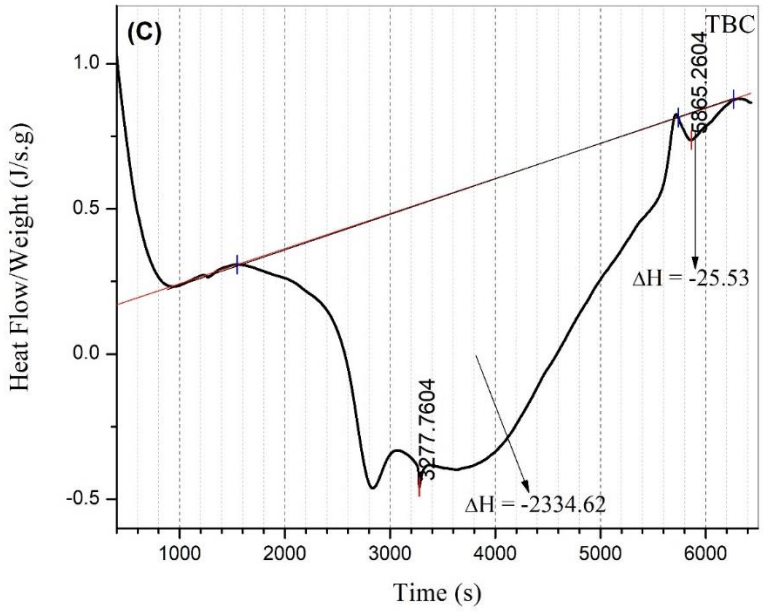

Appendix 3d: Determination of Enthalpy value from DSC data for Tetegu clay

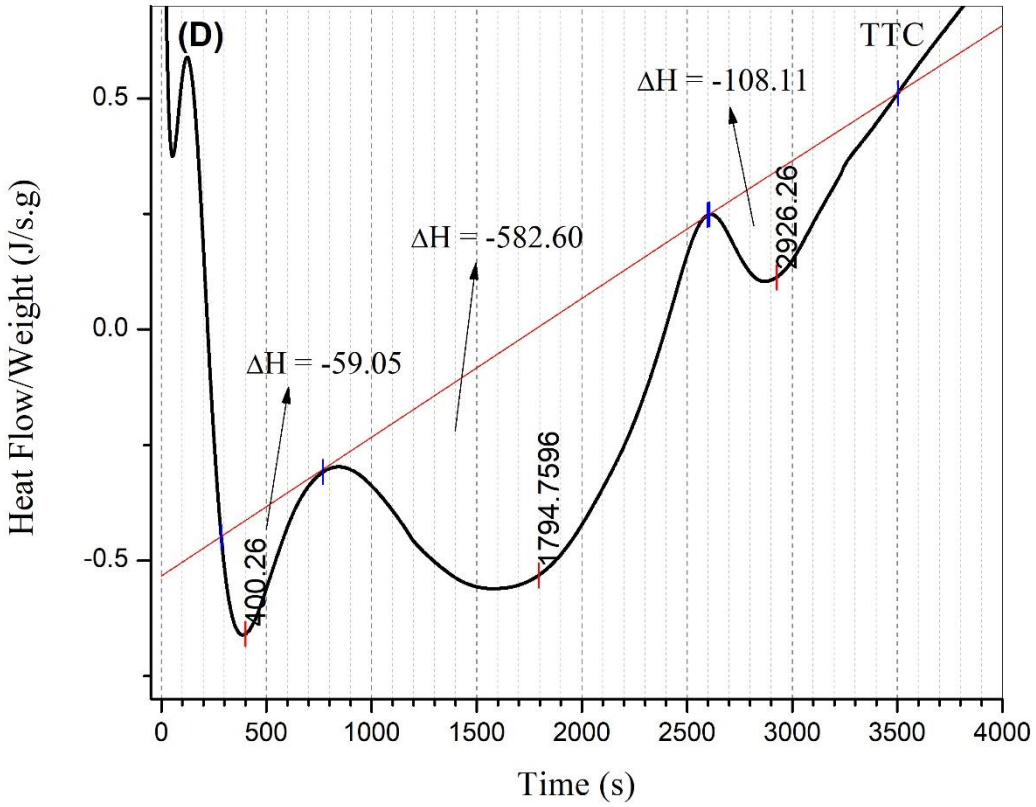

Appendix 4a: FTIR spectra of calcination at 600 ºC, 700 ºC and 800 ºC of Anfoega clay

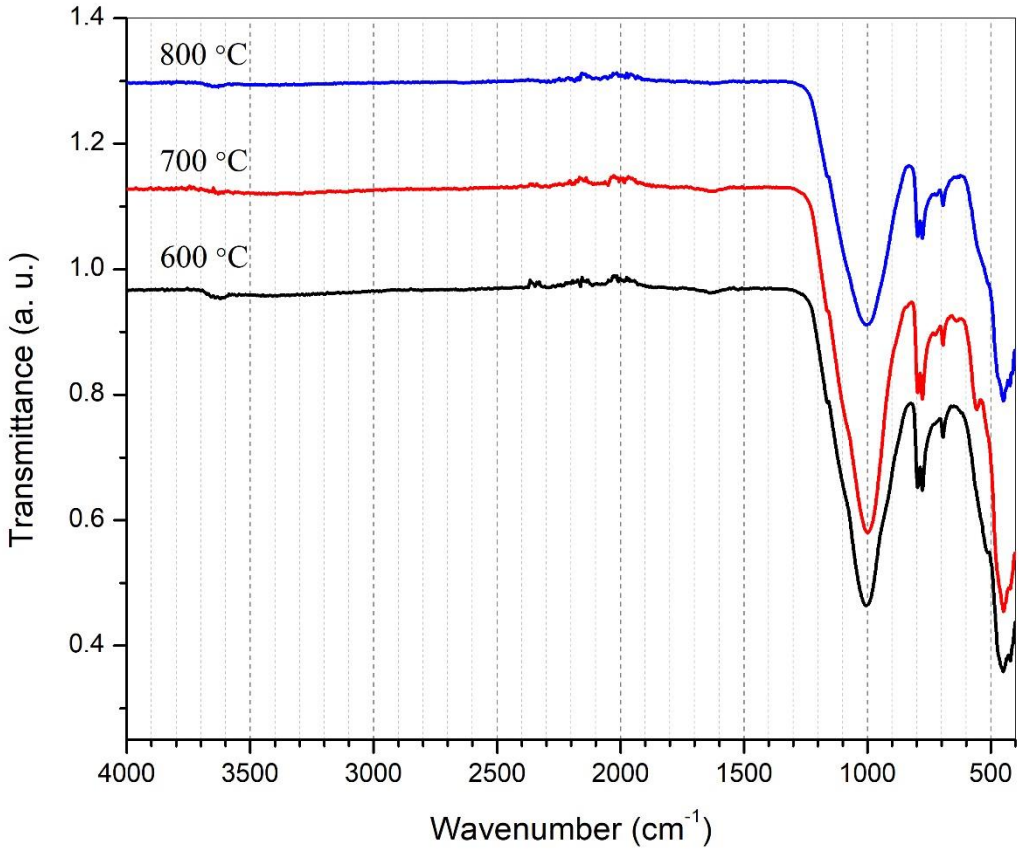

Appendix 4b: FTIR spectra of calcination at 600 ºC, 700 ºC and 800 ºC of Mfensi clay

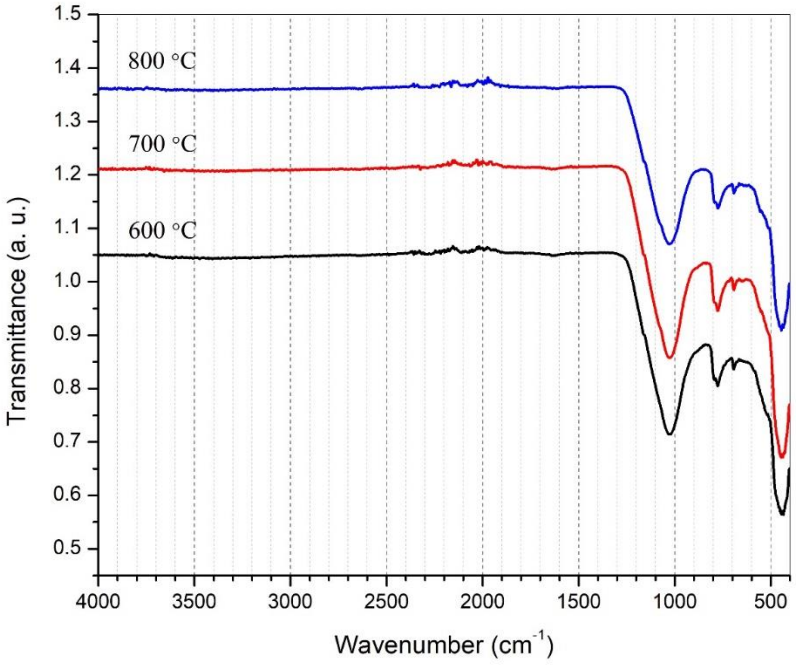

Appendix 4c: FTIR spectra of calcination at 600 ºC, 700 ºC and 800 ºC of Teleku-Bokazo clay

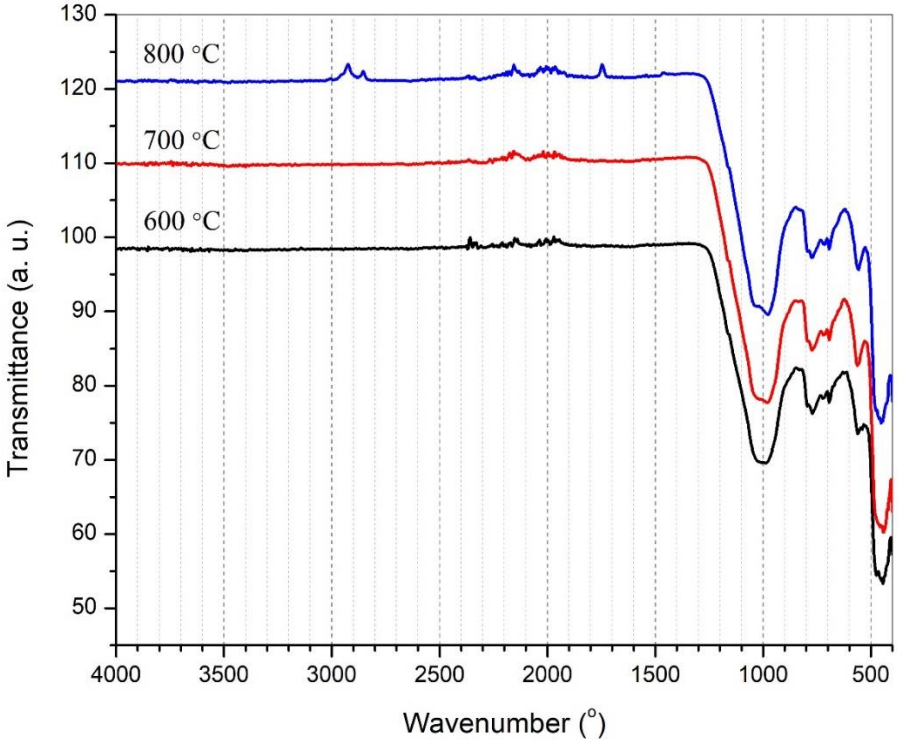

Appendix 4d: FTIR spectra of calcination at 600 ºC, 700 ºC and 800 ºC of Tetegu clay

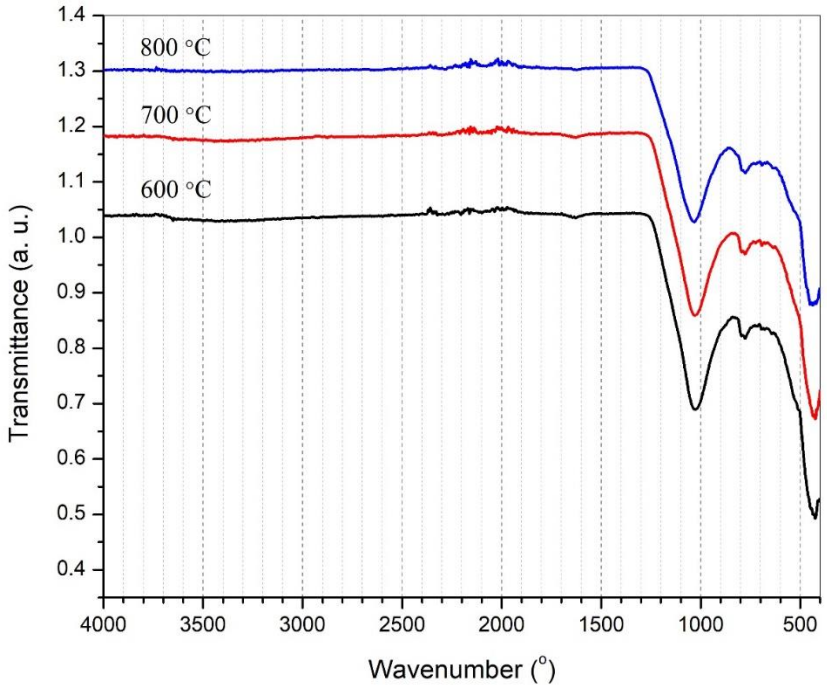

Appendix 5a: XRD pattern of raw, calcined, and acid-leached Anfoega clay

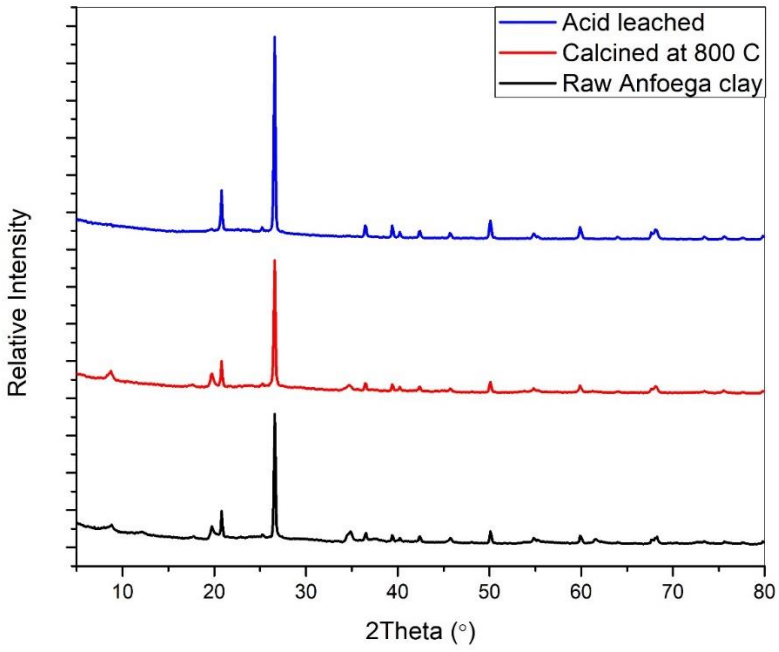

Appendix 5b: XRD pattern of raw, calcined, and acid-leached Mfensi clay

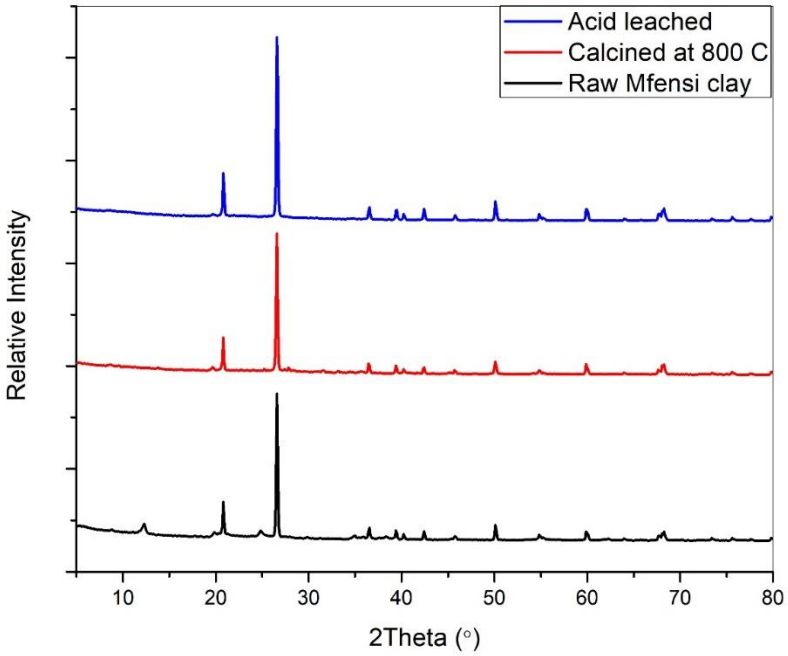

Appendix 5c: XRD pattern of raw, calcined, and acid-leached Teleku-Bokazo clay

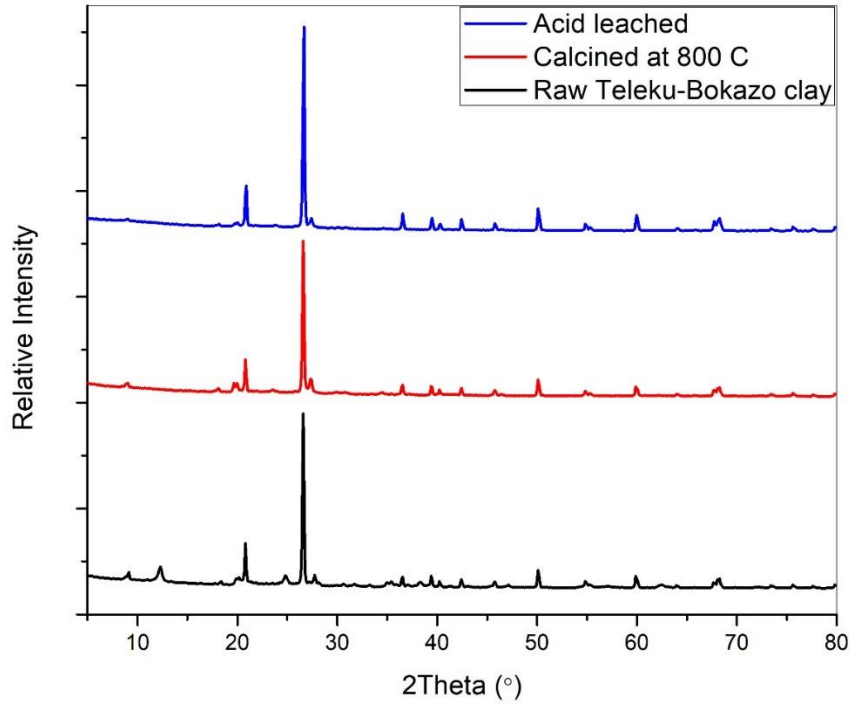

Appendix 5d: XRD pattern of raw, calcined, and acid-leached Tetegu clay

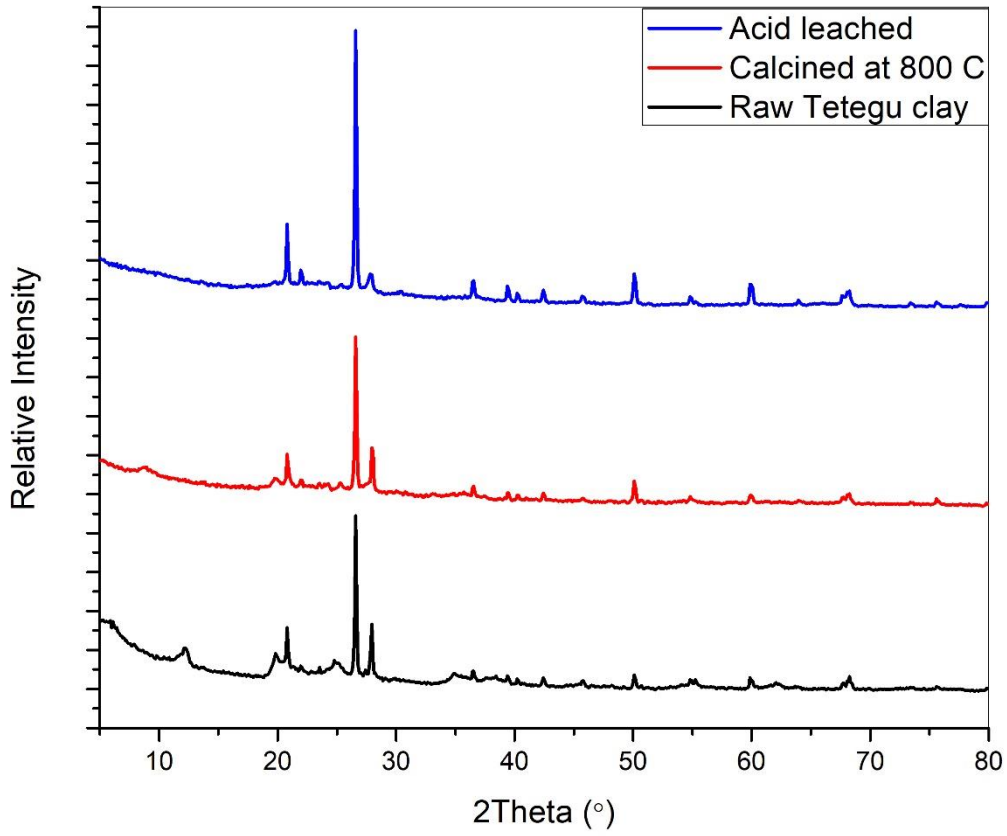

Appendix 6: FTIR spectra of acid leached (a) Anfoega, (b) Mfensi, (c) Teleku-Bokazo, and (d) Tetegu clay

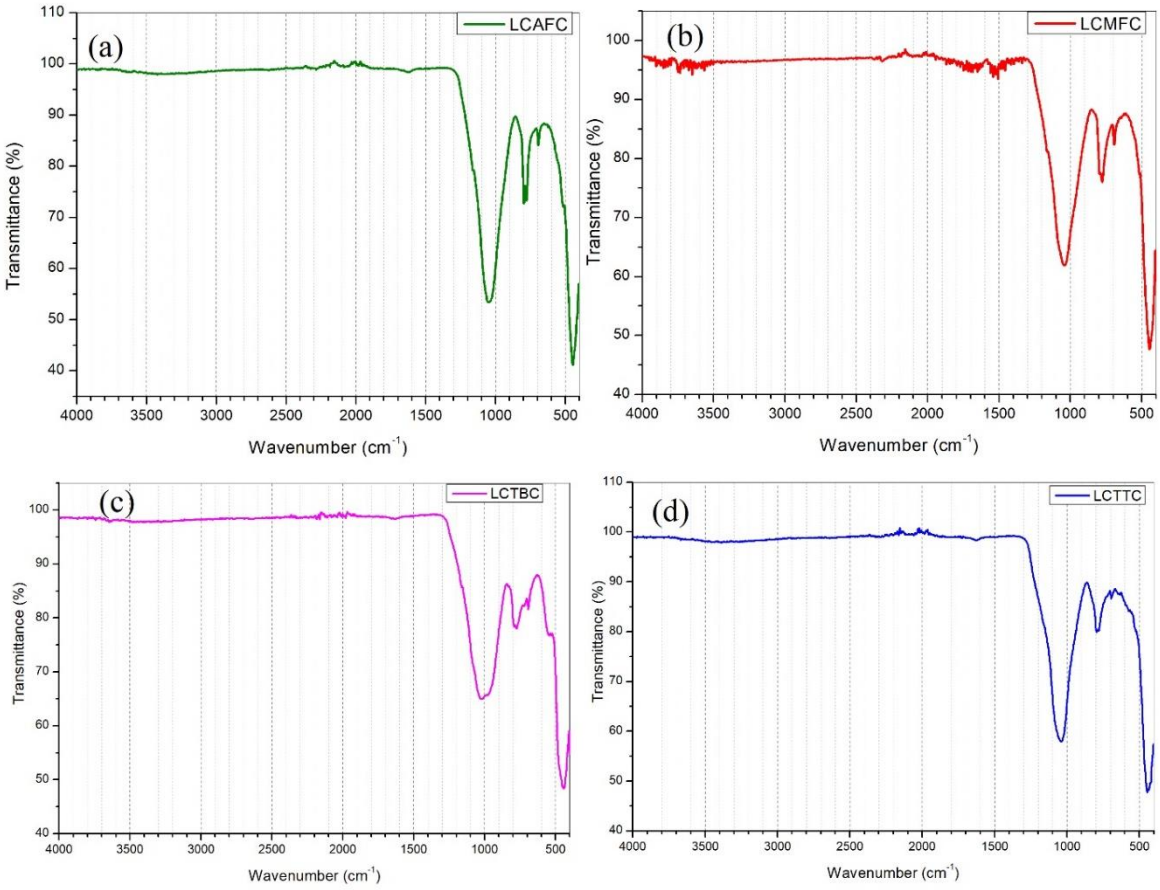

Appendix 7: XRD pattern of as-synthesized product from Anfoega clay using a solid-state method of synthesis.

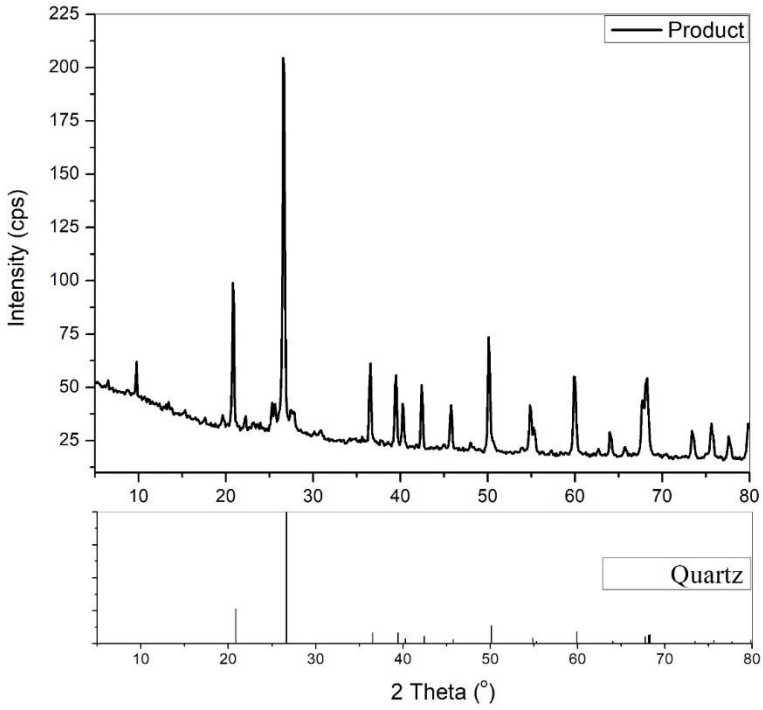

Appendix 8: FTIR spectra of as-synthesized products at different crystallization temperatures.

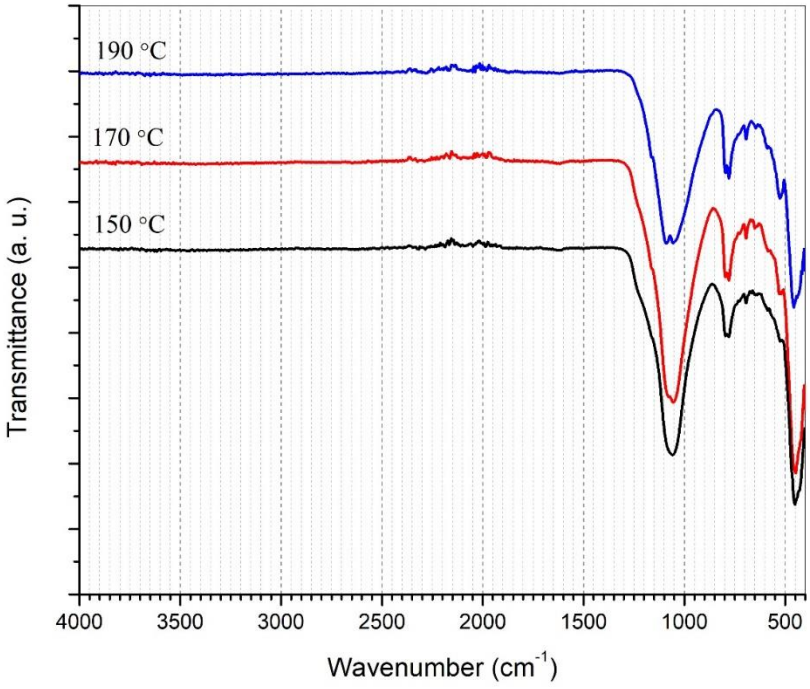

Appendix 9: FTIR spectra of as-synthesized products at different crystallization times.

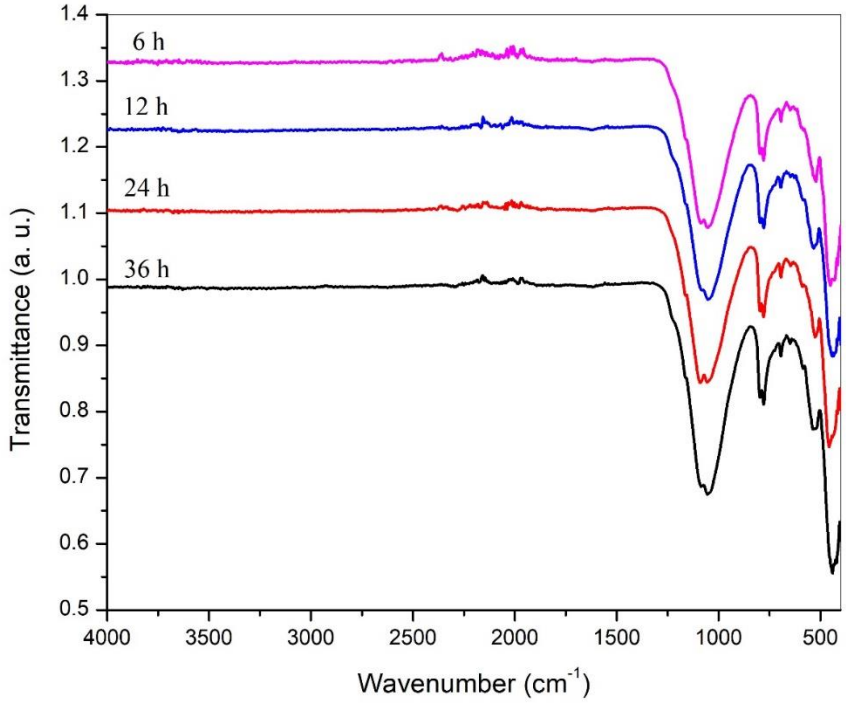

Appendix 10: FTIR spectra of as-synthesized products at different SiO_2/Al_2O_3 molar ratios.

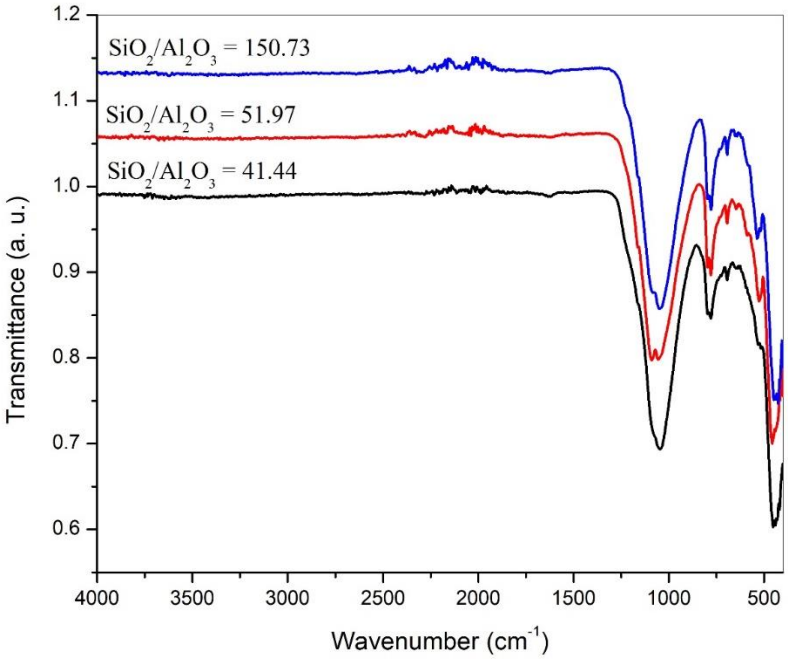

Appendix 11: FTIR spectra of as-synthesized products at different $NaOH/SiO_2$ molar ratios.

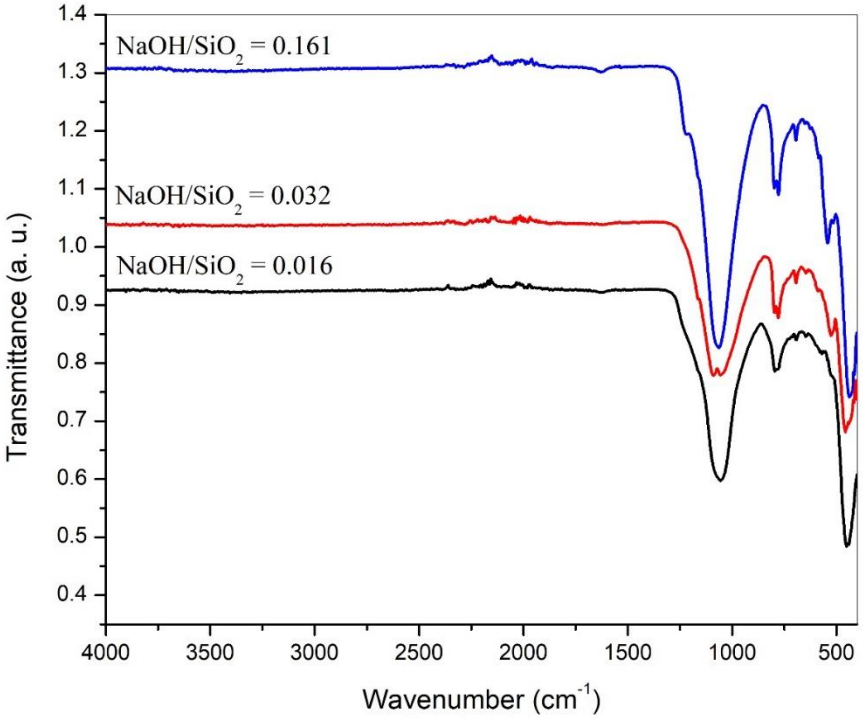

Appendix 12: FTIR spectra of as-synthesized products at different TPABr/SiO_2 molar ratios.

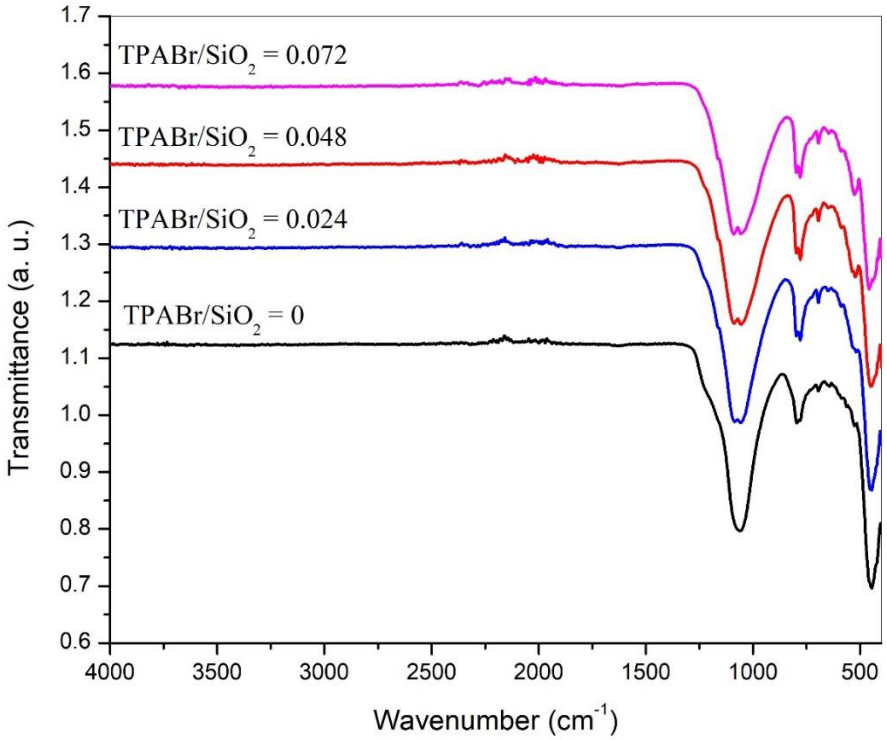

Appendix 13: FTIR spectra of as-synthesized products at different H_2O/SiO_2 molar ratios.

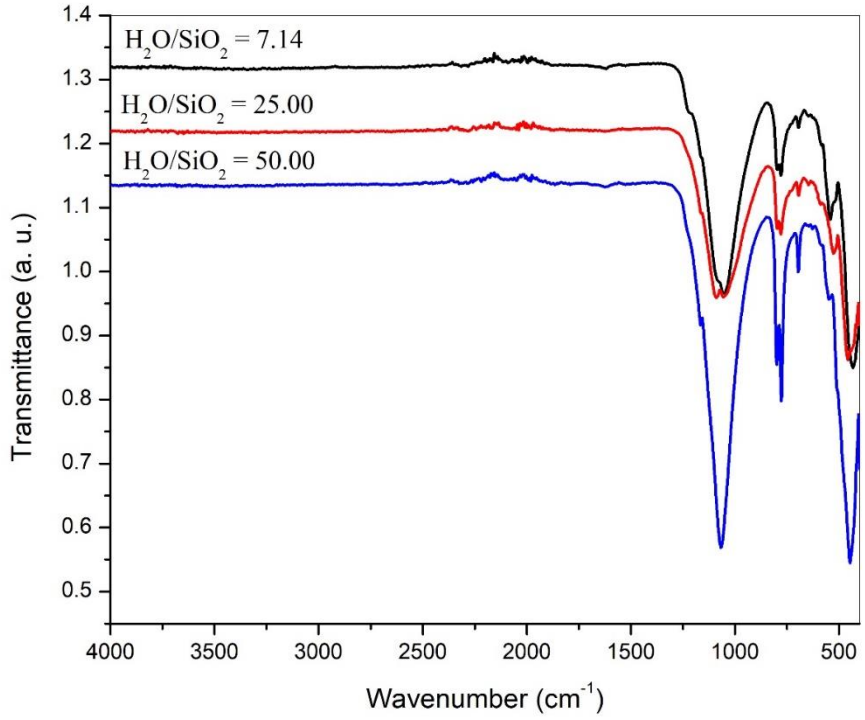

Appendix 14: FTIR spectra of as-synthesized products at different aging conditions.

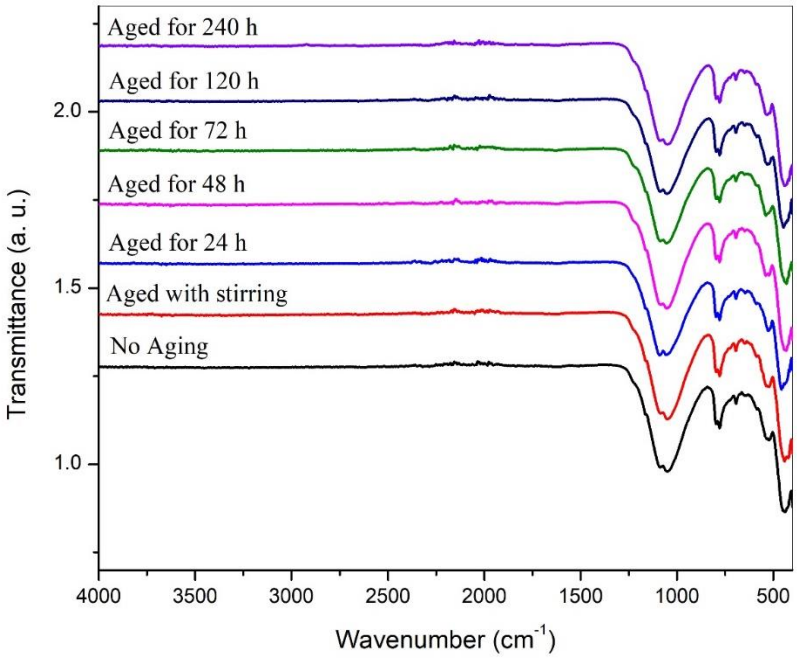

Appendix 15: FTIR spectra of as-synthesized products with and without calcination after dealumination.

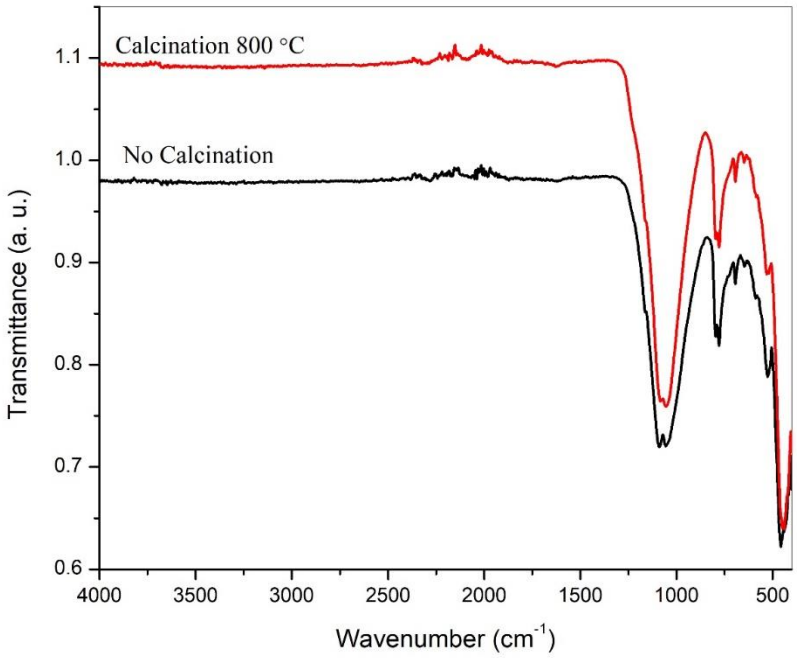

Appendix 16: Semi-quantitative phase analysis of the XRD data of as-synthesized ZSM-5 product from (a) Anfoega (b) Mfensi (c) Teleku-Bokazo (d) Tetegu clay samples (e) commercial ZSM-5.

Semi-Quantitative	(a)	(b)	(c)	(d)	(e)
ZSM-5 phase (%)	42.50	28.40	26.10	60.50	99.60
Quartz phase (%)	57.50	71.60	73.90	39.50	0.40